eTransportation 18 (2023) 100272

Contents lists available at ScienceDirect

eTransportation

journal homepage: www.journals.elsevier.com/etransportation

Challenges and opportunities of practical sulfide-based all-solid-state batteries

Dongsheng Ren [a,b,*], Languang Lu [b], Rui Hua [b], Gaolong Zhu [c], Xiang Liu [d], Yuqiong Mao [b], Xinyu Rui [b], Shan Wang [b], Bosheng Zhao [b], Hao Cui [a], Min Yang [b], Haorui Shen [b], Chen-Zi Zhao [b], Li Wang [a], Xiangming He [a,**], Saiyue Liu [b], Yukun Hou [b], Tiening Tan [c], Pengbo Wang [c], Yoshiaki Nitta [e], Minggao Ouyang [b,***]

[a] Institute of Nuclear and New Energy Technology, Tsinghua University, Beijing, 100084, China
[b] State Key Laboratory of Intelligent Green Vehicle and Mobility, Tsinghua University, Beijing, 100084, China
[c] Ouyang Minggao Academician Workstation, Sichuan New Energy Vehicle Innovation Center Co., Ltd., Sichuan, 644000, China
[d] School of Material Science and Engineering, Beihang University, Beijing, 100084, China
[e] Advanced Materials and Processing Laboratory, Nissan Motor Co., Ltd., 1, Natsushima-cho, Yokosuka, 237- 8523, Japan

ARTICLE INFO

Keywords:
All-solid-state batteries
Sulfide solid electrolytes
Interfacial instability
Composite electrodes
Scaling up

ABSTRACT

All-solid-state batteries (ASSBs) are regarded as the most promising next-generation batteries for electric vehicles in virtue of their potential advantages of enhanced safety, high energy density and power capability. Among the ASSBs based on various solid electrolytes (SEs), sulfide-based ASSBs have attracted increasing attention due to the high ionic conductivity of sulfide SEs which is comparable to that of liquid electrolytes. Extensive efforts from academia and industry have been made to develop sulfide-based ASSBs, and several significant progress has been achieved in recent years. However, successful fabrication of high-performance sulfide-based ASSBs has been rarely reported, and the practical application of sulfide-based ASSBs still faces a variety of challenges. Herein, following a bottom-up approach, we present a comprehensive review of the critical issues of practical sulfide-based ASSBs from the material, interface, composite electrode to cell levels. The existing challenges, recent advances, and future research directions of sulfide-based ASSBs at multiple levels are discussed. Finally, several fabrication processes for scaling up sulfide-based ASSBs and existing pilot/mass production schedules of sulfide-based ASSBs of the leading companies are also introduced. Facing the existing challenges and future opportunities, we highly encourage joint efforts and cooperation across the battery community to promote the practical application of sulfide-based ASSBs.

1. Introduction

Driven by the large-scale application of electric vehicles (EVs), lithium-ion batteries (LIBs) have experienced a high-speed development in the past decade, with the energy density exceeding 300 $Wh{\cdot}kg^{-1}$ and the cost reduced to around $100 per kWh [1–3]. The global EV battery usage reached 517.9 GWh, creating a multi-hundred-billion-dollar industry [4,5]. However, the existing liquid-electrolyte-based LIBs are approaching their energy density limits and exhibit potential safety risks [6–8]. Therefore, driven by the increasing demand for high-energy-density, safe and long-lasting batteries, tremendous research efforts have been devoted to the development of next-generation batteries, including all-solid-state batteries (ASSBs), lithium-sulfur batteries, and lithium-air batteries [9–12]. Among them, ASSBs are regarded as a game-changing technology for accelerating the popularization of EVs. As summarized in Table 1, owing to the improved safety, higher energy density, better power capability, temperature robustness and wide selections of electrode materials, automotive manufacturers have raised high expectations for ASSBs to make EVs more competitive in terms of longer driving range, shorter charging time, lower cost, more efficient integration and better environmental adaptability [13,14].

The performance of ASSBs largely depends on the solid electrolytes

* Corresponding author. Institute of Nuclear and New Energy Technology, Tsinghua University, Beijing, 100084, China.
** Corresponding author. Institute of Nuclear and New Energy Technology, Tsinghua University, Beijing, 100084, China.
*** Corresponding author. State Key Laboratory of Intelligent Green Vehicle and Mobility, Tsinghua University, Beijing, 100084, China.
E-mail addresses: rends@tsinghua.edu.cn (D. Ren), hexm@tsinghua.edu.cn (X. He), ouymg@tsinghua.edu.cn (M. Ouyang).

https://doi.org/10.1016/j.etran.2023.100272
Received 27 April 2023; Received in revised form 28 July 2023; Accepted 13 August 2023
Available online 21 August 2023

Abbreviations

ALD	Atomic layer deposition
AM	Active material
AN	Anode
ASSB	All-solid-state battery
CA	Cathode
CAM	Cathode active material
CBD	Carbon–binder
CE	Coulombic efficiency
CEI	Cathode electrolyte interphase
CMC	Carboxymethyl cellulose
cPAN	Cyclized polyacrylonitrile
DFT	Density functional theory
DOD	Degree of discharge
EIS	Electrochemical impedance spectroscopy
ESW	Electrochemical stability window
EV	Electric vehicle
HSAB	Hard and soft acids and bases
KPI	Key performance indicator
LATP	$Li_{1.4}Al_{0.4}Ti_{1.6}(PO_4)_3$
LGPS	$Li_{10}GeP_2S_{12}$
LIB	Lithium-ion battery
NBR	Nitrile-butadiene rubber
NCA	$LiNi_xCo_yAl_zO_2$
NCM	$LiNi_xCo_yMn_{1-x-y}O_2$
NMP	N-methyl pyrrolidinone
PAA	Polyacrylic acid
PTFE	Polytetrafluoroethylene
PVDF	Poly(vinylidene fluoride)
PVDF-HFP	Poly(vinylidene fluoride-co-hexafluoropropylene)
P(VDF-TrFE)	Poly(vinylidene fluoride-co-trifluoroethylene)
SBR	Styrene-butadiene rubber
SCL	Space charge layer
SE	Solid electrolyte
SEBS	Polystyrene-block-poly(ethylene-ran-butylene)-block-polystyrene
SEI	Solid electrolyte interphase
SNCM	Single-crystalline $LiNi_{0.6}Co_{0.2}Mn_{0.2}O_2$
SOC	State of charge
THF	Tetrahydrofuran
VGCF	Vapor-grown carbon fiber
XPS	X-ray photoelectron spectroscopy

Table 1
Automotive manufacturers' expectations for ASSBs [13,14].

Feasibilities of ASSBs	Rationales & Principles	Expectations
Improved Safety	• Implementing incombustible and thermal stable solid electrolyte • Inhibiting chemical crosstalk by compact electrolyte membrane	• Simplified safety design at battery module and pack level • Freeness of layout in pack
High energy density	• Compatibility to high-capacity materials, like Li metal • Possibility of bipolar stacking	• Up to 2 times energy density • Space saving • Reduced per Wh cost
Better power capability	• Highly conductive solid electrolyte with a different Li^+ transport mechanism (hopping) • Unity Li^+ transference number	• Fast-charging capability • Better dynamic performance • Compatibility to a wider range of vehicles, such as trucks
Temperature robustness	• Stable at a wide temperature range of −30–150 °C without freezing or volatilizing	• Simplified cooling/heating system • Improved environmental adaptability for EVs
Wide selections of electrode materials	• Possibility to materials that suffer from severe side reactions with liquid electrolytes, such as pure Si anode [15], Li-rich cathode [16], etc.	• Reduced raw material cost • Countermeasure for resource issues in the future

(SEs), which not only provide Li^+ transport pathways inside ASSBs but also act as separators to prevent electronic short circuit between the cathode and anode [17]. Several group of SEs have been developed for ASSBs, including polymer SEs, oxide SEs, sulfide SEs and halide SEs [10]. Polymer SEs usually exhibit excellent deformability and good compatibility to the existing manufacturing line of LIBs, and thus have been applied in consumer LIBs [18]. Limited ionic conductivities and poor electrochemical compatibility with high-voltage cathode are the challenges that hinder the market implementation of polymer-based ASSBs. Oxide SEs have excellent (electro-)chemical and thermal stabilities, which are conducive for battery safety [19]. However, the relatively low ionic conductivities and high elastic moduli of oxide SEs lead to large internal resistance and poor rate performance of oxide-based ASSBs, limiting their application in EV power batteries. In recent years, polymer SEs and oxide SEs have been utilized in hybrid solid/liquid LIBs as additives or coating materials for electrodes/separators, to enhance battery safety and cycling stability [6,20]. Halide SEs show higher ionic conductivities than oxide SEs and high stability toward oxidation. Therefore, halide SEs are most suitable as the catholyte in ASSBs [21]. Nevertheless, halide SEs are still in an early stage of research, and efforts are required to improve their compatibility with Li metal and reduce or exclude the use of rare-earth elements (In, Sc, Y, and etc.). Among the four SEs, sulfide SEs exhibit the highest ionic conductivities that are comparable to those of the common liquid electrolytes (≈10 mS cm^{-1}), and are thus the most promising SEs for EV power ASSBs and the main focus of this paper.

Since the first report of $Li_{10}GeP_2S_{12}$ (LGPS)-type [22] superionic conductor in 2011, a series of sulfide SEs with high ionic conductivities of 1–20 mS cm^{-1} have been developed, including Li_2S – P_2S_5 binary system [23–25] (1–10 mS cm^{-1}), argyrodite Li_6PS_5X (X = Cl, Br and I) type [26–28] (1–10 mS cm^{-1}), thio-LISICON type [29–31] (~1 mS cm^{-1}) and LGPS type ($Li_{10}GeP_2S_{12}$ [22] – 12 mS cm^{-1}, $Li_{9.54}Si_{1.74}P_{1.44}S_{11.7}Cl_{0.3}$ [32] – 25 mS cm^{-1}). The discoveries of highly conductive sulfide SEs push the research on ASSBs into a new stage. As shown in Fig. 1 (a), the proportion of papers on sulfide-based ASSBs shows a significant increase since 2011 and reached 20% in 2022. Sulfide-based ASSBs with high energy density (>900 Wh·L^{-1} [33]) or long cycling life (>500 cycles [15,33,34] and even >10000 cycles [35]) have been reported in recent years. Moreover, attracted by their great potential as next-generation EV batteries, a growing number of automotive/battery manufacturers and start-ups have started developing high-performance sulfide-based ASSBs, and some have made significant progress, as presented in Fig. 1 (b). For example, Solid Power [36] and Svolt Energy [37] announced the successful fabrication of 20 Ah sulfide-based ASSBs, Mitsui Kinzoku [38] and POSCO [39] set up pilot factories of sulfide SEs, and Solid Power [36], Samsung [40] and Nissan [41] have started constructing pilot production plants for sulfide-based ASSBs. These achievements considerably raise the community's confidence in ASSBs, making the mass production of sulfide-based ASSBs possible soon.

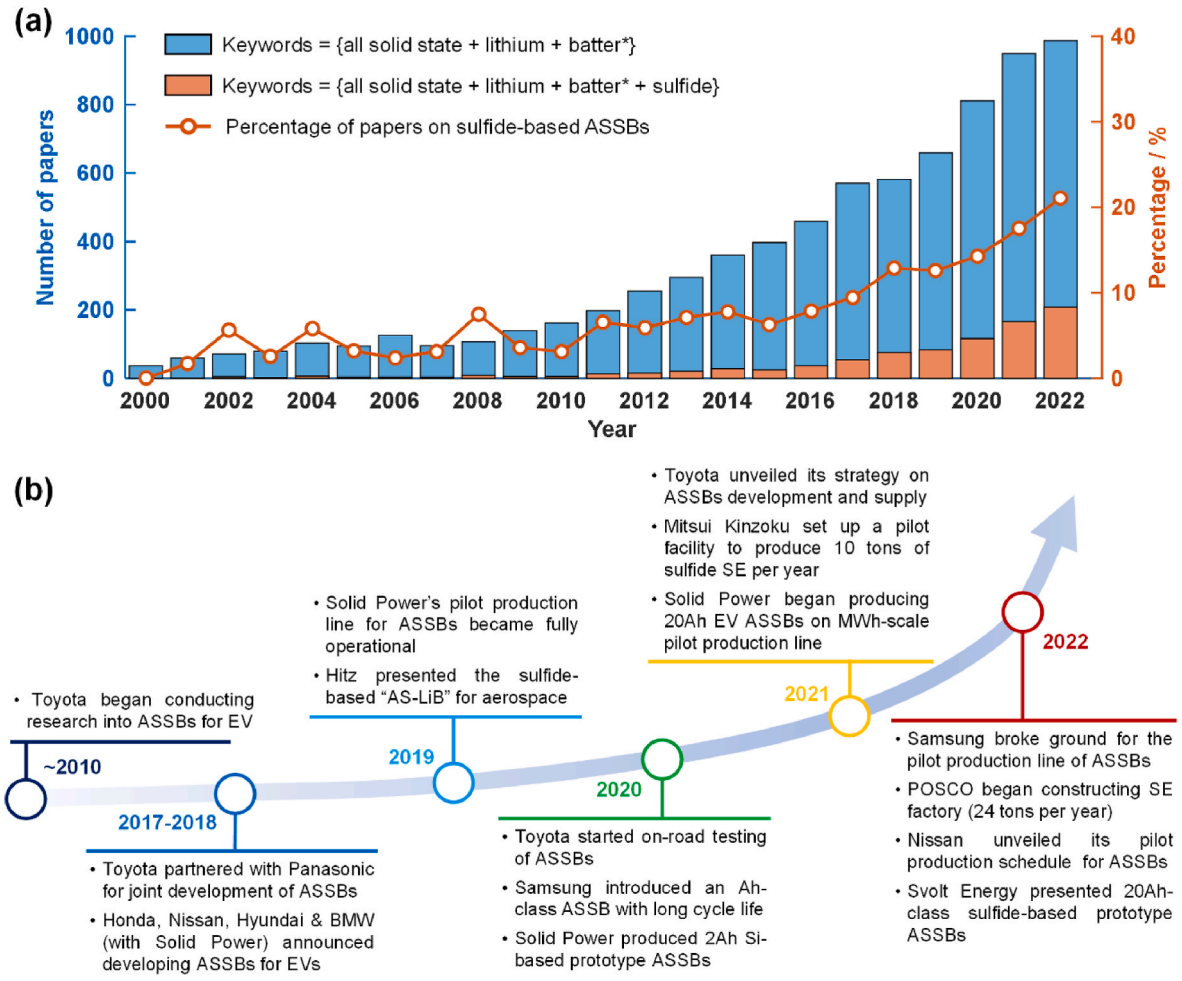

Fig. 1. Academic and industrial progress of sulfide-based ASSBs. (a) The number of papers on ASSBs and sulfide-based ASSBs published each year, and the evolution of the proportion of papers on sulfide-based ASSBs. Statistics from Web of Science Core Collection by searching relevant keywords (March 03, 2023); (b) the important industrial progress of sulfide-based ASSBs in the past decade [36–50].

Although sulfide-based ASSBs are considered a promising candidate for EV batteries, and several breakthroughs have been made in recent years, no company has yet demonstrated the ability to mass manufacture ASSBs. According to ASSB roadmaps from various countries and companies, sulfide-based ASSBs will be commercialized no earlier than 2025 or even after 2030. Before the mass production of sulfide-based ASSBs,

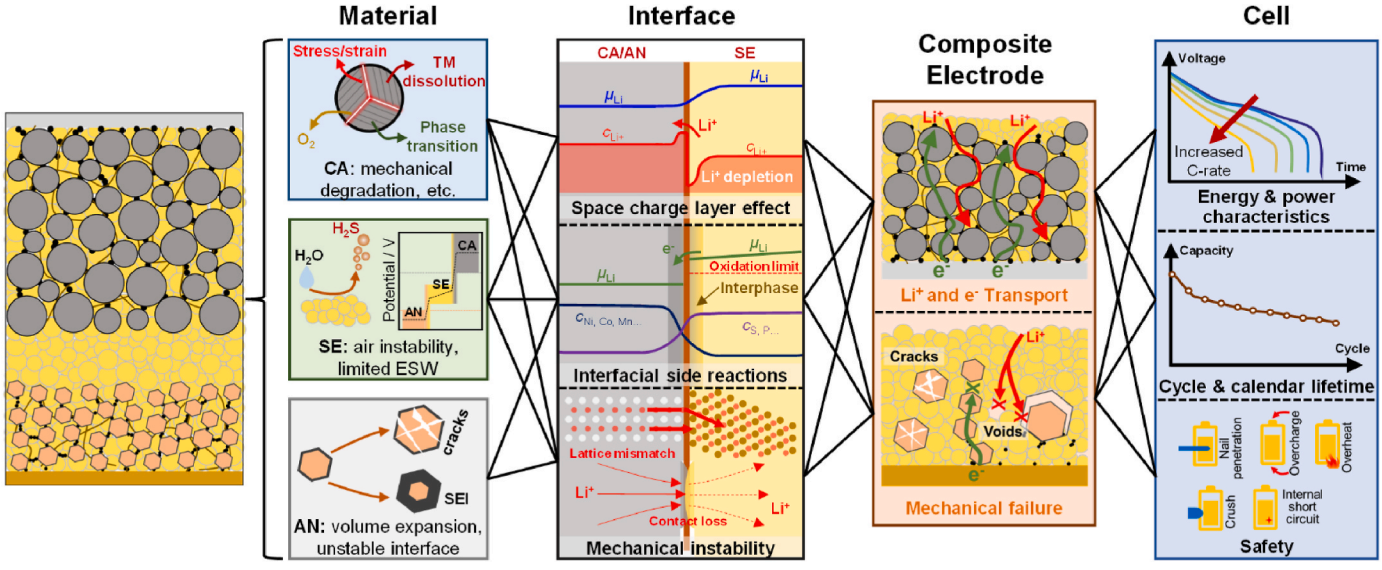

Fig. 2. Challenges of sulfide-based ASSBs: from material (CA = Cathode, SE = Solid electrolyte, AN = Anode), interface, composite electrode to cell.

many challenges remain to be addressed, including material instabilities, interfacial failures, electrode/cell construction and scaling-up, as summarized in Fig. 2. Herein, we discuss current challenges, possible solutions and future opportunities of practical sulfide-based ASSBs, as well as recent significant breakthroughs from companies. By integrating numerous reviews and perspectives on the material [51], interfacial [52–56], electrode [57] and scaling-up [58] problems of sulfide-based ASSBs, we provide a comprehensive overview of the challenges and opportunities of practical sulfide-based ASSBs at different levels and clarify their internal connections. The organization of this paper follows a "bottom-up" approach, i.e., from the material, interface, and composite electrode to cell levels. The scaling-up issues are also introduced according to worldwide players' reports on sulfide-based ASSB strategies.

2. Challenges of sulfide-based all-solid-state-batteries: from material, interface, composite electrode to cell

Fig. 2 summarizes the critical challenges of sulfide-based ASSBs at the material, active material (AM) | SE interface, composite electrode, and cell levels.

At the material level, SEs are the core component of ASSBs. Despite their high ionic conductivity, the large-scale application of sulfide SEs is still hindered by their poor air stability and limited electrochemical stability window (ESW) [51,59,60]. Consequently, most sulfide SEs need to be handled in an inert gas environment, leading to a sharp increase in the manufacturing cost of sulfide SEs and ASSBs [61–64]. Large-scale, low-cost manufacture of sulfide SEs materials is also challenging and requires extensive efforts from academic and industrial partners. For the electrode materials, high-voltage, high-capacity cathode materials (such as Ni-rich $LiNi_xCo_yMn_{1-x-y}O_2$ (NCM) and Li-rich layered materials) and Si-based anode or lithium metal anode will be adopted in sulfide-based ASSBs, to achieve high energy density. However, these high-capacity cathodes and anodes mostly suffer from detrimental structural effects, such as mechanical degradation in the cathode [65,66], and large volume expansion and low Coulombic efficiency (CE) in the anode [67,68]. Despite extensive mechanistic understanding and modification of electrode materials, the optimal design of cathode and anode materials for sulfide-based ASSBs remains to be discovered.

Due to the incompatibilities of electrodes and SEs on electrical, electrochemical, chemical and mechanical aspects, sulfide-based ASSBs face several interfacial problems, including space charge layer (SCL) effect, interfacial side reactions and mechanical instability [52–54]. These interfacial problems result in the formation of Li^+ depletion layer or low-conductivity interphase at the AM | SE interfaces, significantly impeding the transport of Li^+ and e^-. The interfacial problems can be mitigated by introducing a buffer layer to prevent direct contact between AMs and sulfide SEs, such as the coating layer on the cathode surface [69] and artificial solid electrolyte interphase (SEI) on the anode surface [70,71]. An ideal buffer layer is supposed to have excellent chemical/electrochemical stability, high ionic and low electronic conductivities, and a thickness of several nanometers [69]. However, the rational design and construction of homogeneous buffer layers between AMs and sulfide SEs are still challenging.

At the composite electrode level, the slow ionic/electronic transport kinetics and mechanical failure are the bottlenecks that limit the electrochemical performance of ASSBs [57,72,73]. Different from liquid electrolyte batteries, which have continuous and homogeneous Li^+/e^- pathways formed by the flowing electrolyte and the uniform conductive carbon network, Li^+/e^- transports in ASSBs are usually hindered by the nonuniform distribution of AMs, SEs, binder and carbon, leading to low capacity utilization of AMs [74]. Furthermore, the transport kinetics inside composite electrodes is influenced by the mass ratio of AMs, SEs, binder and carbon, morphologies of each component and mixing methods [74,75], and is indeed a vital area requiring further exploration. Moreover, mechanical failures in composite electrodes, including particle cracks and voids formation, would interrupt the Li^+/e^- pathways and lead to possible lithium dendrite growth and internal short circuit [76]. Applying a sufficiently high pressure to the composite electrodes and the cell during fabrication and cycling is the most effective approach to mitigate mechanical failures in ASSBs [77,78]. However, the optimal pressure values and the proper ways to apply the pressure remain elusive.

At the cell level, energy & power characteristics, cycle & calendar life, and safety are the key performance indicators (KPIs) for EV batteries. The energy & power characteristics and lifetime of sulfide-based ASSBs are highly related to the problems at the material, interface, and composite electrode levels. Only after addressing the challenges above will sulfide-based ASSBs be possible to achieve the vision of higher-energy-density, better-power-capability, and longer-lasting batteries. One more critical issue requiring careful consideration is the safety of sulfide-based ASSBs. Some recent results showed that ASSBs are not absolutely safe, as intense heat generation and even explosion were found in ASSBs under certain abuse conditions [79,80]. With the acceleration of the mass production of sulfide-based ASSBs for EVs, mechanistic understanding and comprehensive evaluation of the safety of sulfide-based ASSBs are urgently needed.

Among the above challenges at various levels, the rational design of high-capacity electrode materials, the transport and mechanical issues within composite electrodes, and the cell KPIs are also common for other types of ASSBs. For the sulfide-based ASSBs, several unique challenges resulted from the physicochemical characteristics of sulfide SEs do exist and require special attention. The (electro-)chemical instabilities of sulfide SEs lead to severe interfacial problems such as SCL effect and side reactions with electrode materials. Comprehensive investigation on the sulfide SE | AM interfacial structures and their evolution during the whole life cycle is one of the most important research topic for sulfide-based ASSBs. Moreover, considering the poor air stabilities of sulfide SEs, careful attention should be paid to the fabrication and handling processes of sulfide SEs in battery production line. Therefore, in the following sections, fundamental understandings of the critical issues at the material, interface, composite electrode and cell levels and scaling-up challenges, as well as several promising solutions are presented. The results can not only provide valuable guidance for researchers in sulfide-based ASSBs field, but also promote the research and development of all types of ASSBs.

3. Key materials for sulfide-based all-solid-state batteries

3.1. Sulfide solid electrolytes

With the groundbreaking discovery of superionic conductor $Li_{10}GeP_2S_{12}$ SE by Kanno et al. in 2011 [22], the ionic conductivity of sulfide SEs has entered the 10^{-3}–10^{-2} S cm^{-1} era [51,82,83], approaching or even surpassing that of organic liquid electrolytes. As a result, ionic conductivity is no longer the main bottleneck for the practical application of sulfide SEs in ASSBs. However, sulfide SEs still suffer from air and electrochemical instability, leading to significant difficulties in manufacturing, storing, and utilizing sulfide SEs.

As shown in Fig. 3 (a), sulfide SEs are prone to be hydrolyzed by moisture, following the reaction: $M_xS_y + H_2O \rightarrow M_xO_y + H_2S(g)$ [59,84,85]. The generated H_2S gas is highly toxic and explosive within a certain concentration range, and thus needs to be carefully treated. Moreover, with the chemical change from M_xS_y to M_xO_y, the ionic conductivity of sulfide SEs significantly decrease [59,84,85]. As summarized by Lu et al. [60], the air instability of sulfide SEs can be explained by various theoretical mechanisms, including hard and soft acids and bases (HSAB) theory [86], thermodynamic analysis [87] and kinetics of interfacial reactions [88]. Among them, the HSAB theory proposed by Ralph G. Pearson [86] has been widely accepted and applied to guide the development of air-stable sulfide SEs. According to the HSAB theory, the

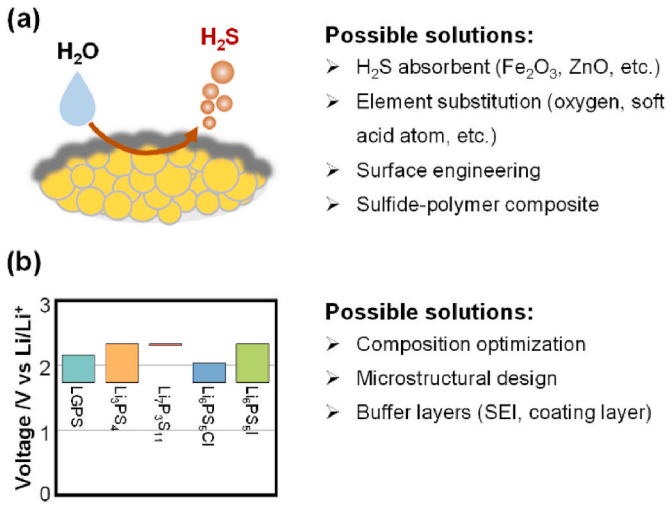

Fig. 3. Air and electrochemical instability problems of sulfide SEs. (a) Air instabilities and possible solutions; (b) the limited ESW and possible solutions. The ESWs of various sulfide SEs are obtained from Ref. [81].

hard acid P in sulfide SEs prefers to react with the hard base O to form P–O bonds instead of maintaining the P–S bonds, while the soft base S is apt to combine with H to generate H_2S gas [31]. Based on these theoretical explanations, several strategies were proposed to develop air-stable sulfide SEs, including H_2S absorbent [89,90], element substitution [91–93], surface engineering [94,95] and construction of sulfide-polymer composite SEs [96,97], as summarized in Fig. 3 (a). Metal-oxide additives like Fe_2O_3 and ZnO can absorb H_2S through chemical reactions [89]. However, the H_2S absorbent can only react with H_2S rather than improve the intrinsic air stability of sulfide SEs, and thus cannot mitigate the reduction of ionic conductivity due to the hydrolysis reaction. Moreover, introducing ionic insulating metal-oxide additives will further decrease the ionic conductivity of sulfide SEs [89]. Element substitution based on the HSAB theory, including O and soft acid atom (e.g., Sb, Sn, and Cu) substitution, can effectively suppress the hydrolysis reaction and enhance the air stability of sulfide SEs [92,93,98]. However, partial substitution will also result in structural changes in sulfide SEs and consequently decrease their ionic conductivity. More computational and experimental efforts are required to find better substitution strategies for sulfide SEs [60]. Surface engineering denotes constructing a functional layer on the surface of sulfide SEs or membranes to protect the SE from direct exposure to moisture. Jung et al. [94] prepared a core-shell oxysulfide-coated Li_6PS_5Cl SE, which can maintain a high ionic conductivity of 2.50 mS cm^{-1} after 30 min air exposure. Xu et al. [95] designed a water-stable Li_6PS_5Cl membrane tolerant to extreme exposure (direct water jetting) by constructing a superhydrophobic Li^+-conducting protective layer. Moreover, sulfide-polymer composite SE is another promising solution to air instability. The polymers can not only serve as a protective layer but also improve the mechanical flexibility and processability of sulfide SEs. Tan et al. [96] incorporated the hydrophobic polymer polystyrene-*block*-poly(ethylene-*ran*-butylene)-*block*-polystyrene (SEBS) into $Li_7P_3S_{11}$, and the composite SE film can even resist water immersion. Despite the promising solutions above to the air instability problem of sulfide SEs, a decrease in ionic conductivity is usually unavoidable. Thus, continuous efforts are required to balance the air stability and ionic conductivity of sulfide SEs. The target for improving air stability is to enable the processing of sulfide SEs in dry room conditions (similar to liquid electrolyte LIBs), which is more economical than processing in an inert gas environment.

The limited ESW is another bottleneck that hinders the application of sulfide SEs. Some studies have shown that sulfide SEs have wide ESWs, even up to 5 V versus Li/Li^+ [22]. However, Han et al. [99] found that the ESWs of SEs had been overestimated due to the poor contact between SEs and current collectors. Based on first-principle calculations, Zhu et al. [81] revealed that the intrinsic ESWs of sulfide SEs were mostly limited between 1.71 and 2.5 V versus Li/Li^+, as presented in Fig. 3 (b). Zhu's computational results are also supported by the experimental results using modified testing cell configurations [99]. The narrow ESWs result in the incompatibility of sulfide SEs with most of the common cathode (>4.0 V) and anode (<1.0 V) materials. The sulfide SEs can be oxidized to sulfites, phosphates, sulfur, and P_2S_x compounds at the cathode, and reduced to Li_2S, Li_3P, LiCl and Li–Ge compounds at the anode, leading to sluggish Li^+ transport across the interface [81,100]. The intrinsic ESWs of sulfide SEs can be improved through composition optimization and microstructural design. According to the experimental [101] and computational [102] results, oxygen doping can enhance the electrochemical stability of Li_6PS_5X (X = Cl, Br) against Li metal and oxide cathode. Wu et al. [103] presented a core-shell microstructural design that can broaden the ESW of $Li_{9.54}Si_{1.74}P_{1.44}S_{11.7}Cl_{0.3}$ SE to 0.7–3.1 V by resisting the decomposition-accompanied expansion. However, despite the efforts to improve the intrinsic ESW of sulfide SEs, the existing sulfide SEs are still far from stable with common electrode materials. Buffer layers (coating layers on the cathode and artificial SEI on the anode) can effectively mitigate the decomposition of sulfide SEs and endow the ASSBs with stable cycle performance when operated at wide voltage windows [71,104]. Design strategies and practical considerations will be discussed in Section 4.2.

Moreover, an efficient and low-cost synthesis route is essential for the commercialization of sulfide SEs. Typical synthesis methods for sulfide SEs include melt-quenching, solid-state reaction and wet chemical reaction techniques [51,82,83]. The melt-quenching and solid-state reaction techniques have been widely applied on a lab scale. The melt-quenching technique is usually used to produce glassy sulfide SEs by melting the precursors (e.g., Li_2S, P_2S_5, and LiCl) at a high temperature (>900 °C) and quenching rapidly [51]. The solid-state reaction technique is usually achieved by high-energy ball-milling and consecutive annealing steps to produce crystalline sulfide SEs [51,82]. However, limited by the high melting temperature or the long milling time (4–8 h), these two methods' energy and time efficiencies are not always desirable for large-scale application and require further improvement. The wet chemical reaction technique is performed by mixing precursors or pre-formed SEs with solvents to form a suspension or solution, and wet-chemical reactions ensue [51,82,83]. The wet chemical reaction technique can reduce the processing time, enable mass production of homogeneous sulfide SEs, and also help to control the size and morphology of SE particles [83]. However, selecting suitable solvents for the wet chemical reaction technique is challenging, as most sulfide SEs undergo chemical degradation when exposed to highly polar and protic solvents [59]. Recently, Zhou et al. [105] presented a solution-engineered approach to produce highly ionic conductive argyrodite Li_6PS_5X (X = Cl, Br, I) SEs using $Li_3PS_4{\cdot}3$ tetrahydrofuran (THF), Li_2S, and LiX (X = Cl, Br, I) as precursors and THF/ethanol mixtures as solvents, indicating a promising future of the wet chemical reaction technique in the mass production of sulfide SEs. Atomic layer deposition (ALD)-based synthesis technique was also reported to achieve rational composition design and size/thickness control of SEs [106]. Meng et al. [107] synthesized a series of Li_xAl_yS sulfide SEs using ALD, and achieved high conductivities of over 1 mS cm^{-1}. Nevertheless, ALD-based SE synthesis technique is still at immature phase and requires much more efforts in developing suitable precursors and controlling the atmosphere. Despite the difficulties and challenges in the synthesis methods above, Mitsui Kinzoku [38] in Japan and POSCO [39] in Korea have set up pilot facilities for sulfide SEs. Their annual production capacities of sulfide SEs would reach 10 and 24 tons, respectively, demonstrating the feasibility of mass production of sulfide SEs.

3.2. Cathode materials

To achieve high energy density, high-voltage, and high-capacity cathode materials such as Ni-rich NCM and Li-rich layered materials will be adopted in sulfide-based ASSBs. However, these cathodes usually suffer from severe problems such as oxygen release, irreversible phase transition, transition metal dissolution and particle fracture, which lead to rapid voltage decay and capacity fade upon cycling [65,108,109]. Most of the problems faced by the cathodes in ASSBs are similar to those in liquid electrolyte LIBs, and are not discussed in detail in this paper. Here, we mainly focus on the mechanical degradation of cathode materials, which is more prominent in ASSBs than liquid electrolyte LIBs [74,76,110].

Mechanical degradation, including the formation of pores and cracks induced by volume contraction/expansion of cathode materials, is a challenging issue for ASSBs, because of the rigid solid-solid contact between cathode materials and SEs [76]. The Li^+ and e^- insulating pores and cracks can impede the charge transport process and deteriorate battery performance. Therefore, cathode materials with robust mechanical properties are desirable in ASSBs. The lattice structure of NCM cathodes can be stabilized by tuning the composition [111] and doping [112] to achieve a zero-strain design. Moreover, rational design of microstructure can also significantly affect the mechanical properties of cathode materials, as shown in Fig. 4. Polycrystalline cathodes composed of randomly packed primary particles show significant internal stresses due to anisotropic expansion and contraction along the *c* and *a* axes [113], resulting in severe intergranular cracking after several cycles [114]. As shown in Fig. 4, the cracks and the anisotropic Li^+ diffusivities in the *c* and *a* directions increases the tortuosity of the Li^+ diffusion pathway within the cathode materials [115], leading to the decay of rate capability. Refining the primary grains (such as radially-aligned grains) inside the secondary cathode particle is one of the most effective solutions to alleviate the internal stress and prevent particle cracking [115,116], as shown in Fig. 4. Jung et al. [115] found that the radially oriented rod-shaped grains in $Li[Ni_{0.75}Co_{0.10}Mn_{0.15}]O_2$ cathode could improve sulfide-based ASSB's performance regarding reversible capacity, initial CE, and capacity retention compared to the cathode with randomly oriented grains. To further enhance the mechanical stability, boundary-free single-crystalline cathode materials with good microstructural integrity and enhanced oxygen redox are favorable in ASSBs. Single-crystalline cathode materials have been proven to exhibit high power density, high energy density, and long cycle life in sulfide-based ASSBs [117–119]. However, it is worth noting that most of the reported single-crystalline cathodes still contain many boundaries and suffer from mechanical degradation during long cycling [120]. Synthesizing fully boundary-free single-crystalline cathodes is still very challenging.

Moreover, particle size and shape can also affect the mechanical degradation of cathode materials. Small-sized cathode particles are beneficial to achieve short diffusion pathways and small absolute volume change [74], which can mitigate the contact loss between cathode materials and SEs. However, careful balancing of the particle sizes of cathodes and SEs is required to maintain continuous Li^+ and e^- transport pathways in the composite electrodes [121,122]. It has been reported that particle shapes can also affect the lithiation uniformity of cathode materials. For example, Mistry et al. [123] found that the aspherical particle shape of $LiNi_{0.6}Mn_{0.2}Co_{0.2}O_2$ cathode can break the symmetry in reaction and transport interactions and cause nonuniform intercalation at the particle surface, leading to accelerated mechanical degradation.

In summary, rational design microstructure and proper control of particle size and shape is the key to addressing the mechanical degradation problems of cathode materials in ASSBs. However, the optimal design of cathode materials for sulfide-based ASSBs remains to be discovered.

3.3. Anode materials

Compared to the relatively clear choices (NCM or Li-rich materials) of cathodes, more uncertainties exist in the anodes for sulfide-based ASSBs. As shown in Fig. 5 (a), Li-intercalation anodes (graphite) [124,126,127], Li alloy anodes (Si, In, Sn) [15,34,128–130], Li metal anode [125,131] and anode-free design [33,132] have been applied in sulfide-based ASSBs. Owing to their ultrahigh capacity, Si-based anode and Li metal anode (including anode-free) are promising choices for sulfide-based ASSBs. However, as summarized in Fig. 5 (b), these high-capacity anodes face several challenges, including large volume expansion (over 300% for Si [133], and infinity for anode-free design [132]), unstable interface towards sulfide SEs [70,134] and lithium dendrite growth [135]. The continuous large volume expansion/contraction of the Si and Li metal anode can result in cracking and pulverization of the anodes, contact loss and even exfoliation from the current collector during cycling, and severe loss of active anode materials finally [57,67,68,136]. Meanwhile, due to the limited ESW of the sulfide SEs, various interphases are formed by (electro)chemical reactions at the anode (AN) | SE interface, which are similar to SEI in liquid electrolyte LIBs [70,134,137]. The interphases with poor mechanical strength would also crack and re-generate along with the volume changes of anode materials, leading to continuous consumption of lithium inventory and thus low CE and poor cycling life. Moreover, for the Li metal anode, contact loss and nonuniform distribution of current density can induce lithium dendrite growth on the anode surface [138,

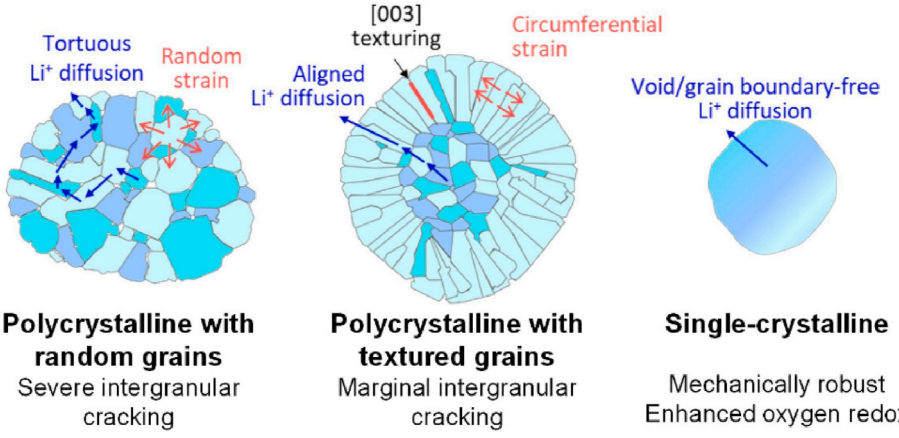

Fig. 4. Microstructural design of cathode materials for ASSBs, i.e., polycrystalline cathodes with randomly oriented grains and textured grains, and single-crystalline cathode. Reproduced with permission from Ref. [76]. Copyright 2022, Elsevier.

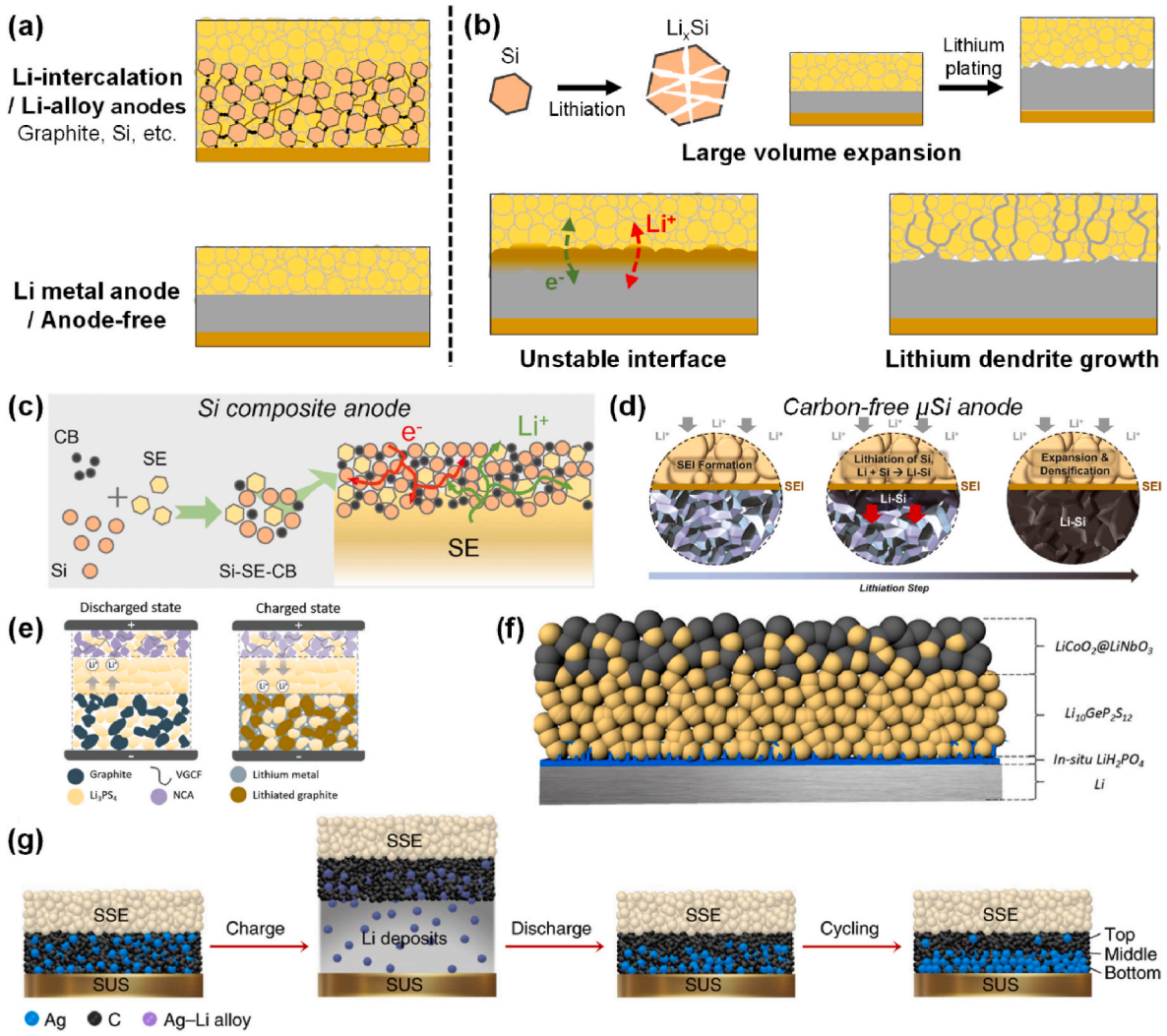

Fig. 5. The existing problems and recent advances in high-capacity anodes for sulfide-based ASSBs. (a) representative anode materials; (b) the main challenges of high-capacity anodes for sulfide-based ASSBs, including large volume expansion, unstable interface and lithium dendrite growth; (c) Si composite anode composed of nano-Si, carbon, and SE. Reproduced with permission from Ref. [34]. Copyright 2022, Wiley-VCH GmbH; (d) carbon-free high-loading μSi anode. Reproduced with permission from Ref. [15]. Copyright 2021, The American Association for the Advancement of Science; (e) lithium-free anode with a 3D framework composed of graphite and sulfide SE. Reproduced with permission from Ref. [124]. Copyright 2021, American Chemical Society; (f) Li metal anode with in-situ-prepared LiH_2PO_4 protective layer. Reproduced with permission from Ref. [125]. Copyright 2018, American Chemical Society; (g) Ag–C composite anode. Reproduced with permission from Ref. [33]. Copyright 2020, Springer Nature.

139]. The rigid lithium dendrite can penetrate through the SE layer, leading to internal short circuit and cell failure [135,140,141]. Fortunately, despite the difficulties, several remarkable advances have been made in high-capacity and cycling-stable anodes for sulfide-based ASSBs in recent years, as presented in Fig. 5 (c)~(g).

As a typical alloy-type anode, Si is receiving increasing attention as the anode for sulfide-based ASSBs due to their high specific capacity and potential for lithium dendrite-free operation [68,128]. Since the first report of Si anode applied in sulfide-based ASSBs by Trevey et al. [142] in 2009, several strategies have been proposed to improve the electrochemical performance of Si anode in sulfide-based ASSBs, including optimizing particle size, controlling stacking pressure and adjusting cutoff voltage. Among them, optimizing particle size is an effective solution to reduce internal stress and mitigate the propagation of cracks within Si particles. Cao et al. [34] constructed a Si composite anode composed of nano Si particles, Li_6PS_5Cl SE and carbon black for sulfide-based ASSBs, as illustrated in Fig. 5 (c). The crystalline nano Si underwent amorphization during cycling and transformed to a dense and homogeneous morphology, which helped to buffer the volume expansion of Si particles [34]. Moreover, the large contact area between nano Si, SE and carbon black enabled fast Li^+ and e^- transport pathways, boosting the rate capability of the Si composite anode [34]. Benefiting from the nano Si design, the Si composite anode showed a high capacity of 2067 $mAh{\cdot}g^{-1}$ and maintained stability for 200 cycles at 0.5 mA cm^{-2} [34]. The size of Si particles also influences the electrochemical performance of the Si/C composite anode. Dunlap et al. [143] found that the Si/C composite anode with 50 nm Si particles outperformed those containing μSi particles in terms of initial capacity, CE, and capacity retention. However, the nano Si particles exhibit a high specific surface area, which inevitably accelerates the side reactions with SEs and irreversible lithium consumption [128]. In addition, developing nano Si particles for industrial application is much less practical and more expensive compared to μSi [144], calling for in-depth studies to examine the feasibility of μSi in sulfide-based ASSBs. Yamamoto et al. [145] showed that μSi composite anode exhibited similar cycling stability as the nano Si anode due to the suppression of Si pulverization using a 75 MPa external pressure. Recently, Tan et al. [15] fabricated a 99.9 wt% μSi anode by limiting the contact area between sulfide SE and Si anode to a 2D plane, which can eliminate continuous interfacial growth and irreversible lithium loss, as presented in Fig. 5

(d). The carbon-free μSi anode achieved high loading (5 mAh·cm^{-2}) and excellent cycling stability with a capacity retention of 80% after 500 cycles. Besides size control, the existing strategies of Si anodes in liquid electrolyte LIBs [68,128,136], such as surface coating, core-shell design, Si/C composite anode, and pre-lithiation, may also improve the capacity and cycling performance of Si anode in ASSBs and require further investigation.

Li metal anode exhibits the highest specific capacity and lowest potential, thus considered as the ideal anode for ASSBs. However, the application of Li metal anode is still hindered by the unstable interface and continuous SEI and lithium dendrite growth, which lead to poor cycling stability and safety concerns [67,146,147]. Regulating the lithium plating and stripping behaviors and suppressing the interfacial reactions are the keys to the practical application of Li metal anode in sulfide-based ASSBs. A 3D-structured electrode can help to prevent lithium dendrite growth by reducing the local current density and providing sufficient space for the deposited lithium. 3D electrode structures can be fabricated by patterning the current collector [132] or the SE [148], which has been widely studied in liquid electrolyte Li metal batteries. However, unlike the liquid electrolyte batteries where the electrolyte can infiltrate into the 3D structures, only the 3D structures with both Li^+ and e^- conducting pathways can be applied in ASSBs to ensure continuous plating and stripping of Li metal. Xing et al. [124] designed a 3D mixed conductive anode network composed of graphite and Li_3PS_4 SE, with extra Li metal deposited into the voids inside the 3D network, as shown in Fig. 5 (e). The graphite-based 3D hybrid anode achieved a three-fold increase in critical current density (1.3 mA cm^{-2}) compared to the planar Li metal anode and improved cycling stability [124]. Constructing a protective layer between Li metal and sulfide SEs can not only alleviate the interfacial reactions but also improve the interfacial physical contact. Zhang et al. [125] prepared a manipulated LiH_2PO_4 protective layer on the Li metal anode to circumvent the chemical stability problems between LGPS and Li metal, as shown in Fig. 5 (f). The protective layer significantly enhanced the interfacial compatibility of Li metal and LGPS. The ASSB using the Li metal anode with a protective layer delivered a long cycle life with a high capacity retention of 86.7% after 500 cycles at 0.1C [125]. LiF [149], Li_3PO_4 [150] and Li_xSiS_x [151] were also applied as protection layers for Li metal anode, and helped to enable high critical current density without lithium dendrite formation. More protection layers for Li metal anode were summarized in Ref. [54].

As the mass production of thin lithium metal films with uniform and smooth surfaces is challenging, developing anode-free solid-state Li metal batteries is attracting increasing attention. Anode-free Li metal batteries face similar but more serious problems as Li metal anodes, such as infinite volume change, severe interfacial reactions and lithium dendrite growth [132]. Similar solutions for Li metal anode, such as 3D electrode structures and protective layers, can also be applied to improve the electrochemical performance of anode-free solid-state Li metal batteries. Recently, Lee et al. [33] designed a Ag–C nanocomposite layer to regulate the lithium deposition in the anode, as shown in Fig. 5 (g). The Ag nanoparticles were firstly alloyed with Li and assisted in uniform and dendrite-free plating of lithium metal at the interface of the Ag–C layer and the current collector, while the carbon layer acted as a buffer layer to prevent direct contact between the plated lithium metal and sulfide SE. A prototype pouch cell (0.6 Ah) using the Ag–C layer as anode exhibited a high energy density (>900 Wh·L^{-1}) and a long cycle life (1000 times under 0.5C) [33]. However, the exact working principle of the Ag–C layer remains unclear. Further studies are required to investigate the Li^+ and e^- transport in this composite layer and find more possible materials to replace the costly Ag nanoparticles.

In summary, Si-based anode and Li metal anode are promising candidates for the anode materials of high-energy-density sulfide-based ASSBs. In recent years, several practical strategies have been proposed to address the critical issues (such as volume expansion, unstable interfaces and lithium dendrites) that hinder the application of Si and Li metal anodes. Significant advances have been achieved in constructing stable anodes for sulfide-based ASSBs. However, to further improve the stability of Si and Li metal anodes and achieve long-cycle-life (>1000 cycles) sulfide-based ASSBs, an in-depth understanding of the vital failure mechanisms (on mechanical, chemical and electrochemical aspects) and practical strategies to improve battery performance are still urgently needed.

4. Interfacial problems in sulfide-based all-solid-state batteries and solutions

Due to the incompatibilities of electrodes and SEs on electrical, electrochemical, chemical and mechanical aspects, several interfacial problems exist in sulfide-based ASSBs, including space charge layer effect, interfacial side reactions and mechanical instability [52–54]. The interfacial problems result in a high energy barrier and slow kinetics at the AM | SE interfaces, significantly impeding the transport of Li^+ and e^-. Therefore, uncovering the nature of the complex interfacial problems and designing stable interfaces with fast charge transfer kinetics are essential to optimizing the power capability and cycling stability of sulfide-based ASSBs. In this section, we discuss the physicochemical characteristics of the interfacial issues and introduce the possible solutions to improve interfacial compatibility.

4.1. Space charge layer effect

The space charge layer usually forms at the oxide cathode | sulfide SE interfaces. As illustrated in Fig. 6 (a)–(d), driven by the difference in chemical potential, Li^+ migrates from the sulfide SE to the oxide cathode, resulting in a Li^+ depletion layer on the SE side [152–154]. As Li^+ is the primary charge carrier inside ASSBs, the Li^+ depletion layer leads to a high migration barrier and resistance at the interface [155,156]. Evidence of the SCL effect was experimentally observed in the initial stage of the charging profile, where an additional oxidation slope appeared prior to voltage changes from the lithium de-intercalation from cathode materials [156–158], as shown in Fig. 6 (a). Experimental observations and theoretical calculations have been applied to better understand the SCL and its effects on ASSBs' performance. Yamamoto et al. [159–161] successfully visualized the changes of the ionic and potential profiles in SCL using quantitative electron holography. Wang et al. [162] showed direct evidence of Li^+ accumulation on the $LiCoO_2$ side at the interface due to Li^+ migration from Li_6PS_5Cl to $LiCoO_2$ using the in-situ differential phase contrast scanning transmission electron microscopy. First-principles simulations were also applied to calculate the interfacial electrochemical potential and energy profiles, which could help to reveal the formation and evolution of SCL [152,161,163–165].

According to the experimental observations and theoretical calculations, the formation and evolution of SCL at the cathode (CA) | SE interface are elucidated in Fig. 6 (b)–(d). μ_{Li} denotes the Li chemical potential versus Li metal determined by Li-vacancy formation energy. $\widetilde{\mu}_{Li^+}$ and $\widetilde{\mu}_{e^-}$ are the electrochemical potentials of Li^+ and e^-, respectively. c_{Li^+} represents the Li^+ concentration in the cathode and SE. The relation between chemical and electrochemical potentials is $\mu_{Li} = \widetilde{\mu}_{Li^+} + \widetilde{\mu}_{e^-}$. When the oxide cathode and sulfide SE with different Li chemical potentials form the CA | SE interface, the Li^+ in the sulfide SE migrates to the oxide cathode due to the relatively higher Li chemical potential, resulting in the formation of SCL at the interface. Meanwhile, electrons also move from the sulfide SE to the cathode to maintain charge neutrality, leading to a potential shift at the interface. Finally, a Li^+ depletion layer forms on the sulfide SE side when the CA | SE interface reaches equilibrium, while Li^+ enrichment occurs on the cathode side, as illustrated in Fig. 6 (b). As Li^+ is the only charge carrier in SE, the decrease in Li^+ concentration will lower the ionic conductivity, resulting in high interfacial resistance. Besides, Gao et al. [163,166] pointed out that Co↔P exchange at the $LiCoO_2$ | β-Li_3PS_4 interface would further induce a high migration barrier in the Li^+ electrochemical potential $\widetilde{\mu}_{Li^+}$

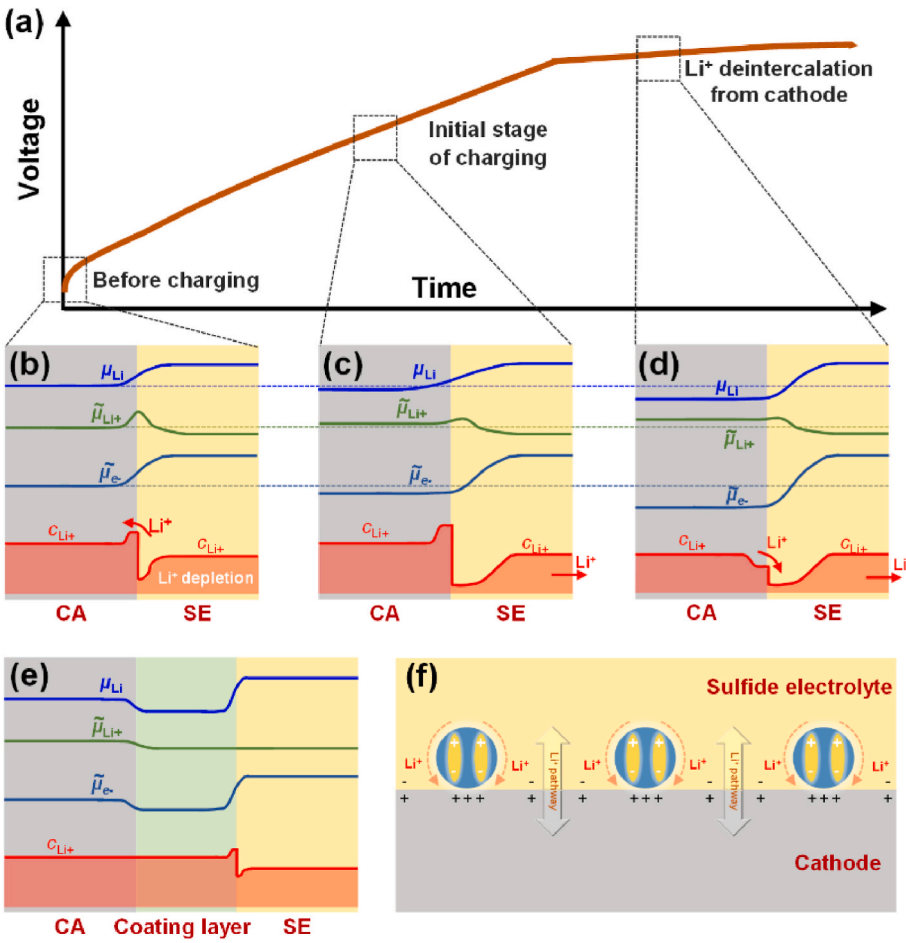

Fig. 6. Evolution of space charge layer at the cathode (CA) | SE interface and solutions. (a)~(d) Schematic illustrations of the formation and evolution of the SCL during the charging process. The SCL effect on battery charging voltage profile is presented in (a), and (b)~(d) illustrate the distribution of the Li chemical potential μ_{Li}, Li^+ electrochemical potential $\tilde{\mu}_{Li^+}$, Li^+ concentration c_{Li+}, and the e^- electrochemical potential $\tilde{\mu}_{e^-}$ [152,163,165,166]; (e) illustration of the surface coating to mitigate the SCL effect [152,163,165]; (f) built-in electric field and chemical potential coupling strategy to reduce SCL formation. Reproduced with permission from Ref. [162]. Copyright 2020, Springer Nature.

distribution, which is unfavorable for the Li^+ transportation across the interface. At the initial stage of charging, the Li^+ in the sulfide SE begins to migrate to the anode, whereas Li^+ de-intercalation from the cathode to the sulfide SE will not start until the electrode potential at the interface reaches the redox potential of the cathode and the Li^+ electrochemical potential is high enough to overcome the energy barrier. Instead, the Li^+ depletion layer on the sulfide SE side thickens, along with the widening of the Li^+ enriched region on the cathode side [167], as in Fig. 6 (c). In this stage, the ASSB voltage profile exhibits an additional oxidation slope, as in Fig. 6 (a), similar to the charging voltage profile of capacitors [168]. As the electrode potential exceeds the voltage plateau of the cathode materials, Li^+ begins to de-intercalate from the cathode and migrate to the sulfide SE to compensate for the Li^+ depletion layer, as in Fig. 6 (d). The Li^+ depletion layer still exists during the following charging and discharging process [166,167], acting as a barrier for Li^+ transport and thus resulting in large interfacial resistance. Nevertheless, the thickness of SCL and its exact contribution to interfacial resistance are still unclear. Moreover, the SCL would also change during battery aging due to the interfacial reactions with ionic exchanges, leading to more complex interfacial chemistry and structure of the SCL. A generalized model to simulate the formation and evolution of SCL is lacking and requires further investigation.

Introducing a coating layer between the electrode and SE has been proven effective in mitigating the SCL effect, as illustrated in Fig. 6 (e) and (f). Takada et al. [155,157,158,165,169] interposed several oxides ($Li_4Ti_5O_{12}$ [157], $LiNbO_3$ [169], and $LiTaO_3$ [158]) as buffer layers between the $LiCoO_2$ cathode and $Li_{3.25}Ge_{0.25}P_{0.75}S_4$ or Li_2S–P_2S_5 SEs. The buffer layers can eliminate the additional oxidation slope and reduce the interfacial resistance in the cathode [157,158,169]. Based on the density functional theory (DFT) + U calculation, Haruyama et al. [152] found that the $LiNbO_3$ coating layer between $LiCoO_2$ and β-Li_3PS_4 introduced smoothly matched interfaces without Li adsorption space and suppressed the growth of SCL. Gao et al. [163] further revealed that the $LiNbO_3$ coating layer lowered the migration barrier in the Li^+ electrochemical potential $\tilde{\mu}_{Li^+}$, and thus reduced the interfacial resistance, as in Fig. 6 (e). The $LiNbO_3$ coating layer could also effectively suppress the preference of ion mixing and SE oxidation [163]. Moreover, since the SCL is driven by the Li chemical potential difference between the cathode and SE and influenced by the electric field, Wang et al. [162] proposed an innovative built-in electric field and chemical potential coupling strategy to suppress the SCL effect. As illustrated in Fig. 6 (f), ferroelectric $BaTiO_3$ nanoparticles were discontinuously coated on the $LiCoO_2$ cathode and generated permanent reverse electric dipoles under the electric field effects of the SCL. The built-in electric field of $BaTiO_3$ led to the redistribution of Li^+ and significantly improved the Li^+ migration kinetics at the CA | SE interface. Overall, coating layers can effectively suppress the formation and evolution of SCL. However, the effects of the materials and thickness of coating layers on the SCL effect and Li^+ distribution remain elusive. Innovative designs of coating layers based on fundamental understandings of the SCL effect are strongly encouraged.

4.2. *Interfacial reactions*

Interfacial side reactions, including electrochemical and chemical reactions, occur at both the CA | SE and AN | SE interfaces, mainly induced by electrochemical and chemical instabilities of the sulfide SEs when in contact with electrodes [52–54]. In the electrochemical aspect, as mentioned above, sulfide SEs will be oxidized at the cathode interface and reduced at the anode interface due to their narrow ESW, leading to

the formation of interphases between electrodes and SEs [81,99,100], as illustrated in Fig. 7 (a). In the chemical aspect, mutual element diffusion between electrodes and SEs caused by the side reactions can result in the decomposition of the electrodes or sulfide SEs and the formation of interphases [166,170], as in Fig. 7 (b). Similar to the SEI and cathode electrolyte interphase (CEI) in liquid electrolyte LIBs, the physicochemical properties of the formed interphases significantly influence ASSBs' performance [104]. Most of the formed interphases have lower ionic conductivity than the sulfide SEs, leading to an increase in interfacial resistance [81,134]. Moreover, the interphases with mixed ionic and electronic conductivity can induce the continuous decomposition of the SE and thickening of the interphases during cycling, resulting in fast degradation of the battery capacity and power capability [171].

At the CA | SE interface, according to the DFT calculations by Richards et al. [134], sulfide SEs with PS_4 groups are prone to be oxidized by the high voltage oxide cathodes, generating PO_4 groups and transition metal sulfides. Haruyama et al. [172] found that Co↔P exchange is energetically favorable at the $LiCoO_2$ | β-Li_3PS_4 interface, enhancing the growth of SCL. Their theoretical calculation results were in good agreement with the experimental findings. Sakuda et al. [170] first observed the formation of a 10 nm interfacial layer at the $LiCoO_2$ | Li_2S–P_2S_5 interface, accompanied by the mutual diffusion of Co, P, and S elements, as in Fig. 7 (b). Auvergniot et al. [173] found that Li_6PS_5Cl is oxidized into elemental sulfur, lithium polysulfides, P_2S_x, phosphates, and LiCl at the interface with typical cathode materials: $LiCoO_2$, $LiNi_{1/3}Co_{1/3}Mn_{1/3}O_2$ and $LiMn_2O_4$. Walther et al. [174] characterized the local structure and morphology of the interfacial layer between $LiNi_{0.6}Co_{0.2}Mn_{0.2}O_2$ and Li_6PS_5Cl, and found that phosphates and sulfates such as Li_3PO_4 and Li_2SO_4 in the interfacial layer play a vital role in the rapid capacity fade of ASSBs. On the cathode side, Wang et al. [175] observed that the $LiNi_{0.5}Mn_{0.3}Co_{0.2}O_2$ cathode also suffered from interfacial oxygen loss and structural changes from layered structure to rock-salt structure, leading to a further increase in interfacial resistance. Moreover, Strauss et al. [176] found that the oxidation of β-Li_3PS_4 SE at the cathode interface under high voltage (>4.5 V) leads to the formation and release of highly corrosive SO_2 gas [176], threatening the safety of sulfide-based ASSBs. The kinetics of the interfacial reactions are important for the long-term cycling performance of ASSBs. Zhu et al. [81] revealed that the oxidation reactions of sulfide SEs at the cathode interface usually exhibit sluggish kinetics with a high overpotential, contributing to a wider ESW observed in the experiments. Richards et al. [134] found that the products of the oxidation reactions are electronically insulating but ionically conductive, and thus act as a passivation layer to mitigate further interfacial reactions. Furthermore, Auvergniot et al. [173] observed that the oxidation of Li_6PS_5Cl at the interface with $LiNi_{1/3}Co_{1/3}Mn_{1/3}O_2$ cathode is partially reversible and does not hinder the cyclability of ASSBs as good capacity retention was observed over 300 cycles for the $LiNi_{1/3}Co_{1/3}Mn_{1/3}O_2$ | Li_6PS_5Cl | Li–In half-cell. In contrast to the self-limited interfacial reaction kinetics reported above, Zuo et al. [177] observed that the interfacial reaction rate between $LiNi_{0.6}Co_{0.2}Mn_{0.2}O_2$ and LGPS accelerates when increasing the cathode potential to higher than 4.2V vs. Li^+/Li and leads to severe capacity degradation, mainly due to the triggering of oxygen-involving reactions and the formation of the rock-salt phase. Despite the efforts, the interfacial reaction kinetics under different voltages and temperatures and its effects on the performance of ASSBs are still elusive.

In terms of the AN | SE interface, there are three types of interfaces between Li metal and SEs according to the reactivity of the SEs and the Li^+/e^- conductivities of the reaction products [171], as illustrated in Fig. 7 (c). In the first type of interface, most binary ionic conductors, such as LiF, Li_2S, Li_3P and LiX (X = Cl, Br, I), are thermodynamically stable against Li metal [81,134], forming a chemically stable interface without any interlayer. However, the poor ionic conductivity of these binary compounds limits their application as SEs in ASSBs. In contrast, most highly ionic conductive SEs, such as sulfide SEs, are all thermodynamically unstable against Li metal. Therefore, interphases are formed by (electro)chemical reactions at the Li | SE interface, as in the second and third situations in Fig. 7 (c). For the sulfide SEs solely based on phosphorus such as Li_3PS_4, $Li_7P_3S_{11}$ and Li_6PS_5X (X = Cl, Br, I), the formed interphases are mainly composed of Li_2S, Li_3P and LiX, which are stable with Li metal [100]. These reaction products are ionic conductive but electronic insulating, and thus act as interlayers to suppress the

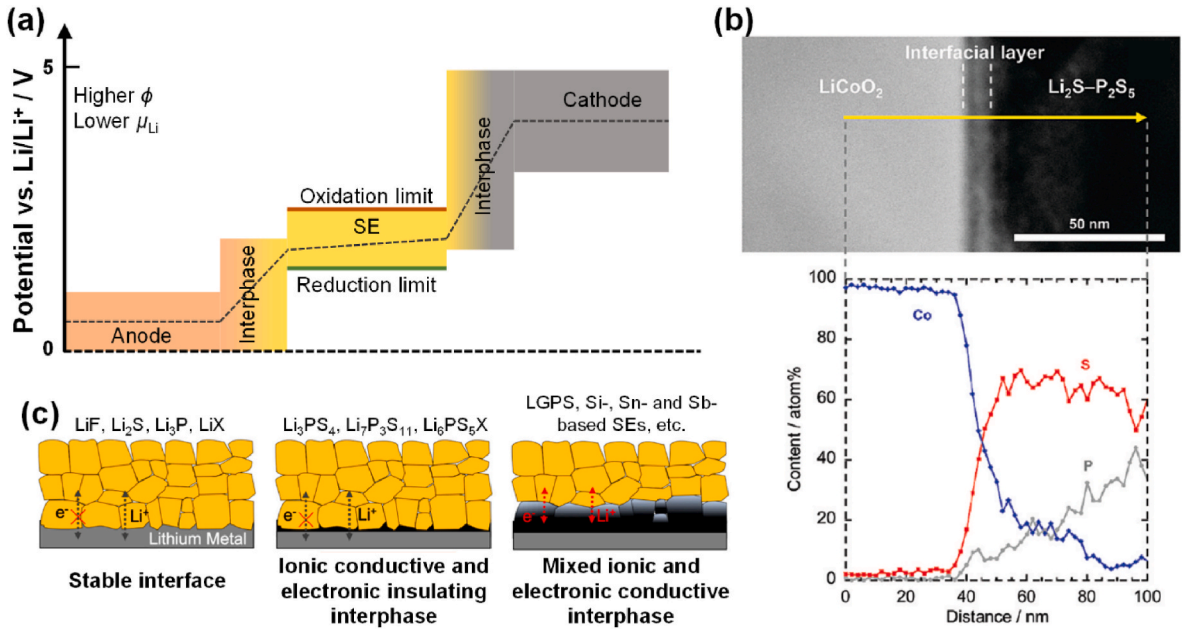

Fig. 7. Interfacial reactions between electrodes and sulfide SEs. (a) illustration of electrochemical side reactions at the CA | SE and AN | SE interfaces. Reproduced with permission from Ref. [81]. Copyright 2015, American Chemical Society; (b) observation of the interfacial layer and mutual diffusion of Co, P and S elements at the $LiCoO_2$ | Li_2S–P_2S_5 interface. Reproduced with permission from Ref. [170]. Copyright 2009, American Chemical Society; (c) three types of interfaces between Li metal and SEs: 1) chemical stable interface; 2) ionic conductive and electronic insulating interphase; 3) mixed ionic and electronic conductive and unstable interphase [54,171]. Reproduced with permission from Ref. [54]. Copyright 2020, American Chemical Society.

further growth of the interphases. For the third type of interface, mixed ionic and electronic conductive interphases containing Li alloys (Li–Ge, Li–Si and Li–Sn alloys) are formed as a result of the reduction of multivalent metal cations in sulfide SEs such as LGPS, $Li_{9.54}Si_{1.74}P_{1.44}Cl_{0.3}$ and $Li_2SnP_2S_{12}$ [171,178]. These interphases continuously grow during cycling, resulting in further decomposition of the SEs and eventually cell failure. Wenzel et al. [179–181] investigated the products of the interfacial reactions between $Li_7P_3S_{11}$, $Li_{10}GeP_2S_{12}$, Li_6PS_5X (X = Cl, Br, I) and Li metal using in situ X-ray photoelectron spectroscopy (XPS) and time-resolved electrochemical impedance spectroscopy (EIS). Consistent with the theoretical analysis, $Li_7P_3S_{11}$ was decomposed into Li_3P and Li_2S at the interface with Li metal, and the formed interphase was limited to a few nanometers [179]. In contrast, continuously growing interphases composed of Li_3P, Li_2S and Li–Ge alloys were observed at the Li | LGPS interface [180]. For the argyrodite sulfide SEs (Li_6PS_5X), interphases composed of Li_3P, Li_2S and LiX were formed when in contact with Li metal [181]. Moreover, the interphase growth kinetics was found to be governed by diffusion across the interphase, following a square root time dependence [179–181]. $Li_7P_3S_{11}$, Li_6PS_5Cl and Li_6PS_5Br show slow rate constants and small interfacial resistances, while $Li_{10}GeP_2S_{12}$ and Li_6PS_5I exhibit much higher reaction rates [179–181]. It is noteworthy that most of the researches on the interfacial reactions at the AN | SE interface focus on the Li metal anode. In contrast, the interfacial reactions between sulfide SEs and graphite/Si-based anodes have rarely been investigated. Sakuma et al. [182] observed the formation of interphases with Li–P–S compound at the interface between Li–M (M = Sn, Si) alloy anodes and $Li_{4-x}Ge_{1-x}P_xS_4$ SEs, and found that the interfacial resistance rises obviously when increasing the Ge content in the sulfide SE or decreasing the redox potential of the alloy. Interfacial reactions between Li_6PS_5Cl and μSi [15]/nano Si [34] have also been observed. Though graphite and Si-based anodes may behave similarly to Li metal considering their similar operating voltages, whether the reaction mechanisms between sulfide SEs and Li metal anode can be extended to graphite and Si-based anodes requires further investigation.

Several strategies have been proposed to alleviate the undesirable interfacial reactions between AMs and SEs. Coating layers on the cathode surface can physically prevent the direct contact between cathode materials and sulfide SEs, thus suppressing the interfacial reactions and formation of SCL [69]. As illustrated in Fig. 8 (a), firstly, an ideal coating layer is chemically compatible with both cathodes and sulfide SEs, and electrochemically stable under the operating voltages. Secondly, it is electronically insulating to block the e^- transport, and ionic conductive to enable fast Li^+ transport across the interface. Moreover, as most of the oxide cathode materials undergo volume expansion/contraction during lithiation/de-lithiation, the coating layer should be mechanically robust

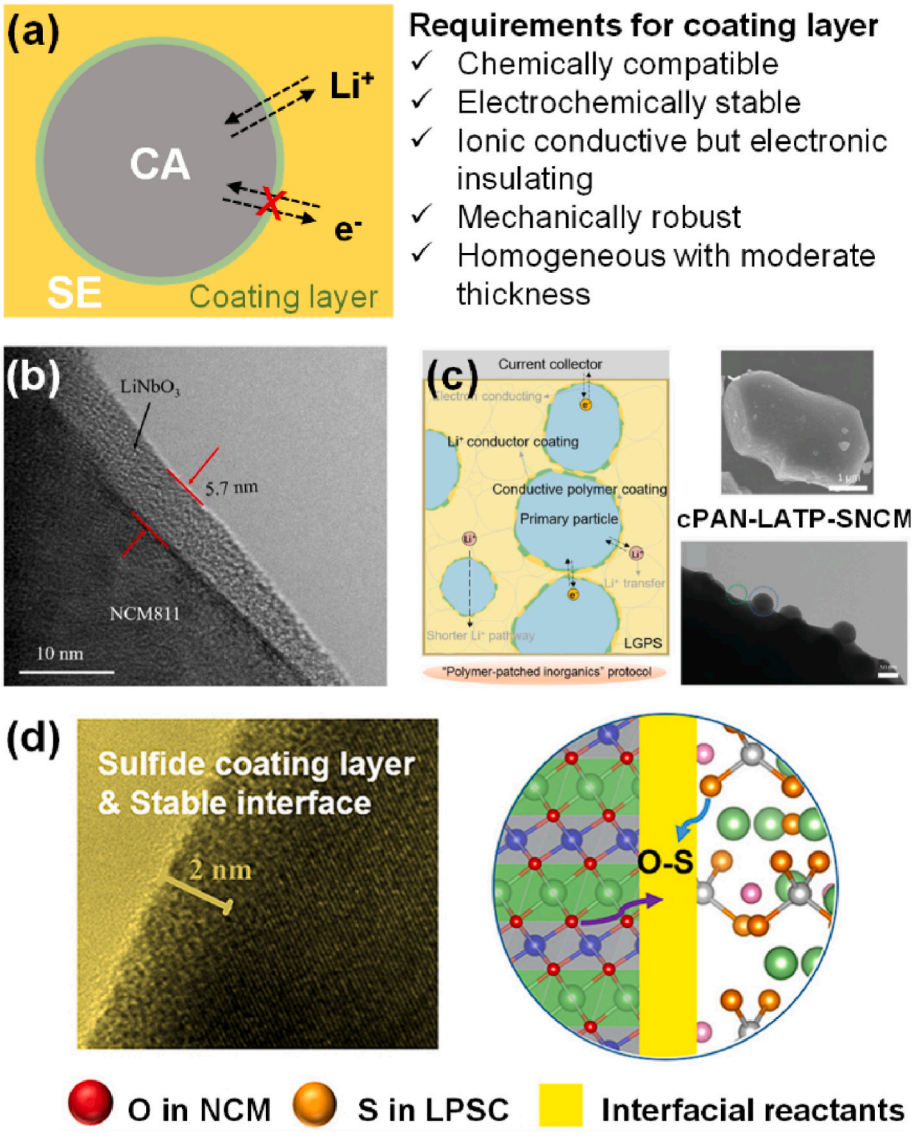

Fig. 8. Surface engineering strategies to mitigate the interfacial reactions at the CA | SE interface. (a) An illustration of the coating layer on the cathode surface and requirements for the coating layer; (b) $LiNbO_3$-coated $LiNi_{0.8}Co_{0.1}Mn_{0.1}O_2$ cathode. Reproduced with permission from Ref. [183]. Copyright 2020, Elsevier; (c) a hybrid coating layer with $Li_{1.4}Al_{0.4}Ti_{1.6}(PO_4)_3$ (LATP) and cyclized polyacrylonitrile (cPAN) on single-crystalline $LiNi_{0.6}Co_{0.2}Mn_{0.2}O_2$ (SNCM) cathode. Reproduced with permission from Ref. [184]. Copyright 2022, Wiley-VCH GmbH; (d) a sulfidation strategy to prepare a $LiNi_{0.88}Co_{0.09}Mn_{0.03}O_2$ cathode with an ultra-thin sulfide surface layer (~2 nm). Reproduced with permission from Ref. [185]. Copyright 2022, KeAi Publishing.

to maintain integrity during long-term cycling. Finally, because most coating materials have lower ionic conductivity than the sulfide SEs, the coating layer should be thin (several nanometers) and homogeneous to perform its essential functions without an apparent increase in interfacial resistance. Xiao et al. [69] conducted a computational screening of cathode coating materials for ASSBs, and identified several oxide materials (including Li_2ZrO_3, $LiNbO_3$, $LiTaO_3$, and LiH_2PO_4) as desirable coating materials. $LiNbO_3$ is the most-commonly used coating material due to its wide ESW that can compromise the mismatch of oxide cathodes and sulfide SEs. Li et al. [183] adopted a 6.3 nm $LiNbO_3$ coating layer on the surface of $LiNi_{0.8}Co_{0.1}Mn_{0.1}O_2$ cathode to improve the interfacial stability, as in Fig. 8 (b). The ASSB using $LiNbO_3$-coated $LiNi_{0.8}Co_{0.1}Mn_{0.1}O_2$ cathode and LGPS SE exhibited high rate performance and significantly improved cycling performance. Oxide SEs such as $Li_{1.4}Al_{0.4}Ti_{1.6}(PO_4)_3$ (LATP) and halide SEs such as Li_3InCl_6 can also be employed as coating materials at the CA | SE interface considering their high ionic conductivity and wide ESW. Liang et al. [184] developed a hybrid layer with LATP and cyclized polyacrylonitrile (cPAN) on a single-crystalline $LiNi_{0.6}Co_{0.2}Mn_{0.2}O_2$ (SNCM) cathode, as in Fig. 8 (c). The LATP coating ensured rapid Li^+ transfer and high oxidation tolerance, while the cPAN patched imperfections in the LATP coating layer and provided extended electronic percolation paths between the interconnected SNCM particles. The ASSB employing the cPAN–LATP–SNCM cathode and LGPS SE demonstrated competitive cycling performance with a capacity retention of 72.7% over 500 cycles at 0.5C. Moreover, stabilizing the surface oxygen of the NCM cathode can also improve the interfacial stability with sulfide SE. Wang et al. [185] proposed a sulfidation strategy to impose a thin sulfide surface layer (~2 nm) on the $LiNi_{0.88}Co_{0.09}Mn_{0.03}O_2$ cathode. With the formation of covalent O–S bonding on the surface, the sulfurized $LiNi_{0.88}Co_{0.09}Mn_{0.03}O_2$ cathode showed a stable interface with Li_6PS_5Cl SE and improved cyclability with a capacity retention of 87% after 500 cycles at 1C.

On the anode side, an interfacial buffer layer is an effective solution to suppress the (electro)chemical side reactions between anodes and sulfide SEs. Examples of buffer layers for Li metal anode include LiF [149], Li_3PO_4 [150] and Li_xSiS_x [151], which are kinetically stable with Li metal and sulfide SEs, as summarized in Ref. [54]. Besides, selecting suitable electrode materials and sulfide SEs with better (electro)chemical compatibilities is also favorable. For example, the interfacial reactions can be mitigated by replacing the pure Li metal anode with lithium alloy that exhibits a working voltage closer to the ESW of sulfide SEs, such as Li–Si, Li–Sn and Li–In Refs. [52,138]. For the sulfide SEs, as mentioned in Fig. 7 (c), Li_3PS_4, $Li_7P_3S_{11}$ and Li_6PS_5X (X = Cl, Br, I) can form kinetically stable interphases to retard further interfacial side reactions and are thus favorable on the anode side. Based on this principle, a multilayered electrolyte configuration has been proposed to combine the advantages of different SEs and achieve interfacial stability. Yao et al. [186] inserted a lithium-compatible $75\%Li_2S–24\%P_2S_5–1\%P_2O_5$ SE layer between the LGPS SE layer and Li metal anode to achieve long-term cycling stability. Ye et al. [187] prepared a multilayered sulfide SE with a less stable SE ($LGPS/Li_{9.54}Si_{1.74}(P_{0.9}Sb_{0.1})_{1.44}S_{11.7}Cl_{0.3}$) sandwiched between more stable SEs ($Li_{5.5}$ $PS_{4.5}Cl_{1.5}$), which can stabilize the primary interface with the Li metal and prevent lithium dendrite growth under high current density. However, it is worth noting that most solutions to anode interfacial reactions focus on Li metal anode. In contrast, solutions to the interfacial reactions between sulfide SEs and Li intercalation or alloy anodes such as graphite and Si-based anodes have rarely been reported.

4.3. Mechanical instability

Multiscale mechanical instability problems, including lattice mismatch, contact loss, cracking and void formation, have detrimental effects on the interfacial charge transfer process and Li^+/e^- transport pathways and are thus pivotal to the performance of ASSBs [76]. To better understand the mechanical instabilities in sulfide-based ASSBs, we carefully distinguish the mechanical problems at the interface and composite electrode levels in this paper. Lattice mismatch and interfacial contact loss resulting in high local current density and stress are considered as mechanical problems at the interface level. The formation of micron-scale cracks and voids that mainly affect the Li^+/e^- transport pathways within the composite electrodes are regarded as mechanical failure at the electrode level and are discussed in section 5.2.

Lattice mismatch occurs at the interface between two solid materials with different lattice parameters, and can result in the formation of a disordered layer and tortuous Li^+ diffusion at the interface [188]. Based on atomic structures, the AM | SE interfaces can be categorized into coherent, semi-coherent and incoherent interfaces [189], as illustrated in Fig. 9 (a) [138]. The coherent interfaces can enable fast Li^+ diffusion across the interface, representing an ideal interface between active materials and SEs. Unfortunately, due to lattice mismatch, typical AM | SE interfaces are mostly semi-coherent or incoherent [138,166,188]. Based on large-scale molecular dynamics simulations, Yang et al. [188] found that the semi-coherent or incoherent interfaces between Li metal and the SE (LLZO) and several SEI components (LiF and Li_2O) result in interfacial disordered Li layers, which is highly detrimental to Li^+ diffusion and can cause interfacial pore formation during cycling and eventually cell failure [188]. At the cathode side, Jand et al. [190] also found that lattice mismatch results in atomic rearrangement and high strain at the $LiCoO_2$ | $Li_7La_3Zr_2O_{12}$ interface. Until now, the limited researches on lattice mismatch mainly focus on the interfaces between active materials and oxide SEs. Nevertheless, the lattice mismatch at the interfaces with sulfide SEs has been rarely studied. Gao et al. [166] predicted disordered heterogeneous crystal structure at the $LiCoO_2$ | β-Li_3PS_4 interface, and estimated the strain induced by the lattice mismatch. However, the effects of lattice mismatch on the performance of sulfide-based ASSBs remain unclear.

Physical contact loss is inevitable at the AM | SE interfaces because of the rigid nature of SEs. The continuous volume expansion/contraction of AMs during cycling deteriorates the interfacial contact [76]. Consequently, as illustrated in Fig. 9 (b), blocked by pores at the interface, Li^+ flux bundles together to pass local spots, named the current constriction phenomenon [138]. The high local current density induces great local strain at limited contact spots, leading to the cracking of the AMs and SEs and the propagation of contact loss. For the Li metal anode, the high local current density induces voids formation during lithium stripping and lithium dendrite growth during plating, finally leading to cell failure [191,192]. Moreover, the morphological instability of the Li | SE interface during cycling also leads to dendrite formation [139,193]. Kasemchainan et al. [139] observed void formation and accumulation at the Li | Li_6PS_5Cl interface when the stripping current density removed Li from the interface faster than it can be replenished, as illustrated in Fig. 9 (c). The reduced contact area led to an increase in the local current density and consequently dendrite formation during plating, short circuit and cell failure. They also observed that the critical current density for Li dendrite growth is determined by the Li stripping process, which is strongly affected by the applied pressure. Proper stacking pressure can enable sufficient contact between Li metal and SE and fast Li transport to the interface by creep [139]. However, excessive pressure may lead to lithium dendrite growth because Li metal creeps into the grain boundary or pores within the SE layer [191]. Doux et al. [191] systematically investigated the effect of stack pressure on lithium dendrite growth in the Li | Li_6PS_5Cl | Li system. As the stack pressure increased from 5 MPa to 25 MPa, the cell lifetime during plating and stripping at 75 μA cm^{-2} shortened due to the slow creeping of Li into the pores of the SE layer to form dendrites. At a high stack pressure of 75 MPa, the cell mechanically shorted before applying a current. This dilemma could be resolved by employing alloy-based anodes (e.g., Li–In and Li–Al) that can withstand much higher stack pressures. However, recent studies have revealed that void formation and dendrite growth also occur in Li alloy anodes under high current density and stack pressure [129,141,194]. Kasemchainan et al. [139] and Banerjee et al. [54] summarized three Li transport

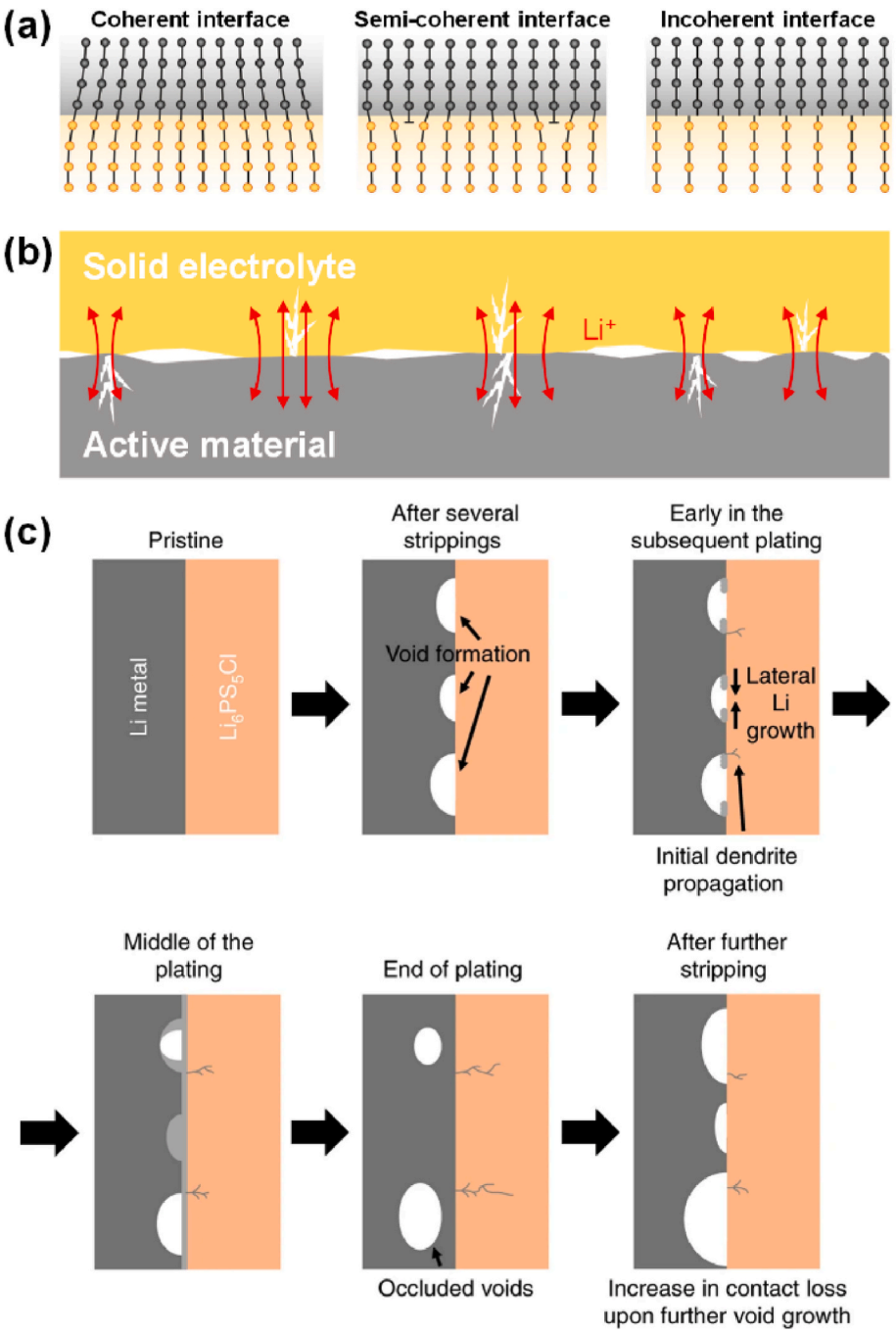

Fig. 9. Mechanical instability issues at the interface between electrode materials and SEs, including (a) lattice mismatch. Reproduced with permission from Ref. [138]. Copyright 2020, American Chemical Society (b) contact loss and (c) lithium dendrite growth at the Li | SE interface. Reproduced with permission from Ref. [139]. Copyright 2019, Springer Nature.

mechanisms that determine lithium plating and stripping behaviors at the Li | SE interface, i.e., Li^+ migration from Li metal to SE, self-diffusion of Li atoms inside Li metal and Li metal creep. The flux of Li^+ migration depends on the magnitude of current density, while the fluxes of Li diffusion and Li creep are correlated with the applied stack pressure and temperature [54,139]. Thus, careful considerations of the applied current density, stack pressure and temperature are required to address the mechanical instability issues at the Li | SE interface. Compared with the Li metal anode, few studies have been reported on the mechanical instability issues at the interface between graphite or Si-based anodes and sulfide SEs. As Si-based anode is promising for sulfide-based ASSBs but exhibits large volume change, further studies are urgently needed.

At the cathode side, interfacial contact loss between $LiNi_{0.8}Co_{0.1}Mn_{0.1}O_2$ cathode and β-Li_3PS_4 SE was observed by Koerver et al. [195]. Jung et al. [115] and Han et al. [117] observed the cracking of polycrystalline cathode particles after cycling, leading to rapid capacity loss of sulfide-based ASSBs. Benefiting from the low Young's Modulus and good deformability of sulfide SEs, mechanical instability issues at CA | sulfide SE interfaces are not so severe as those at CA | oxide SE interfaces, and can be effectively mitigated through improving the mechanical properties of cathode materials (as discussed in section 3.2) and applying proper pressure during fabrication and operation.

5. Transport and mechanical issues in composite electrodes

The emergence of highly ionic conductive sulfide SEs has attracted wide attention and triggered many attempts on practical ASSBs. As presented in Fig. 10 (a), the areal capacity and current density of reported ASSBs exhibit an upward trend in the past decade, and some examples demonstrated high areal capacity (>3 mAh·cm^{-2}) under practical current density (>3 mA cm^{-2}). One example is the work of Lee et al. [33], where a $LiNi_{0.90}Co_{0.05}Mn_{0.05}O_2$ | Li_6PS_5Cl | Ag–C pouch cell showed a high areal capacity of 6.8 mAh·cm^{-2} at 0.2C (1.36 mA cm^{-2}) and 6.3 mAh·cm^{-2} at 1C (6.8 mA cm^{-2}). Recently, Li et al. [196] constructed a high mass loading (36.94 mg cm^{-2}) electrode using Al-modified $Li(Ni_{0.9}Mn_{0.05}Co_{0.05})_{0.8}Co_{0.2}O_2$ cathode, which displayed an areal capacity of 5.86 mAh·cm^{-2} at 0.2C (1.478 mA cm^{-2}) and 4.36 mAh·cm^{-2} at 2C (14.78 mA cm^{-2}). Despite the outstanding performance, high operating temperature and pressure were utilized in the ASSBs above (60 °C and 4 MPa in Lee's work [33] and 45 °C and 980 MPa in Li's work [196]), which may be unpractical. Actually, fabricating practical ASSBs with high areal capacity and high rate capability remains challenging.

Fig. 10 (b) and (c) compare the typical composite electrode microstructures in ASSBs and liquid electrolyte batteries. The composite electrodes in ASSBs inevitably form inhomogeneous and discontinuous Li^+/e^- transport pathways, due to the imperfect distribution of solid particles and insufficient solid-solid contact. The actual tortuosity of both Li^+ and e^- transport in ASSBs thus becomes much higher than the geometric tortuosity [76,197]. Moreover, voids and cracks are unavoidable in ASSBs, as the SEs cannot adapt to the volume change of the AMs during charging/discharging. The voids and cracks further impede the Li^+/e^- transport and lead to the electrochemical–mechanical failure of ASSBs. As a result, the effective ionic conductivity of the composite electrode using SEs decreases to 10^{-3}–10^{-2} mS cm^{-1} [76,197,198], several orders lower than the bulk ionic conductivity of sulfide SEs (1–10 mS cm^{-1}). In contrast, the effective ionic conductivity of the composite electrode employing liquid electrolytes can maintain higher than 1 mS cm^{-1} [199,200]. The well-dispersed carbon additives and penetration of the liquid electrolyte into the porous electrodes enable low-tortuosity Li^+/e^- transport pathways in liquid electrolyte LIBs, as presented in Fig. 10 (c). Furthermore, the liquid electrolyte can also effectively infiltrate the cracks in the particles and thus ensure conformable interfacial contact with AMs during cycling. Therefore, at the composite electrode level, the sluggish Li^+/e^- transport and mechanical failure are the bottlenecks limiting the practical performance of ASSBs.

5.1. Transport limitation in composite electrodes

The microstructural design of composite electrodes is vital to the energy density and power capability of ASSBs. Generally, a composite electrode with a large fraction of SEs and a thin thickness is recommended to ensure fast Li^+/e^- transport and high power capability. However, a thick electrode design with high AM content is necessary to achieve a high energy density for sulfide-based ASSBs [201,202]. The trade-off between energy density and power capability calls for rational optimization of the composite electrodes regarding each component's weight/volume ratio, particle size, morphology and distribution.

First, the compositions and fractions of different components within composite electrodes determine the primary electrochemical performance of ASSBs. As ionic transport is usually identified as the rate-limiting transport process within the composite electrode [197,198], several researchers have studied the effects of SE fraction on ASSBs' performance. Zhang et al. [203] found that a small fraction (20%) of

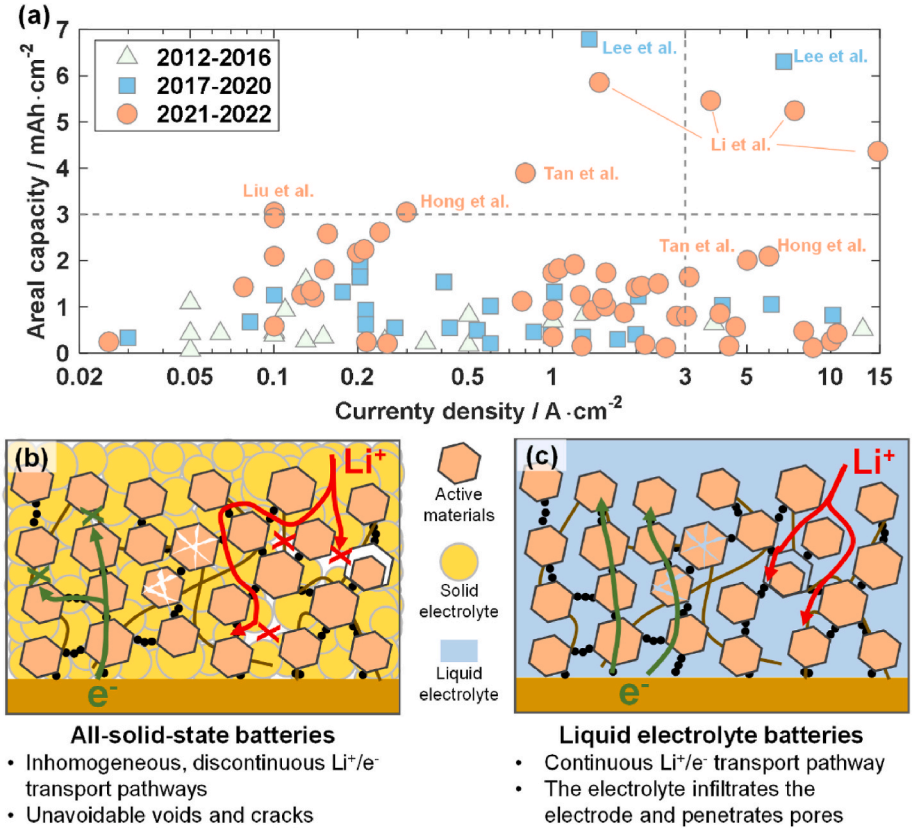

Fig. 10. Transport limitations and mechanical failures in composite electrodes of ASSBs. (a) Summary of the reported current densities and areal capacities of ASSBs in the existing literature (as in Table S1); (b)&(c) comparison of Li^+/e^- transport and mechanical problems in the composite electrodes using SEs (b) and liquid electrolytes (c).

LGPS is sufficient for good electrochemical performance of the $LiCoO_2$–LGPS composite electrode at low current density(<2C). However, a higher LPGS fraction (>40%) is required to ensure fast electrochemically access for all cathode particles when the C-rate exceeds 5C [203]. Nam et al. [75] and Minnmann et al. [198] also found that a low fraction of SE significantly degrades the electrochemical performance of the $LiNi_{0.6}Co_{0.2}Mn_{0.2}O_2$–$Li_6PS_5Cl$ composite electrode, due to the sluggish Li^+ transport. Davis et al. [204] visualized the local state of charge (SOC) heterogeneity in graphite–Li_6PS_5Cl composite electrodes using operando video microscopy. The composite electrode with a high fraction of graphite exhibited fewer interconnected SE regions and significant gradients in local SOC, which limited the rate performance [204]. Besides ionic transport, electronic conductivity is also important to the performance of composite electrodes. Conductive carbon agents are usually added to the composite electrode to promote electronic conductivity [205]. Mizuno et al. [206] and Minnmann et al. [198] found that utilizing vapor-grown carbon fiber (VGCF) can promote the rate performance of composite electrodes with a low fraction of active material. However, carbon additives are reported to cause severe electrochemical decomposition of sulfide SEs within the composite cathode, which is detrimental to cycle life [207,208]. Carefully controlling the morphology and content of carbon additives is essential to balancing the Li^+/e^- transport within the composite electrode and reducing the decomposition of SEs [197]. The VGCF carbon additive with a low surface area can mitigate the decomposition of SEs and form a more continuous e^- conducting path than carbon black or acetylene black, benefiting from their reduced contact area with SEs and increased contact points between carbon additives [206,209]. With the help of mesoscale modeling, Naik et al. [73] presented a microstructure-dependent kinetic and transport regime map of ASSBs, as in Fig. 11 (a). Firstly, low AM content results in an insufficient active area and isolated AM–CBD (carbon–binder) clusters, leading to a kinetically limiting scenario. Secondly, Li^+ transport limitation occurs at high AM content due to increased tortuosity in the SE phase. This scene becomes more severe at a higher CBD content, resulting in low utilization of AMs. Thirdly, e^- transport resistance increases at very low fractions of CBD due to the poor electronic connectivity between AM particles, namely e^- transport limitation. Overall, optimizing the ratios of different components (AM, SE and CBD) within the composite electrode is an essential first step to achieving efficient Li^+/e^- transport networks, which are critical to the electrochemical performance of ASSBs.

The particle sizes of AM and SEs also play an important role in the electrochemical performance of composite electrodes. Strauss et al. [210] found that $LiNi_{0.6}Co_{0.2}Mn_{0.2}O_2$–$Li_3PS_4$ composite electrode with small (D50 = 4.0 μm) $LiNi_{0.6}Co_{0.2}Mn_{0.2}O_2$ particles exhibited superior capacity utilization than those with large (D50 = 15.6 μm) or medium (D50 = 8.3 μm) particles. Operando X-ray diffraction experiments revealed that the composite electrodes with small $LiNi_{0.6}Co_{0.2}Mn_{0.2}O_2$ particles can ensure sufficient electronic transport pathways and full charge/discharge capacity. In contrast, the composite electrodes with large and medium particles suffered from inactive AMs [210]. Recently, Jiang et al. [211] revealed a positive correlation between the particle size and mass fraction of cathode active materials (CAMs) in composite electrode design. They found that more CAMs are required to achieve well-percolated e^- transfer pathways as their particle size increases. Furthermore, Shi et al. [121] demonstrated that the CAM–SE particle size ratio significantly affects the performance of ASSBs with high mass loading, as presented in Fig. 11 (b). A large CAM–SE particle size ratio favored a high packing density and sufficient Li^+ percolation within the composite cathode, enabling high CAM loading and high capacity utilization. Therefore, reducing the particle size of SEs, i.e., SE conditioning, is recommended to achieve a large AM–SE particle size ratio, as overlarge AM particles can result in lengthy lithium diffusion paths within the particles. Nano-sized sulfide SE particles have been synthesized using a solution-based method and demonstrated to improve the electrochemical performance of composite cathodes with high mass loading [212,213]. However, reducing the particle size of SEs by

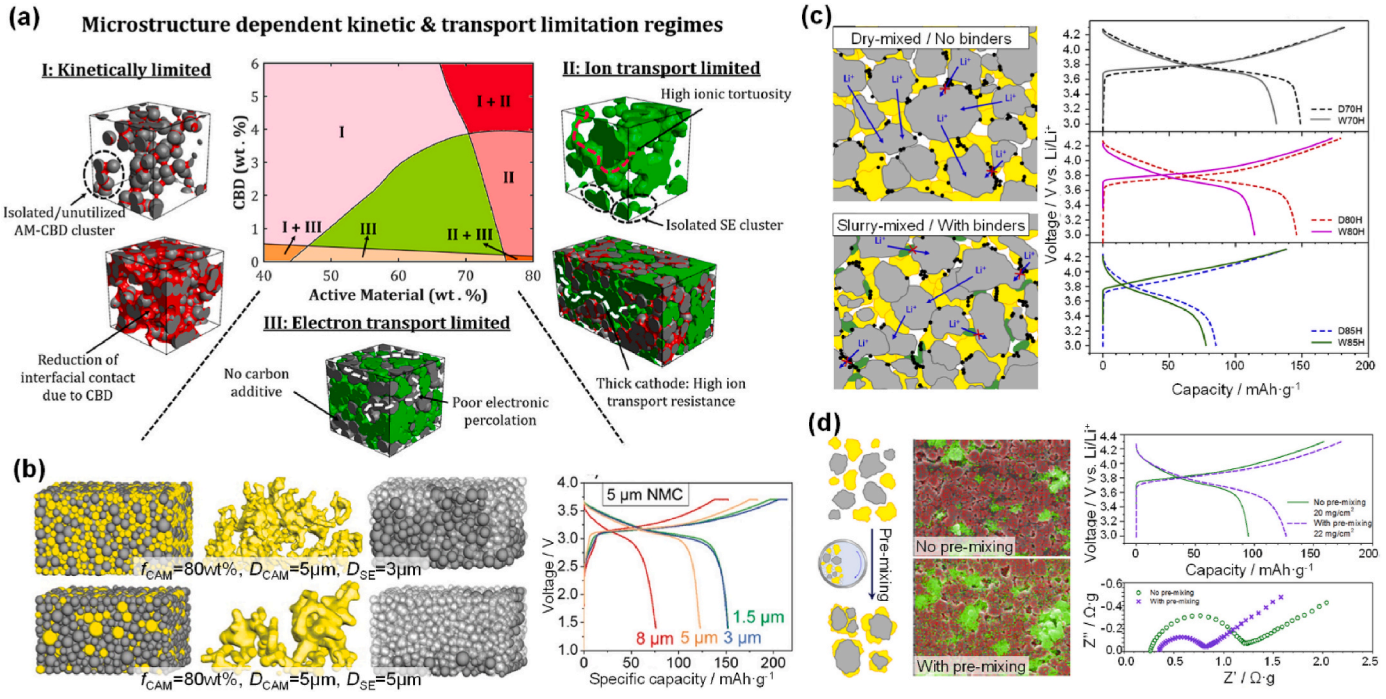

Fig. 11. Critical factors affecting the transport kinetics within the composite electrodes of ASSBs. (a) Evolution of kinetic and transport limitation with the weight ratios of AMs, carbon–binder (CBD) and SEs. Reproduced with permission from Ref. [73]. Copyright 2022, American Chemical Society; (b) effect of cathode active material (CAM) and SE particle sizes on the performance of ASSBs. Reproduced with permission from Ref. [121]. Copyright 2020, Wiley-VCH GmbH; (c) effect of binder content on the performance of ASSBs; (d) effects of mixing protocols on the performance of ASSBs. Reproduced with permission from Ref. [75]. Copyright 2018, Elsevier.

solution-based methods may decrease the bulk ionic conductivity [58,212,213], calling for a balance between the particle size and ionic conductivity. Furthermore, Rajagopal et al. [214] found that the $LiNi_{0.8}Co_{0.1}Mn_{0.1}O_2$–$Li_7P_2S_8I$ composite cathode with mixed-sized SEs has a higher capacity than that with uniform-sized SEs by improving the contact between the SEs and AMs. Park et al. [215] also revealed that the composite cathode using bimodal SEs exhibits a better performance than those using solely fine or coarse-sized SEs, benefiting from the improved packing density and lowered resistance.

To provide mechanical flexibility and good adhesion, polymeric binders are usually introduced into composite electrodes. However, binders are mostly neither ionic nor electronic conductive and would thus interrupt the Li^+/e^- transport within the composite electrode. Rosero-Navarro et al. [216] found that the initial discharge capacities of the ASSBs with different contents of ethyl cellulose binder are lower than that of the ASSB without binder. Nam et al. [75] also revealed that the nitrile-butadiene rubber (NBR) in the slurry-mixed composite electrodes can impede Li^+ conduction by blocking contacts between AMs and SEs, leading to poor performance of ASSBs, as in Fig. 11 (c). In contrast, the dry-mixed composite electrodes without binders exhibited improved capacity and rate capability. Bielefeld et al. [217] found that the binder content has a strong negative influence on the Li^+ transport pathways and active surface area within the composite electrode. However, employing an appropriate binder content has been proven an effective method for improving the cycling performance of ASSBs, by reinforcing the mechanical properties of the composite electrodes [216,218]. Careful consideration should be paid to the composition, content and distribution of binder within the composite electrode to achieve optimal electrochemical performance for ASSBs. Minimizing the binder content through dry-film technology [219–223] or incorporating ionic conductive binders [224–226] are promising strategies to balance the pros and cons of using binders in ASSBs.

Finally, a uniform distribution of AMs and SEs within the composite electrode is critical for high-performance ASSBs. As shown in Fig. 11 (d), Nam et al. [75] found that a pre-mixing process can lead to a more homogenous distribution of AM and SE and significantly improve the electrochemical performance of ASSBs. Hayakawa et al. [227] used a high-shear mixer to fabricate a composite cathode with high SE dispersion and enhanced SE adhesion on the AM particles. The high SE dispersion enabled a composite cathode with fewer voids and well-percolated ionic pathways, which exhibited significantly improved rate and cycle performance. Noh et al. [228] further found that the mixing sequence of AMs, SEs and carbon additives in the composite cathode also influences the electrochemical performance. Their results demonstrated that mixing half of the carbon additive with the SEs and reserving the other half for the final mixing achieved high initial capacity and rate performance. Besides the mixing protocols, Kim et al. [229] and Huang et al. [230] proposed a SE-infiltrated method to fabricate composite electrodes with enhanced physical contact. By infiltrating a SE solution into the conventional porous electrodes, intimate ionic contacts between the SEs and AMs were achieved and ensured better rate capability and more stable cycling performance than the dry-mixed electrodes [230]. Overall, maintaining a homogeneous distribution of the components (AMs, SEs, carbon additives and binders) within the composite electrodes remains challenging and requires a deeper understanding of the fabrication and manufacturing processes.

Despite the experimental efforts mentioned above, microstructural engineering of composite electrodes is still challenging, due to the complex interplay of various components and electrochemical/chemical/physical processes. Computational modeling can facilitate microstructural design by quickly evaluating the effects of different parameters and unraveling valuable but experimentally inaccessible information [231,232]. Bielefeld et al. [217,233,234] established a three-dimensional microstructure model to link the ASSB's performance with microstructural parameters, including the composition, weight/-volume ratio, porosity, particle size, and electrode thickness. Shi et al. [121] built up a particle network model to reveal the effects of the CAM–SE particle size ratio on CAM utilization. Park et al. [232] and Naik et al. [73] also presented comprehensive microstructural models to understand the transport limitation within composite electrodes. Neumann et al. [235] reported 3D microstructure-resolved simulations of sulfide-based composite electrodes with the microstructure obtained by X-ray tomography. Yamakawa et al. [236] further combined the neural network-based regression analysis and phase-field model to unravel the correlation between the power capability and microstructural parameters of the composite electrodes. The rational design of composite electrodes with the help of microstructure-resolved modeling has been proven effective in improving the electrochemical performance of ASSBs [121]. However, systematic comparisons between the simulation and experimental results in terms of microstructural properties, effective Li^+/e^- transport pathways and conductivities, and electrochemical performance of ASSBs are still urgently needed to improve the model's accuracy. Moreover, there is a remarkable lack of computational models to correlate the manufacturing parameters with the microstructure and electrochemical performance of composite electrodes. The ARTISTIC project led by Prof. Alejandro A. Franco aims to develop a digital twin of the manufacturing process of liquid electrolyte LIBs [237–239]. Adaption of ARTISTIC simulation tools to the manufacturing processes of ASSB electrodes has also been carried out but requires more validations [240]. Microstructure-resolved modeling from the manufacturing process to the performance output of the composite electrodes will pave the way toward an accelerated optimization of ASSBs.

5.2. Mechanical failure in composite electrodes

Mechanical failures at the electrode level include the formation of voids, cracking or pulverization of the active material particles, and lithium dendrite growth in the Li metal anode, as illustrated in Fig. 12. Void formation can interrupt the Li^+/e^- transport pathways and reduce the contact area between AMs and SEs, and particle cracking or pulverization results in tortuous Li^+ diffusion pathways within the particles and even isolated particles. Both lead to significant increase in transport and interfacial resistance, and finally drastic capacity loss. For the Li metal anode, void formation and cracking of the SE layer lead to lithium dendrite growth through the SE, and eventually internal short circuit of ASSBs. Mechanical degradation in the composite electrodes has been identified as the major cause of the capacity fading of ASSBs [241,242], highlighting the importance of mechanical considerations in ASSBs.

In the composite cathode, the volume change of CAMs during (de-) lithiation is the major trigger of mechanical failure. $LiCoO_2$ cathode shows a volume increase of ~2% when charged to $Li_{0.5}CoO_2$, while the layered NCM and $LiNi_xCo_yAl_zO_2$ (NCA) cathodes experience a volume reduction of 2–8% during charging, with a positive correlation between the volume change and Ni content [76,243,244]. The formation of voids and contact loss between cathode particles and SEs are unavoidable because of the inelastic nature of SEs. Koerver et al. [195] observed apparent contact loss of $LiNi_{0.8}Co_{0.1}Mn_{0.1}O_2$ particles with β-Li_3PS_4 SEs after 50 cycles, which leads to resistance increase and capacity degradation. Shi et al. [242] found an over threefold increase in void volume within the $LiNi_{0.5}Mn_{0.3}Co_{0.2}O_2$–$75Li_2S$–$25P_2S_5$ composite cathode after 50 cycles. The voids were distributed near the cathode particles with a contact loss area of 10.4% of the total cathode surface area, leading to rapid capacity decay of the ASSBs [195]. Furthermore, cracking of the cathode particles has also been observed in the composite cathodes after long-term cycling due to the anisotropic volume changes [76,115,117,245]. Jung et al. [115] found severe disintegration of secondary particles of $LiNi_{0.80}Co_{0.16}Al_{0.04}O_2$ with randomly oriented grains. Unlike the liquid electrolyte that can infiltrate into the intergranular cracks within the secondary particles, SEs cannot flow into the cracks, which remain as voids interrupting intergranular Li^+ diffusion [241,245]. Liu et al. [246] and Han et al. [117] observed microcracks within the particles and obvious voids in the composite cathodes with polycrystalline NCM or

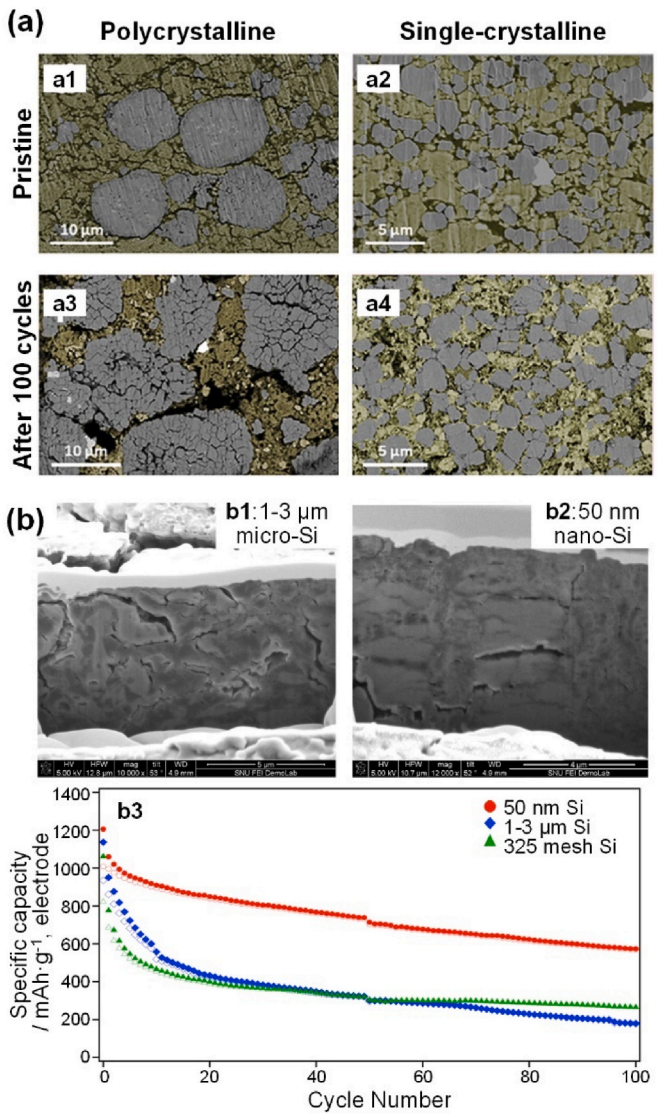

Fig. 12. Mechanical failures in sulfide-based ASSBs. (a) Void formation and particle cracking in composite cathodes with single-crystalline and polycrystalline CAMs. Reproduced with permission from Ref. [117]. Copyright 2021, Wiley-VCH GmbH; (b) cracking, delamination and pulverization in the Si–C–SE composite anodes with different sizes of Si and their cycling performance. Reproduced with permission from Ref. [143]. Copyright 2018, Elsevier.

NCA, as presented in Fig. 12 (a). Conforto et al. [241] found that the secondary particle cracking within the polycrystalline $LiNi_{0.8}Co_{0.1}Mn_{0.1}O_2$ cathode led to a 3–4 times increase in the length of Li^+ diffusion pathways inside the primary particle after 40 cycles. Improving the cathodes' mechanical integrity has been proven as an effective strategy to mitigate mechanical failure in composite cathodes. As shown in Fig. 12 (a), Han et al. [117] demonstrated that the cracking-free single-crystalline cathode can suppress both the void formation and particle cracking during cycling, significantly improving the cycling stability of ASSBs. Moreover, regulating the mechanical properties of sulfide SEs can also improve the mechanical stability of composite cathodes. Teo et al. [247] proposed the application of a glassy SE ($1.5Li_2S$–$0.5P_2S_5$–LiI) as a "soft" SE instead of the crystalline SE (Li_6PS_5Cl) to maintain tight contact with NCM cathode during volume changes, significantly improving the capacity retention after 200 cycles (from 39% to 58%).

On the anode side, the volume changes of graphite and Si-based anodes are much more severe than those in cathodes. The graphite has a volume expansion of 13.2% during lithiation, and the Si expands 320% when fully lithiated to $Li_{22}Si_5$ [133]. Micron-scale cracks were widely observed in Si–C composite or pure Si anodes for ASSBs after cycling [15,34,143,145,248,249], as shown in Fig. 12 (b). Yamamoto et al. [145] and Cao et al. [34] found vertical cracks in the Si–SE composite anodes due to the horizontal tension, while the vertical strain was alleviated by the elastic deformation of the SE layer and the counter electrode's volume changes. The vertical cracks could buffer the Si anode's volume changes and maintain most Li^+/e^- transport pathways, providing good cycling stability [34,145]. The Si particles will also suffer from pulverization during cycling, leading to a severe loss of active materials and increased internal resistance. As presented in Fig. 12 (b), Dunlap et al. [143] observed severe cracking, Si particle pulverization and delamination at the interfaces between SEs and Si–C anodes with micro-Si particles. Reducing the Si particle size to nanometers can mitigate the formation and propagation of cracks within Si due to the stress relaxation, as in Fig. 12 (b). The composite anode with 50 nm Si particles outperformed that with micro-Si particles (1–3 μm and 325 mesh Si) in terms of initial capacity and cycling stability, and exhibited fewer cracks after cycling. Kim et al. [250] also found that the Si–C composite anode using nano-Si particles exhibited a larger contact area between Si and graphite than that using micro-Si particles. Moreover, the mechanically compliant graphite could accommodate the volume change of nano-Si particles, enabling high areal and volumetric capacities of 2.94 $mAh{\cdot}cm^{-2}$ and 997 $mAh{\cdot}cm^{-3}$. Okuno et al. [249,251,252] further proposed a nano-porous Si composite anode design with the nano-porous Si homogeneously dispersed in adequate Li_3PS_4 SEs. Both the nanopores in Si particles and the elastic deformation of SE effectively relieved the stress derived from the volume change of Si, improving the cycling stability of Si anode for ASSBs. Nevertheless, research on the mechanical failure mechanism and mitigation strategies of Si anodes in ASSBs is still in the infant stage, especially when compared with the mechanical issues in composite cathodes. A fundamental study of Si anodes and technical exploration of their application in sulfide-based ASSBs are urgently needed.

Employing proper pressure during the fabrication and operation of ASSBs can mitigate mechanical failures in composite electrodes. The fabrication pressure of electrodes is usually hundreds of MPa or several GPa, while the external pressure during operation (stack pressure) is less than 100 MPa [78,244]. The fabrication pressure directly affects the porosity and Li^+/e^- conductivities of the composite electrode and SE layers [77,253–256]. As shown in Fig. 13 (a), the increased fabrication pressure can effectively densify the composite electrode and SE layers, and increase the contact area fraction between the AMs and SEs [77]. The decreased porosity significantly improved the effective ionic conductivity, while the enhanced contact area fraction led to an order-of-magnitude reduction in charge transfer resistance. Both can promote the electrochemical performance of ASSBs. Doux et al. [253] found that the increase of fabrication pressure can significantly improve the cycling stability and rate performance of sulfide-based ASSBs, as presented in Fig. 13 (b). Meanwhile, appropriate stack pressure is important for the contact between the AMs and SEs during battery operation. Yamamoto et al. [248] observed significant improvements in the cycling stability and rate performance of various ASSBs with the increase of stack pressure, as in Fig. 13 (c). Moreover, the improvements in battery performance varied with the volume changes of the active materials. The Si anode exhibited the greatest improvement in cycling stability when the stack pressure increased from 50 to 75 MPa. The high stack pressure could prevent the crack formation in Si particles, heal fine cracks, and facilitate close contact between the SE and Li_xSi via plastic deformation, thus resulting in more stable cycling. Though the existing results suggest a positive correlation between battery electrochemical performance and fabrication/stack pressure, excessive pressures may harm the performance of ASSBs. Rapid buildup of stress between large electrode particles has been observed under excessive fabrication pressure (>300 MPa), leading to microcracks in AM particles and even

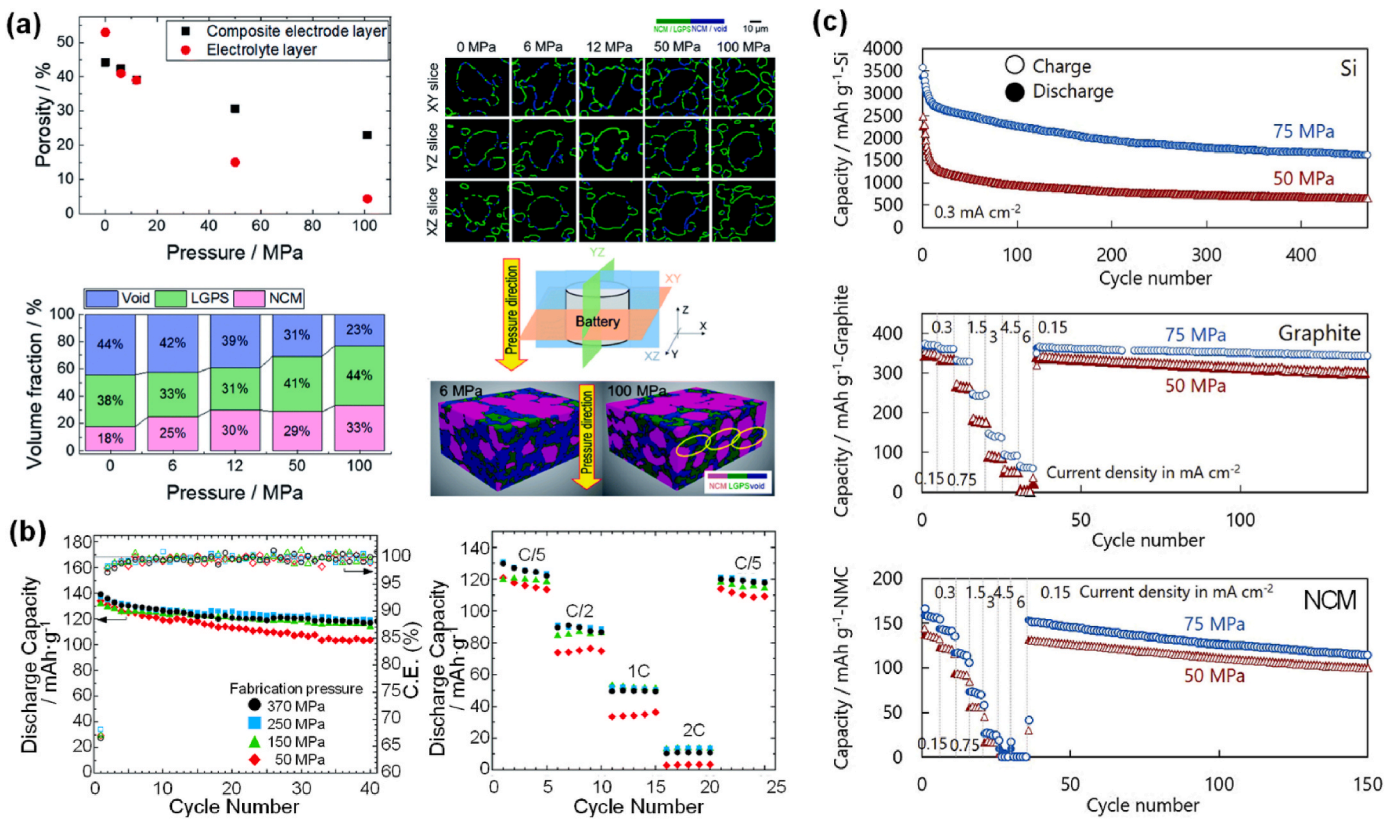

Fig. 13. Effects of fabrication and operating stack pressure on the performance of ASSBs. (a) Porosity and contact area fraction of LGPS–$LiNi_{1/3}Mn_{1/3}Co_{1/3}O_2$ composite cathodes under different pressures. Reproduced with permission from Ref. [77]. Copyright 2022, Royal Society of Chemistry; (b) effects of fabrication pressure on the cycling stability and rate performance of NCA | Li_6PS_5Cl | Li–In ASSBs. Reproduced with permission from Ref. [253]. Copyright 2020, Royal Society of Chemistry; (c) effects of stack pressure on the cycling stability and rate performance of Si |Li_3PS_4 | Li–In, graphite |Li_3PS_4 | Li–In, $LiNi_{1/3}Mn_{1/3}Co_{1/3}O_2$ | Li_3PS_4 | Li–In ASSBs. Reproduced with permission from Ref. [248]. Copyright 2020, Elsevier.

particle fracturing [117,246,254,257]. Piper et al. [258] and Kim et al. [229] found decreases in the capacity utilization and rate performance of nano-Si-based composite electrodes with increased stack pressure. A high stack pressure of 75 MPa even directly leads to short circuit of Li metal ASSBs due to the creeping of Li metal [191]. Therefore, rational optimizations of the fabrication and stack pressures considering the physical properties of the AMs and SEs (such as Young's modulus, shear modulus, bulk modulus and volume changes) are vital for achieving long-cycling-life ASSBs. Moreover, applying a high and uniform stack pressure to ASSBs is very challenging for module and pack design. Ideally, the stack pressure for ASSBs should be close to that for the existing liquid electrolyte LIBs (<1 MPa) [244], but 3–5 MPa may also be technically acceptable to module/pack design [58,259]. Novel materials (such as low-expansion electrode materials and high-mechanical-strength binders) and electrode structure designs are urgently needed to reduce the required stack pressure of ASSBs.

6. Key performance indicators of sulfide-based all-solid-state batteries

A comprehensive evaluation of several KPIs for ASSBs is necessary to meet the requirements of automotive application. As presented in

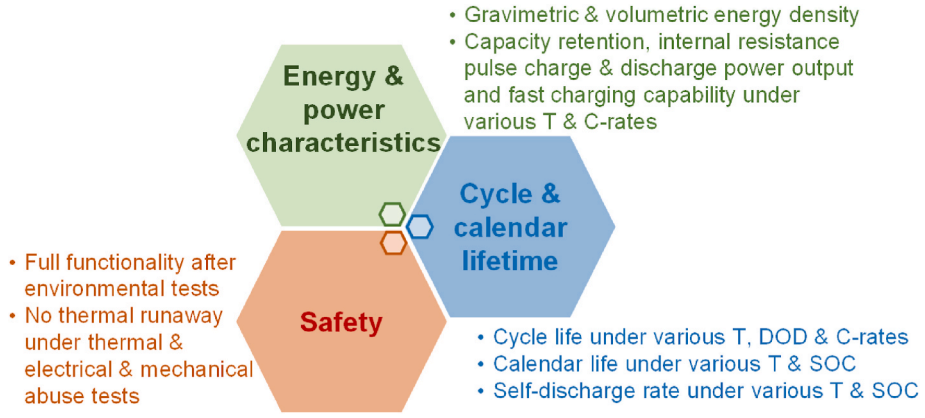

Fig. 14. Key performance indicators and test specifications of sulfide-based ASSBs for automotive applications regarding energy & power characteristics, cycle & calendar life and safety performance.

Fig. 14, the relevant KPIs are divided into three categories, i.e., energy & power characteristics, cycle & calendar lifetime and safety. The energy and power characteristics determine the basic capabilities of an ASSB, including the gravimetric & volumetric energy density, capacity retention, internal resistance, pulse charge & discharge power output under various temperatures and C-rates. The EV batteries should exhibit high capacity retention ratios of around 95%, 90% and 85% under 1C, 2C and 3C, respectively, as indicated in Fig. 15 (a). Fast charging capability with a maximum charging C-rate of over 4C and a wide operating temperature range of around −30–90 °C are also preferred for ASSBs in EV. The cycle and calendar lifetimes determine the ASSB's service life, and are evaluated through cycling or storage tests over a range of test conditions (temperature, the degree of discharge (DOD) range during cycling and the SOC during storage). To fulfill the EV requirements, batteries usually should deliver 1000+ cycles under 1C/100%DOD at room temperature, and maintain 800+ cycles at high temperatures (45 or 60 °C). The battery calendar life depends largely on the temperature and SOC during storage test, and a high capacity retention rate of >97% and a low self-discharge rate of <3% are usually required after 30-days high-temperature storage. Moreover, the cycle and calendar aging performance of ASSBs at extreme temperatures (for example, < −30 °C and >60 °C) should also be evaluated to demonstrate their temperature robustness. Finally, safety is the utmost important performance during the application of ASSBs. An ideal ASSB remains fully functional after environmental tests such as vibration, thermal shock and extremely cold temperature tests. Moreover, ASSBs should exhibit no thermal runaway

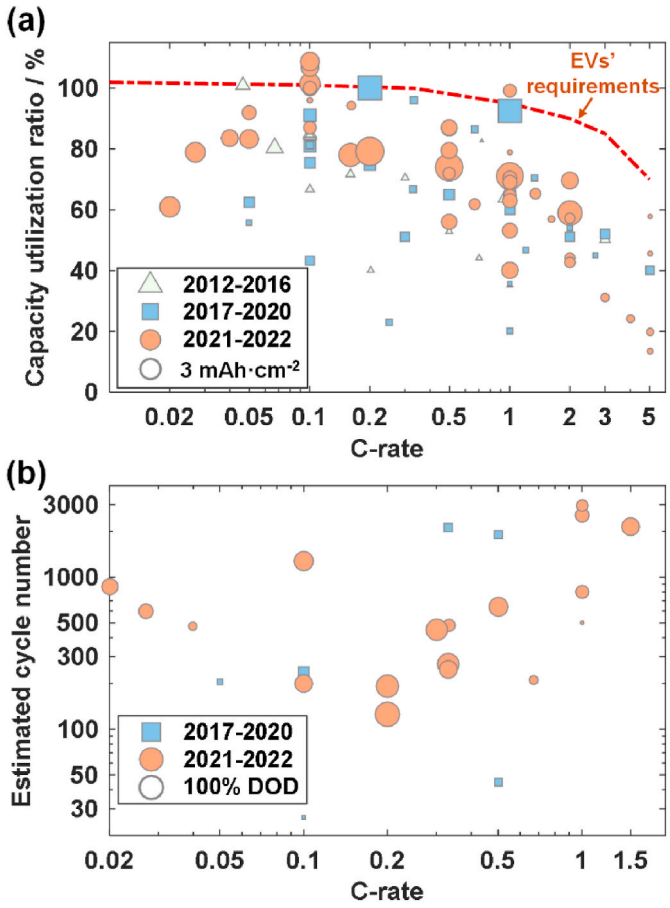

Fig. 15. Summary of the rate performance and cycle lifetime of sulfide-based ASSBs reported in the literature. (a) The capacity utilization ratios of ASSBs under different C-rates compared to their theoretical capacities, and the sizes of the symbols represent the areal capacity of the tested ASSBs; (b) the estimated cycle numbers of the ASSBs before reaching 80% of their initial capacities, and the sizes of the symbols represent the DOD range during cycling.

under thermal (overheat), electrical (overcharge, over-discharge and short circuit) and mechanical (nail penetration and crush) abuse tests. Several organizations also classify the battery behaviors during safety tests into different hazard levels: from level 0 (no effect, no functional impairment) to level 7 (explosion) [260]. A level 3 (no fire, no smoke egress, no explosion) or lower usually represents an acceptable level of performance [261]. Overall, many standards and regulations have been specifically developed to facilitate and regulate battery use in EVs [260–262]. Academic and industrial researchers of ASSBs should consider all the KPIs rather than only one or two, especially when bringing ASSBs to market.

Unfortunately, the aforementioned KPIs of sulfide-based ASSBs have not been thoroughly evaluated, and most of the KPIs require further improvements. We summarize the rate performance and cycle lifetime of sulfide-based ASSBs reported in the literature, as in Fig. 15, with the detailed data in Table S1. It should be noted that the stack pressure and temperature during the rate capability and cycling tests are not presented in Fig. 15 to avoid being verbose. Nevertheless, stack pressure and temperature undoubtedly play vital roles in the electrochemical performance of ASSBs, and require careful optimizations during practical application.

Fig. 15 (a) presents the capacity utilization ratios of the existing ASSBs under different C-rates. Most of the existing ASSBs exhibit poor rate performance with capacity utilization ratios of less than 85% when the C-rate exceeded 0.5C and were still far below the requirements of EVs. Moreover, those operating above 0.5C mostly have low areal capacities (<2 mAh·cm^{-2}). Despite the difficulties, a few examples of ASSBs achieved good rate performance. Lee et al. [33] designed a 0.6 Ah pouch ASSB with a high areal capacity of 6.8 mAh·cm^{-2} and a high capacity retention rate of 92.65% under 1C. Li et al. [196] presented a high areal capacity (7.39 mAh cm^{-2}) mold ASSB, with moderate capacity retention rates of 71.04% and 59.00% under 1C and 2C, respectively. Zhang et al. [263] fabricated a mold-ASSB with a high capacity retention rate of 99.21% under 1C, but with a low areal capacity of 1.26 mAh·cm^{-2}. Besides, sulfide-based ASSBs that can operate under ultra-high C-rates have also been reported. Ye et al. [187] developed a mold ASSB that maintained 36.05% and 25.58% of its theoretical capacity under 10C and 20C, respectively, benefiting from a multilayer electrolyte design. Although the rate capabilities of most existing ASSBs are still below the EVs' requirements, the areal capacity of ASSBs shows an uptrend without deteriorating the rate performance, as in Fig. 15 (a). This indicates continuous improvements in the Li^+/e^- transport and interfacial charge transport kinetics within the composite electrodes, which substantially contribute to the rate performance of ASSB. As discussed in Sections 4 and 5, we believe that overcoming the transport limitations at the interface and composite electrode levels will help boost the rate performance of ASSBs to meet the EVs' requirements.

For the cycle lifetime, as shown in Fig. 15 (b), there are several reports on sulfide-based ASSBs with long cycle lives of over 1000 times, presenting sulfide-based ASSBs' potential for long-term stability. Lee et al. [33] developed an ASSB with superior cycle life (>1000 times) under 0.5C through a Ag–C composite anode design. Shi et al. [264] designed a $LiNi_{0.8}Co_{0.1}Mn_{0.1}O_2$-based sulfide-based ASSB with remarkable cycling stability up to 5650 cycles with a decay rate of 0.0069% per cycle under 1C. This long cycle life was enabled by suppressing the interfacial side reactions using a coupling design of Li_7TaO_6 surface buffer coating with bulk Ta-doping for the cathode. Recently, Liu et al. [35] designed a super long-cycling sulfide-based ASSB with a stable capacity retention rate of 71% even after 20000 cycles at 1.61C, much superior to existing liquid electrolyte LIBs. Start-ups such as Solid Power also demonstrated prototype sulfide-based ASSBs with a long cycle life of 1000+ cycles under 1/5C [265]. However, it should be noted that the ASSBs with super long cycle life are mostly operated within a relatively narrow DOD range below 80%, which is mainly limited by the large polarization under high rate. In contrast, the ASSBs operated under low rate and wide DOD (95–100%) exhibit much shorter lifetimes, as in

Fig. 15 (b). This might be induced by the more severe volume change and mechanical failure within the composite electrode. Compared to the cycling stability of ASSBs, only a few papers reported the calendar life of sulfide-based ASSBs. Yoon et al. [266] found severe capacity decay of a Li_6PS_5Cl-based ASSB after 6-day storage at 4.3 V and 70 °C, due to the decomposition of the Li_6PS_5Cl SE. Rapid impedance increase and capacity degradation of sulfide-based ASSBs at high temperature and high voltage storage were also observed by Zuo et al. [177] and Morino et al. [267]. Nevertheless, the calendar aging performance of sulfide-based ASSBs has not been thoroughly evaluated and requires more attention. Compared with the rate performance, the cycle and calendar lifetimes of ASSBs are more susceptible to operating conditions (such as C-rate, DOD, temperature and pressure). Proper galvanostatic and dynamic charging-discharging test procedures should be built to accurate evaluate ASSB's service life in EVs. Generally, the charging C-rate of EV batteries is around 1/5–1/10C for slow charging and 1–4C for fast charging, and the average discharging C-rate is around 1/3–1/5C. Dynamic test procedures can be acquired by simplifying the EV driving cycle profiles [268]. Moreover, the degradation mechanisms of ASSBs have not been quantitatively characterized. The effective tools/methods that have been applied in the failure analysis of liquid electrolyte LIBs, such as reference electrodes [269–271], incremental capacity and differential voltage analysis [66,266,272], EIS [273–275] and high precision coulometry [276–278] can also facilitate the degradation diagnosis of ASSBs and are worth further explorations.

Safety always comes first in the practical application of batteries. ASSBs are expected to be safer than conventional liquid LIBs by replacing the volatile and flammable liquid electrolytes with nonflammable SEs. Lee et al. [33] demonstrated the high safety of the 0.6 Ah pouch sulfide-based ASSB under a 210 °C oven test. Solid Power and Svolt Energy also announced that their Ah-level prototype sulfide-based ASSBs can pass a series of safety tests such as nail penetration, external short circuit and overcharge [37,279]. However, recently, researchers argued that the safety of ASSBs might have been overestimated, especially considering the high reactivities of sulfide SEs and Li metal [280–282]. The safety of ASSBs largely depends on the thermo-chemical reactions between AMs and SEs rather than the flammability or thermal stabilities of individual components [283]. Tsukasaki et al. [284–287] firstly reported the noticeable exothermic reactions between $LiNi_{1/3}Mn_{1/3}Co_{1/3}O_2$ and Li_3PS_4 at elevated temperatures due to the oxidation of Li_3PS_4 by the oxygen released from the cathode. Violent exothermic reactions between layered cathodes ($LiNi_{0.8}Co_{0.1}Mn_{0.1}O_2$ and $LiCoO_2$) and various sulfide SEs (Li_6PS_5Cl, $Li_7P_3S_{11}$, $Li_{9.54}Si_{1.74}P_{1.44}S_{11.7}Cl_{0.3}$, Li_4SnS_4) were also observed, along with the generation of a significant amount of SO_2 gas [79,80]. Our recent study showed that the sulfide SEs react not only with the oxygen from the layered cathode but also with the solid decomposition products of the cathode [288]. Two distinct exothermic reaction mechanisms between sulfide SEs and CAMs were revealed, i.e., gas-solid and solid-solid reaction mechanisms. Moreover, Vishnugopi et al. [283] observed thermal runaway behaviors of a Li | $Li_{10}SnP_2S_{12}$ | Li symmetrical ASSB with an extreme-high self-heating rate of 196.3 °C/min. The results above demonstrate that safety hazards still exist in ASSBs and highlight the need to comprehensively investigate their safety characteristics. Here, we propose the potential safety hazards of sulfide-based ASSBs according to the physical/chemical properties of the components, as illustrated in Fig. 16. At the cathode side, the highly oxidative CAMs and the released oxygen are prone to react with the lithiated graphite/Si anodes, Li metal anode and sulfide SEs [289,290], generating a significant amount of heat and gases such as SO_2, CO and CO_2. Lithium dendrite growth is the major safety threat at the anode side and can induce internal short circuit of ASSBs. Exothermic reactions between sulfide SEs and the lithiated graphite/Si anode or Li metal anode also occur at a high temperature, as observed in Ref. [283]. Moreover, Li metal melting at a high temperature requires special considerations for the safety of solid-state Li metal batteries. Molten Li metal reacts violently with SEs and O_2 from the cathode or air, leading to intense heat generation [291,292]. Finally, the chemical hazards of sulfide-based ASSBs upon rupture of package, venting or even explosion are additional challenges [293]. Especially, sulfide SEs are known to react with moisture to form H_2S, a highly toxic, flammable and explosive gas. The generation of toxic SO_2 from the oxidation of sulfide SEs at high voltage [176] or temperature has also been observed [79,294]. Nevertheless, the toxicity, flammability and explosibility of the emissions from ASSBs under various conditions remain elusive and need comprehensive evaluation.

7. Scaling up sulfide-based all-solid-state batteries

Currently, most sulfide-based ASSBs are constructed of stacking pellet-type electrodes and thick SE layers. However, the fabrication of pellet-type ASSBs is time-consuming and discontinuous, and can hardly be scaled up. For the mass production of sulfide-based ASSBs, it is essential to fabricate sheet-type electrodes and SE membranes through continuous processes. This section introduces several fabrication methods for sheet-type electrodes and SE membranes, including slurry casting, SE solution infiltration and solvent-free dry-film methods. The

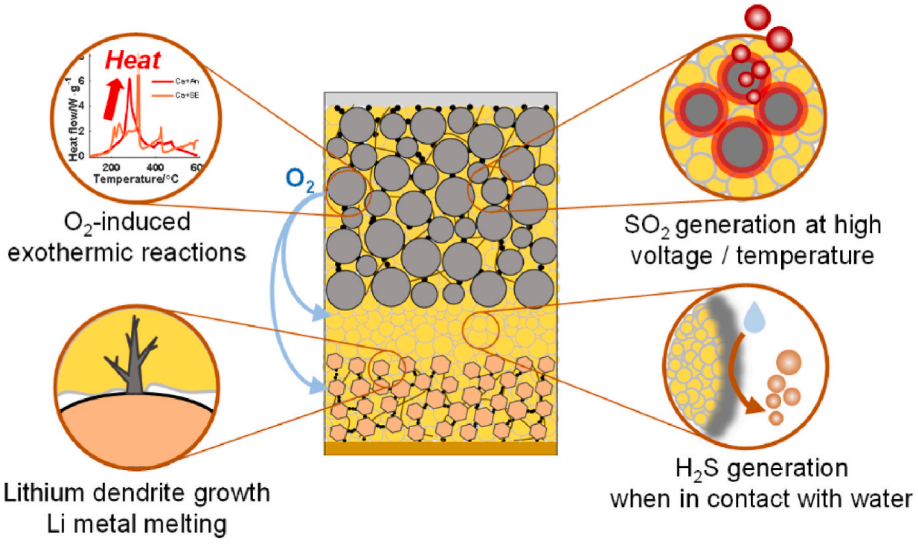

Fig. 16. Potential safety hazards of sulfide-based ASSBs.

typical procedures, representative examples, advantages and disadvantages of each fabrication process are discussed.

7.1. Fabrication of sheet-type electrodes for sulfide-based all-solid-state batteries

Fig. 17 illustrates the three representative sheet-type electrode fabrication processes of sulfide-based ASSBs. Since the first report on the fabrication of Mo_6S_8 electrode using a $Li_{3.25}Ge_{0.25}P_{0.75}S_4$ SE in 2009 [295], many studies have adopted the slurry casting method in conventional liquid electrolyte LIBs to fabricate sheet-type electrodes for sulfide-based ASSBs. As shown in Fig. 17 (a), in the slurry casting process, a slurry is first prepared by dispersing the AMs, SE, conductive carbon and binder in a solvent. The slurry is cast on a current collector, then dried to remove the solvent. High-pressure pressing is conducted before or after stacking the cathode, SE membrane and anode to solidify the electrodes. The slurry casting method is a good candidate for processing sheet-type electrodes considering the accumulated experience in manufacturing conventional liquid electrolyte LIBs and only minor modifications to the existing equipment. The slurry casting method can also facilitate the application of solvate-ionic-liquid-based polymeric binders [225,296–298] in the composite electrodes, which can increase the effective interfacial area and overcome the Li^+/e^- transport limitation induced by the insulating polymeric binders. One-step fabrication of sheet-type electrodes from SE precursors can also be achieved via the slurry casting method, providing an efficient protocol for ASSBs fabrication [216,299]. However, due to their poor chemical stability, it is quite difficult to find appropriate solvent–binder pairs compatible with sulfide SEs. As sulfide SEs tend to dissolve in polar solvents and suffer from decreased ionic conductivity, nonpolar or weakly polar solvents are usually utilized to prepare slurries containing sulfide SEs [59]. This restriction on solvents consequently limits the binders to nonpolar or less polar ones based on the principle of solubility match [59,82,300,301]. However, most nonpolar and less polar binders usually have poor adhesivity and dispersibility, so the choices of sulfide SEs, solvents and binders need careful consideration [301–303]. Efforts have been made to screen solvent-binder pairs for sulfide SEs [300]. The donor number was proposed as an indicator to predict the compatibility of solvent with sulfide SEs [222]. Nonpolar or less polar solvents (e.g., heptane, toluene and xylene) and binders (e.g., rubber binders, cellulose and ethyl cellulose) that can dissolve in these solvents were employed in the slurry-casting process of sulfide SE-based electrodes [301]. Ito et al. [304] prepared a sheet-type $LiNi_{0.8}Co_{0.15}Al_{0.05}O_2$–$Li_2S$–$P_2S_5$(80:20 mol %) composite electrode using NBR-based hydrocarbon polymer binder and dehydrated xylene solvents. Zhang et al. [218] developed the $LiNi_{0.8}Co_{0.1}Mn_{0.1}O_2$–$Li_6PS_5Cl$ composite electrodes using ethyl cellulose binder and anhydrous ethanol solvents. To overcome the dilemma of selecting solvent–binder pairs, Lee et al. [305] proposed a protection−deprotection chemistry-based strategy. In their work, the carboxylic acid groups of the binder were protected by *tert*-butyl groups to allow homogeneous dispersion of the binder in a less polar solvent. The protecting group was thermally cleaved during the drying process, leaving the polar functional groups to engage in hydrogen bonding with the AMs. Besides the incompatibility issues, the distribution of multiple components in the slurries is critical to the electrochemical and mechanical performances of sheet-type electrodes [306]. Chen et al. [307] revealed that composite electrodes using different binders (styrene-butadiene rubber (SBR) and SEBS) with different solvents (anisole for SBR and heptane for SEBS) showed different extents of reaction inhomogeneity. The composite electrode with SEBS suffered from a nonuniform electrode structure, leading to poor ionic conductivity and electrochemical performance [307]. Yamamoto et al. [257] found that

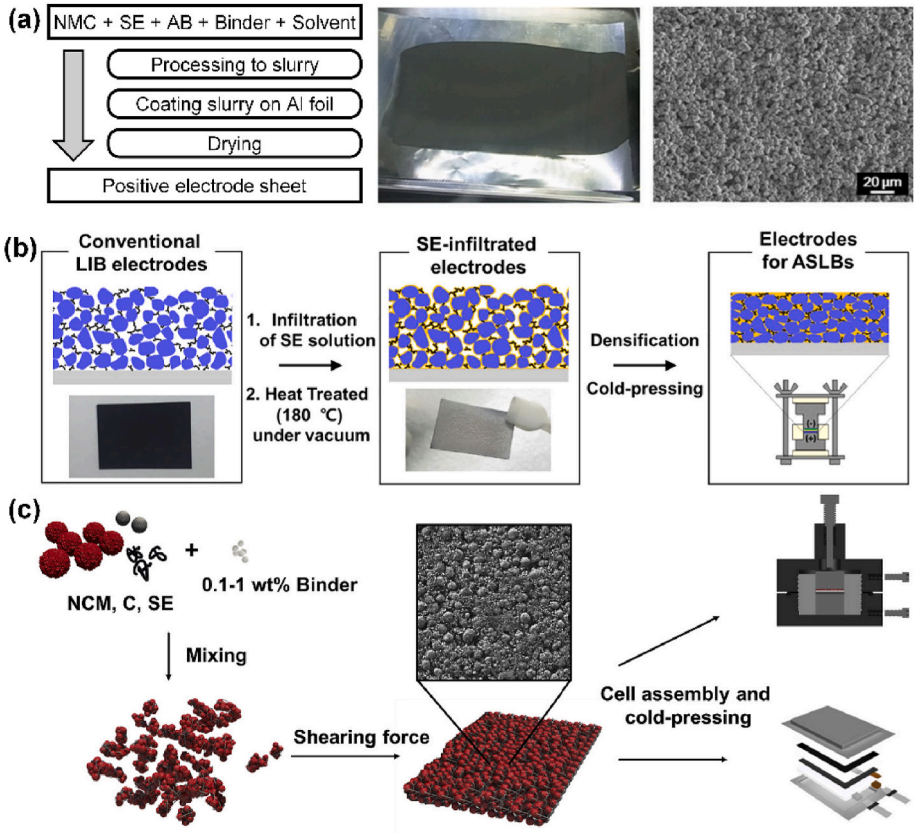

Fig. 17. Representative sheet-type electrode fabrication processes of sulfide-based ASSBs. (a) Slurry casting process. Reproduced with permission from Ref. [311]. Copyright 2017, IOP Publishing; (b) the SE solution infiltration process. Reproduced with permission from Ref. [312]. Copyright 2017, American Chemical Society; (c) the solvent-free dry-film process. Reproduced with permission from Ref. [219]. Copyright 2019, Elsevier.

the composite electrode fabricated using volatile 1,2-dichloroethane had a rough surface with some bulges and delaminated from the current collector, while the electrode fabricated using less volatile n-decane had a dense and smooth surface without aggregations. Binder migration during the fast evaporation of the solvents is responsible for poor electrode performances. To suppress binder migration, Kim et al. [308] combined the highly volatile ethyl acetate and less volatile hexyl butyrate as cosolvents, and used the cosolvents and poly(vinylidene fluoride-*co*-hexafluoropropylene) (PVDF-HFP) binder to fabricate $LiNi_{0.7}Co_{0.15}Mn_{0.15}O_2$–$Li_6PS_5Cl_{0.5}Br_{0.5}$ composite cathodes. The sheet-type $LiNi_{0.7}Co_{0.15}Mn_{0.15}O_2$ electrodes containing PVDF-HFP showed superior performance to those containing NBR binder [308]. Nevertheless, the effects of the solvent, binder and process (mixing, casting and drying) parameters on the performance of slurry-based composite electrodes remain elusive. The experience in the manufacturing processes of conventional liquid electrolyte LIBs [237,309,310] could facilitate the slurry casting-based fabrication of sheet electrodes for sulfide-based ASSBs, but more research is still required.

The SE solution infiltration method is another candidate for fabricating sheet-type composite electrodes. As illustrated in Fig. 17 (b), an SE solution is infiltrated into the conventional LIB electrode fabricated through slurry casting. Heat treatment is then performed to remove the solvents and allow the precipitation of the SE, followed by cold pressing to densify the electrode. Kim et al. [229,312] firstly fabricated sheet-type Li_6PS_5Cl-infiltrated $LiCoO_2$, graphite and Si electrodes using Li_6PS_5Cl/ethanol solutions. Compared to the slurry casting method, the SE solution infiltration method can relax the restrictions on the binders by separating the processing of binders, solvents and sulfide SEs. In Kim's work [229,312], conventional polymeric binders such as poly (vinylidene fluoride) (PVDF), polyacrylic acid (PAA) and carboxymethyl cellulose (CMC), and solvents such as N-methyl pyrrolidinone (NMP) and water were used to fabricate the porous electrodes, while the SE solutions were prepared separately using ethanol or methanol. Moreover, for the composite electrodes fabricated via the SE solution infiltration method, the e^- transport network is firstly constructed by the conductive carbons within the conventional porous electrodes, while the Li^+ transport pathways are formed subsequently during the infiltration and precipitation of sulfide SEs. This can avoid the simultaneous constructions and interactions of Li^+ and e^- pathways in the slurry-casted composite electrodes, thus achieving favorable Li^+/e^- percolation. As a result, Kim et al. [229,312] demonstrated that the Li_6PS_5Cl–infiltrated $LiCoO_2$, graphite and Si electrodes showed high reversible capacities, which were not only superior to those of conventional dry-mixed and slurry-mixed electrodes but also comparable to those of liquid electrolyte cells. However, solution-processed sulfide SEs usually exhibit insufficient ionic conductivities (~ 0.1 mS cm^{-1}). A high temperature is required for the precipitation of SEs, which can cause side reactions at AM | SE interfaces and decomposition of the binders. Song et al. [313] tailored the solution-processable argyrodite $Li_{6+x}P_{1-x}M_xS_5I$ (M = Ge, Sn) SEs to improve their ionic conductivities. However, the highest ionic conductivity (0.54 mS/cm) was still lower than common values (1–10 mS cm^{-1}) of sulfide SEs. Further development of solution-processable sulfide SEs with high ionic conductivity is essential for the application of SE solution infiltration-based fabrication of ASSBs.

Recently, a solvent-free dry-film process has been developed for sheet-type ASSB fabrication to avoid the instability issues caused by the solvents [223,314]. The solvent-free dry-film technology can also eliminate the pollution caused by organic solvents and the high energy consumption during the solvent-drying process. As illustrated in Fig. 17 (c), during the dry-film fabrication process, the AMs, SEs, conductive carbon and a limited amount of fibrous binder (such as polytetrafluoroethylene (PTFE)) are firstly dry-premixed, followed by high shearing force induced film formation. The shearing force can transform PTFE beads into fibrils, which blend between the AM and SE particles and hold them together. Hippauf et al. [219] first reported the solvent-free dry-film fabrication of a sheet-type $LiNi_{0.9}Co_{0.05}Mn_{0.05}O_2$–$Li_6PS_5Cl$ composite electrode. A freestanding composite electrode with a high loading of 6.5 mAh·cm^{-2} was fabricated using only 0.3 wt% PTFE, and exhibited excellent rate performance. Li et al. [315] also fabricated a long-cycle-life sheet-type $LiNi_{0.6}Co_{0.2}Mn_{0.2}O_2$–$Li_6PS_5Cl$ composite cathode using 0.5 wt% PTFE. As demonstrated by Hippauf et al. [219] and Li et al. [315], only 1 wt% PTFE or less is required for dry-film fabrication of sheet-type electrodes, and the fibrous PTEF can form a bridge-like connection among the particles with high specific areas. Both can help to reconstruct the electrode microstructures and reduce the Li^+/e^- transport blocking effects resulting from binders. To further improve the Li^+ transport within the composite electrodes, Hong et al. [224] developed a Li^+-conducting ionomer binder for dry-processed $LiNi_{0.7}Co_{0.1}Mn_{0.2}O_2$–$Li_6PS_5Cl$ composite cathode, which exhibited higher discharge capacity and more stable cycling performance than that using PTFE binder. Despite its potential virtues, the solvent-free dry-film technology is still a new fabrication strategy with nearly no available large-scale processing tools. The PTFE binder is reported to be unstable with anodes [223]. Thus, it is questionable whether the PTFE-based dry-film technology can be applied to the fabrication of composite anode. Moreover, the correlations between the binder properties (e.g., composition and molecular weight), AMs properties (e.g., sizes, shapes, and mechanical strength), processing parameters (e.g., the mixing rate, the calendaring pressure and temperature) and the final performance of the dry-film fabricated electrodes remain elusive and require further exploration.

7.2. Fabrication of sulfide solid electrolyte membranes

Fabrication of sulfide SE membranes is crucial for scaling up high-energy-density sulfide-based ASSBs [82,303,316]. An ideal sulfide SE membrane has high ionic conductivity (>1 mS cm^{-1}), thin thickness (<50 μm) competitive with the polymeric separator in liquid electrolyte LIBs, robust mechanical properties (high Young's modulus and tensile strength) to prevent lithium dendrite growth and be compatible to the roll-to-roll process, and also low cost [82]. Similar to the fabrication of sheet-type electrodes, there are also three representative methods to fabricate sulfide SE membranes, as presented in Fig. 18.

In the slurry-based processing, a slurry is prepared by dispersing the sulfide SE and binder in a solvent and is then coated on the substrate, followed by drying and pressing processes to remove the solvent and densify the SE membrane, as presented in Fig. 18 (a). After exfoliated from the substrate, a freestanding SE film is obtained. Alternatively, a non-freestanding SE membrane can be transferred from a sacrificial substrate to or directly cast on an electrode sheet. Similar to the fabrication of electrodes, the solvent–binder pairs are critical for the slurry casting fabrication of SE membranes. The compatible solvent–binder pairs for electrode fabrication are also suitable for fabricating SE membranes. Cao et al. [317] fabricated a freestanding Li_6PS_5Cl membrane with a low thickness of 47 μm and a superior ionic conductivity of 1.65 mS cm^{-1}, using ethyl cellulose as the binder and toluene as the solvent. A cosolvent strategy consisting of a less polar solvent to stabilize sulfide SEs and a more polar solvent to enhance the solubility of specific binders has also been proposed to prepare sulfide SE membranes. Lee et al. [33] prepared a Li_6PS_5Cl membrane using acrylate-type binder and a xylene-isobutyl isobutyrate mixed solvent (50:50 in weight). The SE membrane achieved a low thickness of 40 μm and a high ionic conductivity of 1.31 mS cm^{-1}. Moreover, the binder content and cosolvent ratio are also crucial to the ionic conductivity and processability of sulfide SE membranes. Chen et al. [318] presented a machine learning-guided optimization of sulfide SE films by deconvoluting the interdependencies between the manufacturing parameters and performance metrics. The optimized Li_6PS_5Cl film had a thickness of 40 μm and an ionic conductivity of 0.86 mS cm^{-1}. Despite the many similarities in the slurry casting fabrication of electrodes and SE membranes, we should note the differences in their compositions and performance requirements. The main target of the composite electrodes is to improve

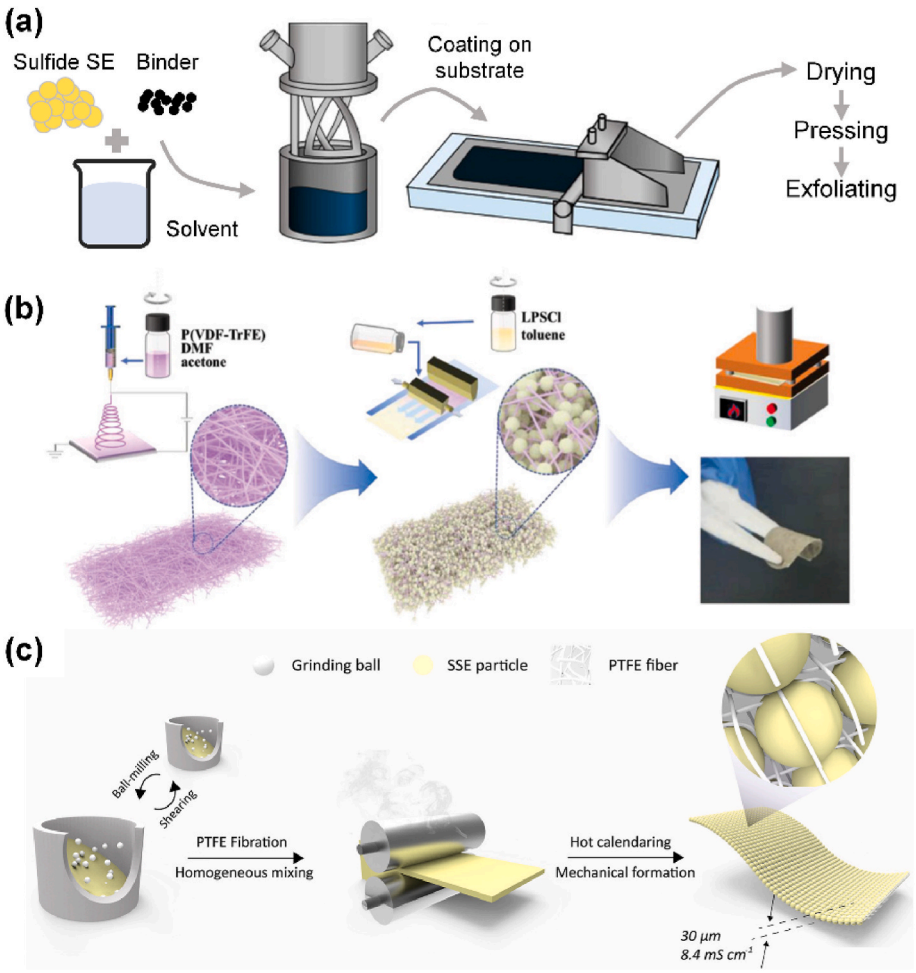

Fig. 18. Methods to fabricate SE membranes. (a) The slurry casting method. Reproduced with permission from Ref. [303]. Copyright 2021, American Chemical Society; (b) the scaffold-assisted SE solution infiltration method. Reproduced with permission from Ref. [35]. Copyright 2022, Wiley-VCH GmbH; (c) the solvent-free dry-film method. Reproduced with permission from Ref. [319]. Copyright 2021, American Chemical Society.

the AMs' utilization and loading with favorable Li^+/e^- transport networks. In contrast, the SE membranes should be as thin as possible while maintaining sufficient mechanical strength. Therefore, the solvent–-binder pairs and the process parameters for slurry casting fabrications of electrodes and SE membranes need to be carefully reconsidered.

The scaffold-assisted solution infiltration method has been developed to fabricate sulfide SE membranes with improved mechanical properties and reduced binder content. Scaffolds with interconnected frameworks, including wood [320], Kevlar nonwoven fiber [321], nylon mesh [322], polyimide [323] and cellulose fiber [324], are utilized to maintain mechanical integrity. SE solutions are infiltrated into the porous scaffolds to provide Li^+ transport pathways, followed by drying and pressing to densify the SE membranes. Zhu et al. [324] designed a 60 μm Li_6PS_5Cl SE film with a high ionic conductivity of 6.3 mS cm^{-1} using cellulose fiber as a scaffold. To ensure the precipitation process of sulfide SE from the solution, Kim et al. [323] used a thermal-stable polyimide nonwoven to enable the solution infiltration fabrication of $Li_6PS_5Cl_{0.5}Br_{0.5}$ SE membranes. The 40 μm $Li_6PS_5Cl_{0.5}Br_{0.5}$-infiltrated polyimide membrane was dried in a glovebox to remove the solvent and then heated at 400 °C to achieve a high ionic conductivity of 2 mS cm^{-1}. Moreover, ion-conducting scaffolds were also designed to further increase the ionic conductivity of SE membranes. Liu et al. [35] designed a thin SE membrane by infiltrating Li_6PS_5Cl–toluene solution into a poly (vinylidene fluoride-*co*-trifluoroethylene) P(VDF-TrFE) scaffold, as shown in Fig. 18 (b). The interaction between Li_6PS_5Cl and P(VDF-TrFE) ensured an ionic conductivity of 1.2 mS cm^{-1}, and the ASSB using the SE membrane presented an ultra-long cycle life of 20000 cycles at 1.0 mA cm^{-2} [35]. The scaffold-assisted SE solution infiltration method for SE membranes is similar to the SE solution infiltration process of sheet-type electrodes in Fig. 17 (b). The chemical incompatibility between sulfide SEs and solvents is still the main challenge, which can degrade the ionic conductivity of solution-processed sulfide SEs. Moreover, proper methods for the large-scale fabrication of appropriate scaffolds are also required.

Solvent-free dry-film technology can also be applied to fabricate SE membranes. Yersak et al. [325] presented an aramid-fiber-reinforced $(Li_2S)_{70}$–$(P_2S_5)_{30}$ SE membrane via hot-pressing at 240 °C and 200 MPa. The 100 μm SE membrane with 10 wt% aramid fiber achieved a relative density of 99.8% and an ionic conductivity of 2.4 mS cm^{-1}. However, the large-scale application of the hot-pressing process is quite challenging due to the required high-temperature, high-pressure processing conditions and the difficulties in reducing the thickness of SE membranes. Dry-film technology using PTFE binders has also been adopted in manufacturing sulfide SE membranes, as presented in Fig. 18 (c). SE particles and PTFE binders are uniformly mixed through ball-mixing or double-blade blending, which can provide a large shear force to fibrillate the binders and form a homogeneous network connecting SE particles [223,314]. Freestanding and continuous SE membranes can be obtained by hot-calendaring the mixed powders. Wang et al. [326] fabricated a 20 μm Li_6PS_5Cl membrane with only a small amount (0.5 wt%) of PTFE, and the ionic conductivity of the SE membrane reached 1.7 mS cm^{-1}. Zhang et al. [319] reduced the PTFE

content to 0.2 wt%, and fabricated a 30 μm $Li_{5.4}PS_{4.4}Cl_{1.6}$ membrane with a high ionic conductivity of 8.4 mS cm^{-1}, as in Fig. 18 (c). As discussed in the section above, the solvent-free dry-film method is a promising technology that can reduce production costs, improve overall performance, and promote the updating of the whole battery industry. Further investigations on the process parameters and scaling-up tools of solvent-free dry-film technology are required.

7.3. Large-scale production of sulfide-based all-solid-state batteries

Fig. 19 presents the potential manufacturing schemes for ASSBs. In the freestanding scheme, the sheet-type cathodes, anodes and SE membranes are prepared separately through the slurry casting, SE solution infiltration or dry-film methods. Calendaring is required for the individual sheets to reduce the porosity and ensure effective Li^+ transport, while drying is optional and depends on whether the solvent is used. After cutting into designed sizes, the three individual layers are stacked together, followed by pressing to improve the interfacial contact, tab welding and finally packaging. Sakuda et al. [311] demonstrated the manufacturing of sulfide-based ASSB using the individual sheet-type $LiNi_{1/3}Co_{1/3}Mn_{1/3}O_2$ cathode, graphite anode and $75Li_2S–25P_2S_5$ membrane fabricated by slurry casting methods. Hippauf et al. [219] also fabricated a 3 × 3 cm^2 sized ASSB using dry-processed $LiNi_{0.9}Co_{0.05}Mn_{0.05}O_2$ cathode, Li_6PS_5Cl membrane and Li–In foil. Another manufacturing strategy is the cathode-supported scheme, where an electrolyte slurry is cast directly onto the surface of the sheet-type cathode, as illustrated in Fig. 19. The sheet-type anode or Li foil is attached on the surface of the cathode–electrolyte layer, and the prototype cell is then cut and pressed. Ates et al. [327] demonstrated that the cathode-supported process could facilitate the formation of tight interfacial contact between the cathode sheet and the SE layer. However, the solvent should be carefully selected to be compatible with the components in the cathode sheet. In both the freestanding and cathode-supported schemes, densification of the sheet-type electrodes and SE membranes towards near zero percent porosity by calendaring or stacking is the most challenging process. The frequent-used line and areal pressing techniques are difficult to achieve high-pressure and homogeneous densification of the electrodes and SE membranes [58,328,329]. To overcome this challenge, isostatic pressing (including cold, warm and hot isostatic pressing) has been utilized to apply ultra-high pressure uniformly in all directions to densify ASSBs [330]. Lee et al. [33] introduced the warm isostatic pressing technique to fabricate pouch ASSBs, and realized significant improvement in the densities of both the electrode and SE. The resultant density and uniformity of the compacted samples depend on three key parameters: time, temperature, and pressure, which still need to be optimized to achieve optimum densification [330]. However, the relatively high cost and lengthy processing time may hinder the application of isostatic pressing in the large-scale production of ASSBs [58,330].

Up to now, there is no available manufacturing line for sulfide-based ASSBs. Although some companies such as Solid Power and Samsung have started the construction of pilot lines [36,40], details of their processes and equipment remain confidential. In order to successfully develop scalable ASSB prototypes, it is imperative to fully utilize existing LIB manufacturing facilities and minimize the need for new machines. Nevertheless, re-inventing or retrofitting new machinery (e.g., dry-film fabrication equipment, high-pressure pressing equipment) is unavoidable to support the large-scale manufacturing of sulfide-based ASSBs. Furthermore, careful control of the gas atmosphere is also vital to avoiding deterioration of the air-unstable sulfide SEs during the manufacturing processes. Corrosion between sulfide SEs and stainless steel equipment is also observed by several ASSBs manufacturers, calling for special attention in equipment design for sulfide-based ASSBs. Therefore, joint efforts and cooperation across the universities/research institutes, battery manufacturers, equipment manufacturers and material suppliers are highly recommended to promote the research and

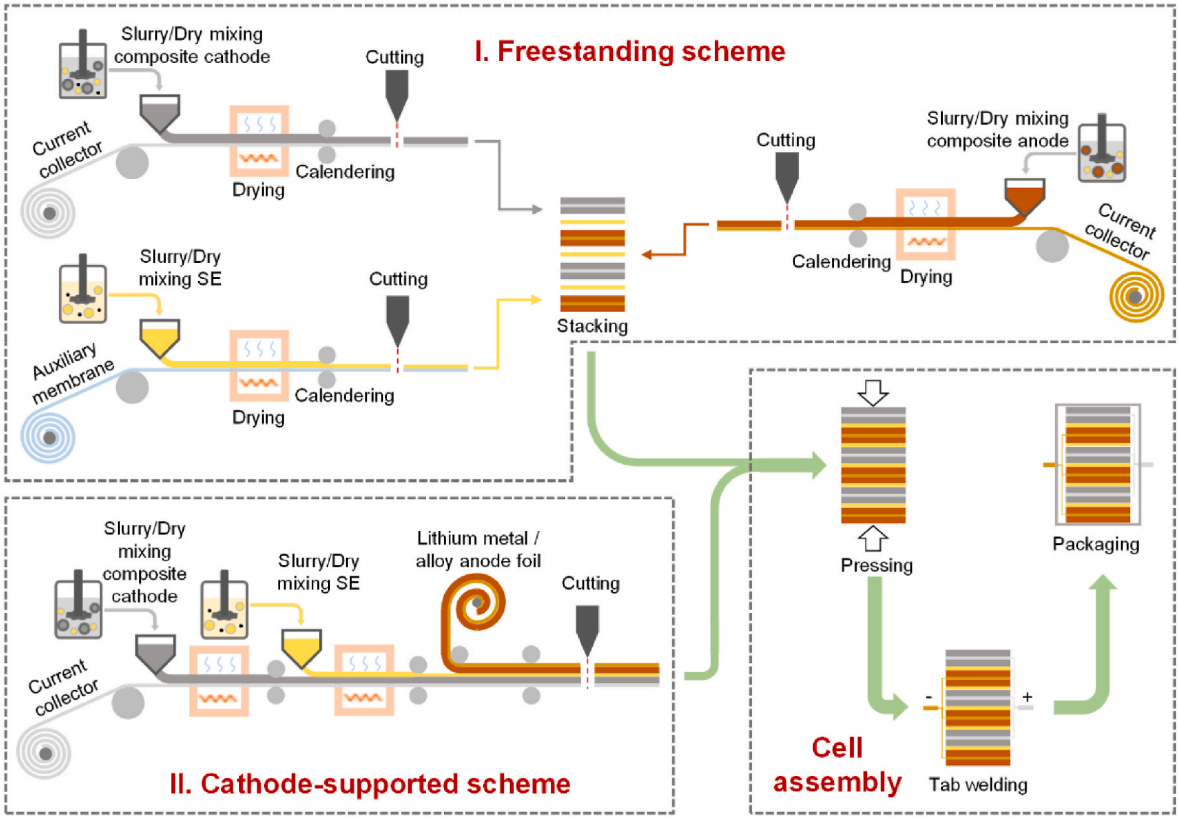

Fig. 19. Illustration of the freestanding and cathode-supported ASSB assembly schemes.

development of sulfide-based ASSBs.

Despite the difficulties from the material, cell to manufacturing aspects, several leading companies have announced their production schedules of sulfide-based ASSBs, as summarized in Fig. 20. Ah-level prototype sulfide-based ASSBs were successfully fabricated in the laboratory [37,279]. According to their roadmaps and production schedules, the large-scale production of sulfide-based ASSBs with be carried out in two stages. In the first stage (2024–2027), the first-generation ASSBs with conventional NCM cathodes and graphite/Si anodes will be launched. The first-generation ASSBs are predicted to have energy densities of 300–400 $Wh{\cdot}kg^{-1}$, close to those of the next-generation liquid electrolyte LIBs and semi-solid LIBs. The first-generation ASSBs have the advantage of much better safety performance, and can simplify the safety design at the battery module and pack level, thus increasing the gravimetric & volumetric energy density of the battery pack. The second-generation ASSBs will be commercialized in around 2030 along with the application of next-generation cathodes (e.g., Li-rich and high-voltage cathodes), anodes (e.g., high Si anode, Li metal anode, and anode-free design) and ultrathin SE membranes, as well innovative battery designs such as the bipolar design [331,332]. The second-generation ASSBs will exhibit high energy density of over 450 $Wh{\cdot}kg^{-1}$ and 1000 $Wh{\cdot}L^{-1}$, superior power characteristics, cycle life and safety performance. Moreover, the continuous research and development of ASSBs will bring comprehensive innovations in advanced structural designs of cells, modules and packs, and also a revolution in the manufacturing process of batteries.

7.4. Summary and prospects

Driven by their prospects of improved safety, high energy density and enhanced power capability, automotive/battery manufacturers raise high expectations for sulfide-based ASSBs as a game-changing technology to make EVs more competitive. Despite the extensive efforts and significant advances that have been made so far, the practical application of sulfide-based ASSBs still faces several critical challenges, calling for joint cooperation across the battery community. This review summarizes the critical challenges of sulfide-based ASSBs, from material instabilities, interfacial failures, transport and mechanical issues within composite electrodes, and cell KPIs, to eventual scaling-up fabrication processes. Recent advances and future opportunities in fundamental understanding and promising solutions are highlighted, aiming to provide a comprehensive overview of the research and development of practical sulfide-based ASSBs.

At the material level, sulfide SEs, cathode materials and anode materials are the core materials for sulfide-based ASSBs. Sulfide SEs suffer from air instability and limited ESW, which hinder the mass manufacturing and application of sulfide SEs. The HSAB theory has been generally applied to interpret the air instability problem and guide the development of air-stable sulfide SEs. Introduction of H_2S absorbent, element substitution, surface engineering and constructing sulfide-polymer composite SEs are several practical strategies to improve the air stability of sulfide SEs. However, a decrease in ionic conductivity is usually unavoidable. Thus, continuous efforts are required to balance the air stability and ionic conductivity of sulfide SEs. For electrochemical instability problems, it is very challenging to widen the intrinsic ESWs of sulfide SEs to ensure their compatibility with the operating voltage windows of the common electrode materials. Therefore, buffer layers on the CA/AN | SE interfaces are recommended to mitigate the decomposition of sulfide SEs. For the electrode materials, electrochemo-mechanical degradation is the major challenge of cathode materials in ASSBs. Refining primary grains within the secondary particles and using a single-crystalline design are effective strategies to alleviate internal stress in CAMs and prevent particle cracking during long-term cycling. Compared to the sulfide SEs and cathode materials, large uncertainties exist in the choice of anode materials for ASSBs, and several critical issues remain to be tackled. Si-based and Li metal anodes are the most promising candidates. However, they suffer from large volume expansion, unstable interface towards sulfide SEs and lithium dendrite growth. Fortunately, we have witnessed significant progress in Si-based and Li metal anodes for sulfide-based ASSBs in recent years, such as the nano-Si composite anode [34], carbon-free μSi anode [15], Li metal anode with a protective layer [125], and Ag–C composite anode [33]. These achievements significantly raise the battery community's confidence in the practical application of long-cycle-life Si-based and Li metal anodes for sulfide-based ASSBs.

At the interface level, the major concerns are the SCL effect, (electro-)chemical side reactions and mechanical instability. The formation of the Li^+ depletion layer due to the SCL effect, the interphases from side reactions, and the voids due to mechanical instability can impede the Li^+/e^- transport across the interface, resulting in high energy barrier and slow charge transfer kinetics. The interfacial issues at the AM | SE interface are multi-interdisciplinary problems that require joint research efforts from various fields, such as chemistry, physics, material science and mechanics. First-principle calculations combined with advanced characterization techniques are highly recommended to understand the nature of the complex interfacial behaviors. Quantitative electrochemical analysis and modeling are also suggested to decouple the interactions of various interfacial problems and quantify their individual effects on the interfacial charge transport process. Constructing a buffer layer (or coating layer) to avoid direct contact between AMs and sulfide SEs is the most effective strategy to mitigate the interfacial problems within sulfide-based ASSBs. Effective coating layers at the CA | SE interface have been widely reported. In contrast, the buffer layer at the AN | SE interface requires further explorations, especially for Si-based anodes. Innovative interfacial design (such as the built-in electric field strategy [162] and surface sulfidation strategy [185]) based on fundamental understandings of interfacial behaviors is also strongly encouraged.

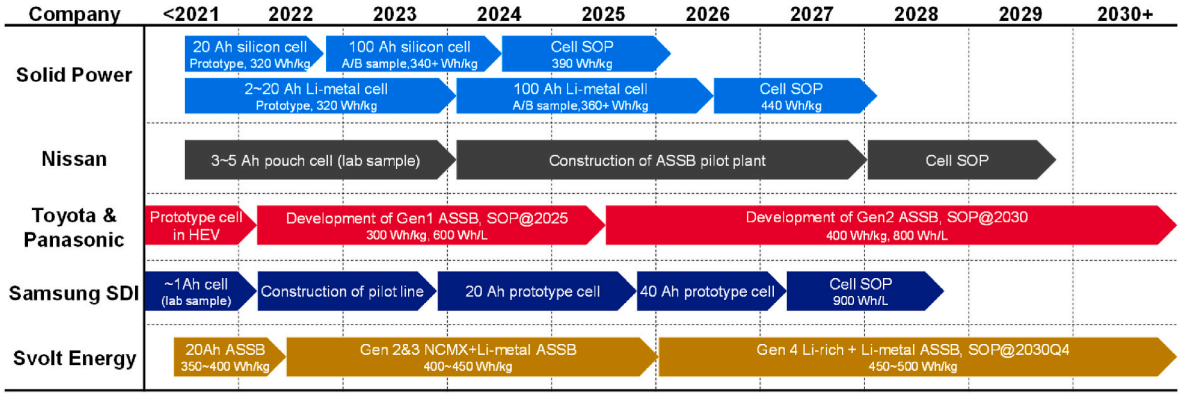

Fig. 20. Production schedules of sulfide-based ASSB from representative companies [41,333–336].

At the composite electrode level, transport limitation and mechanical failure are the bottlenecks limiting the capacity utilization of sulfide-based ASSBs under high loading and C-rates. Highly tortuous and sluggish Li^+/e^- transport pathways are usually formed in the composite electrodes of ASSBs due to the non-uniform distribution of solid particles and insufficient solid-solid contact. The microstructural design regarding weight/volume ratio, particle size, morphology and distribution of each component is essential to achieve high energy density and high power capability of composite electrodes. Recently, 3D microstructure-resolved modeling has been proven an effective tool for the rational optimization of composite electrodes. Though there are still some limitations, we believe that microstructural modeling combined with advanced characterization techniques and artificial intelligence tools will accelerate the rational design of composite electrodes for ASSBs. In the mechanical aspect, void formation and cracking/pulverization of the AM particles are regarded as the primary cause of the capacity degradation of ASSBs. Using mechanical robust cathodes (e.g., single-crystalline cathodes), nano-sized Si anode and appropriate binders can effectively mitigate the mechanical failure of ASSBs. Applying proper fabrication and stack pressures can also help to tackle the mechanical problems in ASSBs, but the optimal pressure values require careful consideration.

At the cell level, we emphasize the necessity of a comprehensive evaluation of the KPIs (energy & power characteristics, cycle & calendar lifetime, and safety) of sulfide-based ASSBs before their practical application. Based on a survey of the literature, we conclude that the rate performance and cycle lifetime of existing sulfide-based ASSBs are still below the EVs' requirements. Nevertheless, several sulfide-based ASSBs with high rate performance and long cycle life have been reported in recent years, benefiting from the continuous progress at the material, interface and composite electrode levels. For safety performance, we point out that safety concerns still exist in sulfide-based ASSBs. Moreover, potential safety hazards of sulfide-based ASSBs that require further investigation are proposed, including exothermic reactions induced by highly oxidative cathodes and oxygen, lithium dendrite growth and Li metal melting, and the chemical hazards related to released gases such as H_2S and SO_2.

Finally, critical issues for scaling up sulfide-based ASSBs are discussed in this paper. Three representative fabrication methods for sheet-type electrodes and SE membranes, and potential schemes for ASSB assembly are introduced. The wet-processing methods, i.e., slurry casting and SE solution infiltration, would be firstly applied in scaling up sulfide-based ASSBs, considering the accumulated experience in manufacturing conventional LIBs. The solvent-free dry-film method is an innovative technology that can reduce production costs and improve the overall battery performance, and worth further investigation. A forecast of future development and application of sulfide-based ASSBs is also presented based on the production schedules from several leading companies. Considering the interdisciplinary nature of battery research, we strongly encourage joint efforts and cooperation across the universities/research institutes, battery/equipment/automotive manufacturers and material suppliers to promote the development of sulfide-based ASSBs.

CRediT authorship contribution statement

Dongsheng Ren: Conceptualization, Methodology, Investigation, Data curation, Visualization, Formal analysis, Writing – original draft. **Languang Lu:** Conceptualization, Methodology, Formal analysis, Reviewing & Revising Draft. **Rui Hua:** Investigation, Data curation, Reviewing & Revising Draft. **Gaolong Zhu:** Investigation, Data curation. **Xiang Liu:** Formal analysis, Reviewing & Revising Draft. **Yuqiong Mao:** Investigation, Data curation, Reviewing & Revising Draft. **Xinyu Rui:** Investigation, Data curation, Reviewing & Revising Draft. **Shan Wang:** Investigation, Data curation, Reviewing & Revising Draft. **Bosheng Zhao:** Investigation, Data curation, Reviewing & Revising Draft. **Hao Cui:** Reviewing & Revising Draft. **Min Yang:** Investigation, Data curation. **Haorui Shen:** Data curation, Reviewing & Revising Draft. **Chen-Zi Zhao:** Investigation, Data curation. **Li Wang:** Formal analysis, Reviewing & Revising Draft. **Xiangming He:** Formal analysis, Reviewing & Revising Draft. **Saiyue Liu:** Investigation, Data curation. **Yukun Hou:** Investigation, Data curation. **Tiening Tan:** Investigation, Data curation. **Pengbo Wang:** Investigation, Data curation. **Yoshiaki Nitta:** Reviewing & Revising Draft. **Minggao Ouyang:** Methodology, Supervision, Funding acquisition, Reviewing & Revising Draft.

Declaration of competing interest

The authors declare that they have no known competing financial interests or personal relationships that could have appeared to influence the work reported in this paper.

Data availability

Data will be made available on request.

Acknowledgements

This work was supported by the National Key R&D Program-Strategic Scientific and Technological Innovation Cooperation [2022YFE0207900], the National Key R&D Program of China [2022YFB2502102, 2022YFB2404300], the National Natural Science Foundation of China [52007099, 52076121, 52177217, 22005200], and Sichuan Science and Technology Program [23QYCX0034, 2021ZYGY022, 2022ZYD0125]. The first author thanks the support from Young Elite Scientists Sponsorship Program by CAST [No. YESS20220063].

Appendix A. Supplementary data

Supplementary data to this article can be found online at https://doi.org/10.1016/j.etran.2023.100272.

References

[1] Frith JT, Lacey MJ, Ulissi U. A non-academic perspective on the future of lithium-based batteries. Nat Commun 2023;14:420. https://doi.org/10.1038/s41467-023-35933-2.
[2] Sun X, Ouyang M, Hao H. Surging lithium price will not impede the electric vehicle boom. Joule 2022;6:1738–42. https://doi.org/10.1016/j.joule.2022.06.028.
[3] McKinsey, Company. Building better batteries : insights on chemistry and design from China. 2023. https://www.mckinsey.com/industries/automotive-and-assembly/our-insights/building-better-batteries-insights-on-chemistry-and-design-from-china. [Accessed 27 March 2023].
[4] SNE Research. Global EV battery usage posted 517.9 GWh. 71.8% YoY growth 2023. 2022 Jan-Dec. https://www.sneresearch.com/en/insight/release_view/68/page/0. [Accessed 27 March 2023].
[5] Li Y, Wei Y, Zhu F, Du J, Zhao Z, Ouyang M. The path enabling storage of renewable energy toward carbon neutralization in China. ETransportation 2023;16:100226. https://doi.org/10.1016/j.etran.2023.100226.
[6] Li Q, Yu X, Li H. Batteries: from China's 13th to 14th five-year plan. ETransportation 2022;14:100201. https://doi.org/10.1016/j.etran.2022.100201.
[7] Feng X, Ren D, He X, Ouyang M. Mitigating thermal runaway of lithium-ion batteries. Joule 2020;4:743–70. https://doi.org/10.1016/j.joule.2020.02.010.
[8] Ma J, Li Y, Grundish NS, Goodenough JB, Chen Y, Guo L, et al. The 2021 battery technology roadmap. J Phys D Appl Phys 2021;54:183001. https://doi.org/10.1088/1361-6463/abd353.
[9] Zhao L, Lakraychi AE, Chen Z, Liang Y, Yao Y. Roadmap of solid-state lithium-organic batteries toward 500 Wh kg-1. ACS Energy Lett 2021;6:3287–306. https://doi.org/10.1021/acsenergylett.1c01368.
[10] Wu D, Wu F. Toward better batteries: solid-state battery roadmap 2035+. ETransportation 2023;16:100224. https://doi.org/10.1016/j.etran.2022.100224.
[11] Zhao M, Li BQ, Zhang XQ, Huang JQ, Zhang Q. A perspective toward practical lithium-sulfur batteries. ACS Cent Sci 2020;6:1095–104. https://doi.org/10.1021/acscentsci.0c00449.
[12] Fichtner M. Recent research and progress in batteries for electric vehicles. Batter Supercaps 2022;5:e202100224. https://doi.org/10.1002/batt.202100224.

[13] https://www.nissan-global.com/EN/INNOVATION/TECHNOLOGY/ARCHIVE/ASSB/. [Accessed 27 March 2023].
[14] https://global.honda/innovation/advanced-technology/all-solid-state-battery.html. [Accessed 27 March 2023].
[15] Tan DHS, Chen YT, Yang H, Bao W, Sreenarayanan B, Doux JM, et al. Carbon-free high-loading silicon anodes enabled by sulfide solid electrolytes. Science 2021; 373:1494–9. https://doi.org/10.1126/science.abg7217. 80.
[16] Wu Y, Zhou K, Ren F, Ha Y, Liang Z, Zheng X, et al. Highly reversible Li_2RuO_3 cathodes in sulfide-based all solid-state lithium batteries. Energy Environ Sci 2022;15:3470–82. https://doi.org/10.1039/d2ee01067d.
[17] Song Y, Sheng L, Wang L, Xu H, He X. Electrochemistry Communications from separator to membrane : separators can function more in lithium ion batteries. Electrochem Commun 2021;124:106948. https://doi.org/10.1016/j.elecom.2021.106948.
[18] Shen M, Wang Z, Cheng D, Cheng H, Xu H, Huang Y. Molecular regulated polymer electrolytes for solid-state lithium metal batteries : mechanisms and future prospects. ETransportation 2023;18:100264. https://doi.org/10.1016/j.etran.2023.100264.
[19] Kim KJ, Balaish M, Wadaguchi M, Kong L, Rupp JLM. Solid-state Li–metal batteries: challenges and horizons of oxide and sulfide solid electrolytes and their interfaces. Adv Energy Mater 2021;11:1–63. https://doi.org/10.1002/aenm.202002689.
[20] Yu X, Chen R, Gan L, Li H, Chen L. Battery safety: from lithium-ion to solid-state batteries. Engineering 2023;21:9–14. https://doi.org/10.1016/j.eng.2022.06.022.
[21] Li X, Liang J, Yang X, Adair KR, Wang C, Zhao F, et al. Progress and perspectives on halide lithium conductors for all-solid-state lithium batteries. Energy Environ Sci 2020;13:1429–61. https://doi.org/10.1039/c9ee03828k.
[22] Kamaya N, Homma K, Yamakawa Y, Hirayama M, Kanno R, Yonemura M, et al. A lithium superionic conductor. Nat Mater 2011;10:682–6. https://doi.org/10.1038/nmat3066.
[23] Mizuno F, Hayashi A, Tadanaga K, Tatsumisago M. High lithium ion conducting glass-ceramics in the system Li_2S-P_2S_5. Solid State Ionics 2006;177:2721–5. https://doi.org/10.1016/j.ssi.2006.04.017.
[24] Yamane H, Shibata M, Shimane Y, Junke T, Seino Y, Adams S, et al. Crystal structure of a superionic conductor. $Li_7P_3S_{11}$. Solid State Ionics 2007;178:1163–7. https://doi.org/10.1016/j.ssi.2007.05.020.
[25] Homma K, Yonemura M, Kobayashi T, Nagao M, Hirayama M, Kanno R. Crystal structure and phase transitions of the lithium ionic conductor Li3PS4. Solid State Ionics 2011;182:53–8. https://doi.org/10.1016/j.ssi.2010.10.001.
[26] Deiseroth HJ, Kong ST, Eckert H, Vannahme J, Reiner C, Zaiß T, et al. Li6PS5X: a class of crystalline Li-rich solids with an unusually high Li+ mobility. Angew Chem, Int Ed 2008;47:755–8. https://doi.org/10.1002/anie.200703900.
[27] Boulineau S, Courty M, Tarascon JM, Viallet V. Mechanochemical synthesis of Li-argyrodite Li 6PS 5X (X = Cl, Br, I) as sulfur-based solid electrolytes for all solid state batteries application. Solid State Ionics 2012;221:1–5. https://doi.org/10.1016/j.ssi.2012.06.008.
[28] Rao RP, Adams S. Studies of lithium argyrodite solid electrolytes for all-solid-state batteries. Phys Status Solidi Appl Mater Sci 2011;208. https://doi.org/10.1002/pssa.201001117. 1804–7.
[29] Kanno R, Hata T, Kawamoto Y, Irie M. Synthesis of a new lithium ionic conductor, thio-LISICON-lithium germanium sulfide system. Solid State Ionics 2000;130: 97–104. https://doi.org/10.1016/S0167-2738(00)00277-0.
[30] Kanno R, Murayama M. Lithium ionic conductor thio-LISICON: the Li2S-GeS2-P2S5 system. J Electrochem Soc 2001;148:A742. https://doi.org/10.1149/1.1379028.
[31] Sahu G, Lin Z, Li J, Liu Z, Dudney N, Liang C. Air-stable, high-conduction solid electrolytes of arsenic-substituted Li4SnS4. Energy Environ Sci 2014;7:1053–8. https://doi.org/10.1039/c3ee43357a.
[32] Kato Y, Hori S, Saito T, Suzuki K, Hirayama M, Mitsui A, et al. High-power all-solid-state batteries using sulfide superionic conductors. Nat Energy 2016;1: 16030. https://doi.org/10.1038/nenergy.2016.30.
[33] Lee YG, Fujiki S, Jung C, Suzuki N, Yashiro N, Omoda R, et al. High-energy long-cycling all-solid-state lithium metal batteries enabled by silver–carbon composite anodes. Nat Energy 2020;5:299–308. https://doi.org/10.1038/s41560-020-0575-z.
[34] Cao D, Sun X, Li Y, Anderson A, Lu W, Zhu H. Long-cycling sulfide-based all-solid-state batteries enabled by electrochemo-mechanically stable electrodes. Adv Mater 2022;34:2200401. https://doi.org/10.1002/adma.202200401.
[35] Liu S, Zhou L, Han J, Wen K, Guan S, Xue C, et al. Super long-cycling all-solid-state battery with thin Li6PS5Cl-based electrolyte. Adv Energy Mater 2022;12: 2200660. https://doi.org/10.1002/aenm.202200660.
[36] https://www.solidpowerbattery.com/about/. [Accessed 27 March 2023].
[37] Svolt successfully develops solid state cell with sulfide-based electrolyte. 2022. https://batteriesnews.com/svolt-successfully-develops-solid-state-cell-sulfide-based-electrolyte/. [Accessed 27 March 2023].
[38] Mitsui Kinzoku initiates supply of A-SoliD. A solid electrolyte for all-solid- state batteries , from its mass production testing facility. 2021. https://www.mitsui-kinzoku.com/LinkClick.aspx?fileticket=yZ3Xf%2BC1Kfo%3D&tabid=278&mid=824. [Accessed 27 March 2023].
[39] POSCO Group produces solid electrolyte “dream material” in earnest. 2022. https://newsroom.posco.com/en/posco-group-produces-solid-electrolyte-dream-material-in-earnest/. [Accessed 27 March 2023].
[40] Samsung SDI. Began construction of the solid-state battery’s pilot line. 2022. https://www.samsungsdi.com/sdi-news/2602.html. [Accessed 27 March 2023].
[41] Nissan unveils prototype production facility for all-solid-state batteries. 2022. https://global.nissannews.com/en/releases/nissan-prototype-production-facility-for-all-solid-state-batteries. [Accessed 27 March 2023].
[42] Solid Power. BMW partner to develop next-generation EV batteries. 2017. https://www.reuters.com/article/us-bmw-solid-power/solid-power-bmw-partner-to-develop-next-generation-ev-batteries-idUSKBN1EC16V. [Accessed 27 March 2023].
[43] Next-generation batteries options: storage battery technologies for automotive applications. 2019. https://www.marklines.com/en/report_all/rep1840_201903. [Accessed 27 March 2023].
[44] Day L. Toyota is road testing a prototype solid state battery EV. 2021. https://www.thedrive.com/tech/42287/toyota-is-road-testing-a-prototype-solid-state-battery-ev. [Accessed 27 March 2023].
[45] Samsung presents groundbreaking all-solid-state battery technology to ‘nature energy’. 2020. https://news.samsung.com/global/samsung-presents-groundbreaking-all-solid-state-battery-technology-to-nature-energy. [Accessed 27 March 2023].
[46] Maeda M. Toyota’ s battery development and supply. 2021. https://global.toyota/pages/news/images/2021/09/battery/battery_01_en.pdf. [Accessed 27 March 2023].
[47] Robinson BAL. Solid-state batteries enter EV fray. MRS Bull 2014;39:1046–7.
[48] Walz E. Toyota expands partnership with panasonic on battery technology. 2018. https://www.futurecar.com/1751/Toyota-Expands-Partnership-With-Panasonic-on-Battery-Technology. [Accessed 27 March 2023].
[49] Honda considers developing all solid-state EV batteries. 2017. https://www.reuters.com/article/us-honda-nissan-idUSKBN1EF0FM. [Accessed 27 March 2023].
[50] Honda and Nissan said to be developing next-generation solid-state batteries for electric vehicles. 2017. https://www.japantimes.co.jp/news/2017/12/21/business/honda-nissan-said-developing-next-generation-solid-state-batteries-electric-vehicles/. [Accessed 27 March 2023].
[51] Zhang Q, Cao D, Ma Y, Natan A, Aurora P, Zhu H. Sulfide-based solid-state electrolytes: synthesis, stability, and potential for all-solid-state batteries. Adv Mater 2019;31:1901131. https://doi.org/10.1002/adma.201901131.
[52] Wang H, Zhu J, Su Y, Gong Z, Yang Y. Interfacial compatibility issues in rechargeable solid-state lithium metal batteries: a review. Sci China Chem 2021; 64:879–98. https://doi.org/10.1007/s11426-021-9985-x.
[53] Chen C, Jiang M, Zhou T, Raijmakers L, Vezhlev E, Wu B, et al. Interface aspects in all-solid-state Li-based batteries reviewed. Adv Energy Mater 2021;11: 2003939. https://doi.org/10.1002/aenm.202003939.
[54] Banerjee A, Wang X, Fang C, Wu EA, Meng YS. Interfaces and interphases in all-solid-state batteries with inorganic solid electrolytes. Chem Rev 2020;120: 6878–933. https://doi.org/10.1021/acs.chemrev.0c00101.
[55] Zhang Q-B, Gong Z-L, Yang Y. Advance in interface and characterizations of sulfide solid electrolyte materials. Acta Phys Sin 2020;69:228803–228803. https://doi.org/10.7498/aps.69.20201581.
[56] Wang C, Adair K, Sun X. All-solid-state lithium metal batteries with sulfide electrolytes: understanding interfacial ion and electron transport. Acc Mater Res 2022;3:21–32. https://doi.org/10.1021/accountsmr.1c00137.
[57] Deysher G, Ridley P, Ham S-Y, Doux J-M, Chen Y-T, Wu EA, et al. Transport and mechanical aspects of all-solid-state lithium batteries. Mater Today Phys 2022;24: 100679. https://doi.org/10.1016/j.mtphys.2022.100679.
[58] Tan DHS, Meng YS, Jang J. Scaling up high-energy-density sulfidic solid-state batteries: a lab-to-pilot perspective. Joule 2022;6:1755–69. https://doi.org/10.1016/j.joule.2022.07.002.
[59] Nikodimos Y, Huang CJ, Taklu BW, Su WN, Hwang BJ. Chemical stability of sulfide solid-state electrolytes: stability toward humid air and compatibility with solvents and binders. Energy Environ Sci 2022;15:991–1033. https://doi.org/10.1039/d1ee03032a.
[60] Lu P, Wu D, Chen L, Li H, Wu F. Air stability of solid-state sulfide batteries and electrolytes. Electrochem Energy Rev 2022;5:3. https://doi.org/10.1007/s41918-022-00149-3.
[61] Liang Y, Liu H, Wang G, Wang C, Ni Y, Nan CW, et al. Challenges, interface engineering, and processing strategies toward practical sulfide-based all-solid-state lithium batteries. InfoMat 2022;4:1–66. https://doi.org/10.1002/inf2.12292.
[62] Karabelli D, Birke KP, Weeber M. A performance and cost overview of selected solid-state electrolytes: race between polymer electrolytes and inorganic sulfide electrolytes. Batteries 2021;7:18. https://doi.org/10.3390/batteries7010018.
[63] Bai X, Yu T, Ren Z, Gong S, Yang R, Zhao C. Key issues and emerging trends in sulfide all solid state lithium battery. Energy Storage Mater 2022;51:527–49. https://doi.org/10.1016/j.ensm.2022.07.006.
[64] Batzer M, Heck C, Michalowski P, Kwade A. Current status of formulations and scalable processes for producing sulfidic solid-state batteries. Batter Supercaps 2022;5:e202200328. https://doi.org/10.1002/batt.202200328.
[65] Zhang H, Zhang J. An overview of modification strategies to improve LiNi0·8Co0·1Mn0·1O2 (NCM811) cathode performance for automotive lithium-ion batteries. ETransportation 2021;7:100105. https://doi.org/10.1016/j.etran.2021.100105.
[66] Han X, Lu L, Zheng Y, Feng X, Li Z, Li J, et al. A review on the key issues of the lithium ion battery degradation among the whole life cycle. ETransportation 2019;1:100005. https://doi.org/10.1016/j.etran.2019.100005.
[67] Oh P, Yun J, Choi JH, Saqib KS, Embleton TJ, Park S, et al. Development of high-energy anodes for all-solid-state lithium batteries based on sulfide electrolytes. Angew Chem 2022;134:e202201249. https://doi.org/10.1002/ange.202201249.

[68] Wang X, He K, Li S, Zhang J, Lu Y. Realizing high-performance all-solid-state batteries with sulfide solid electrolyte and silicon anode: a review. Nano Res 2022:1–25. https://doi.org/10.1007/s12274-022-4526-9.

[69] Xiao Y, Miara LJ, Wang Y, Ceder G. Computational screening of cathode coatings for solid-state batteries. Joule 2019;3:1252–75. https://doi.org/10.1016/j.joule.2019.02.006.

[70] Shen Z, Zhang W, Zhu G, Huang Y, Feng Q, Lu Y. Design principles of the anode–electrolyte interface for all solid-state lithium metal batteries. Small Methods 2020;4:1900592. https://doi.org/10.1002/smtd.201900592.

[71] Wu B, Wang S, Lochala J, Desrochers D, Liu B, Zhang W, et al. The role of the solid electrolyte interphase layer in preventing Li dendrite growth in solid-state batteries. Energy Environ Sci 2018;11:1803–10. https://doi.org/10.1039/C8EE00540K.

[72] Kaiser N, Spannenberger S, Schmitt M, Cronau M, Kato Y, Roling B. Ion transport limitations in all-solid-state lithium battery electrodes containing a sulfide-based electrolyte. J Power Sources 2018;396:175–81. https://doi.org/10.1016/j.jpowsour.2018.05.095.

[73] Naik KG, Vishnugopi BS, Mukherjee PP. Kinetics or transport: whither goes the solid-state battery cathode? ACS Appl Mater Interfaces 2022;14:29754–65. https://doi.org/10.1021/acsami.2c04962.

[74] Minnmann P, Strauss F, Bielefeld A, Ruess R, Adelhelm P, Burkhardt S, et al. Designing cathodes and cathode active materials for solid-state batteries. Adv Energy Mater 2022;12:2201425. https://doi.org/10.1002/aenm.202201425.

[75] Nam YJ, Oh DY, Jung SH, Jung YS. Toward practical all-solid-state lithium-ion batteries with high energy density and safety: comparative study for electrodes fabricated by dry- and slurry-mixing processes. J Power Sources 2018;375:93–101. https://doi.org/10.1016/j.jpowsour.2017.11.031.

[76] Bae Song Y, Kwak H, Cho W, Kim KS, Seok Jung Y, Park KH. Electrochemo-mechanical effects as a critical design factor for all-solid-state batteries. Curr Opin Solid State Mater Sci 2022;26:100977. https://doi.org/10.1016/j.cossms.2021.100977.

[77] Sakka Y, Yamashige H, Watanabe A, Takeuchi A, Uesugi M, Uesugi K, et al. Pressure dependence on the three-dimensional structure of a composite electrode in an all-solid-state battery. J Mater Chem A 2022;10:16602–9. https://doi.org/10.1039/d2ta02378d.

[78] Zhang F, Guo Y, Zhang L, Jia P, Liu X, Qiu P, et al. A review of the effect of external pressure on all-solid-state batteries. ETransportation 2023;15:100220. https://doi.org/10.1016/j.etran.2022.100220.

[79] Kim T, Kim K, Lee S, Song G, Jung MS, Lee KT. Thermal runaway behavior of Li6PS5Cl solid electrolytes for LiNi0.8Co0.1Mn0.1O2 and LiFePO4 in all-solid-state batteries. Chem Mater 2022;34:9159–71. https://doi.org/10.1021/acs.chemmater.2c02106.

[80] Wang S, Wu Y, Ma T, Chen L, Li H, Wu F. Thermal stability between sulfide solid electrolytes and oxide cathode. ACS Nano 2022;16:16158–76. https://doi.org/10.1021/acsnano.2c04905.

[81] Zhu Y, He X, Mo Y. Origin of outstanding stability in the lithium solid electrolyte materials: insights from thermodynamic analyses based on first-principles calculations. ACS Appl Mater Interfaces 2015;7:23685–93. https://doi.org/10.1021/acsami.5b07517.

[82] Liu H, Liang Y, Wang C, Li D, Yan X, Nan C, et al. Priority and prospect of sulfide-based solid-electrolyte membrane. Adv Mater 2022:2206013. https://doi.org/10.1002/adma.202206013.

[83] Park KH, Bai Q, Kim DH, Oh DY, Zhu Y, Mo Y, et al. Design strategies, practical considerations, and new solution processes of sulfide solid electrolytes for all-solid-state batteries. Adv Energy Mater 2018;8:1800035. https://doi.org/10.1002/aenm.201800035.

[84] Tsukasaki H, Sano H, Igarashi K, Wakui A, Yaguchi T, Mori S. Deterioration process of argyrodite solid electrolytes during exposure to humidity-controlled air. J Power Sources 2022;524:231085. https://doi.org/10.1016/j.jpowsour.2022.231085.

[85] Cai Y, Li C, Zhao Z, Mu D, Wu B. Air stability and interfacial compatibility of sulfide solid electrolytes for solid-state lithium batteries: advances and perspectives. Chemelectrochem 2022;9:e202101479. https://doi.org/10.1002/celc.202101479.

[86] Pearson RG. Hard and soft acids and bases. J Am Chem Soc 1963;85:3533–9. https://doi.org/10.1021/ja00905a001.

[87] Zhu Y, Mo Y. Materials design principles for air-stable lithium/sodium solid electrolytes. Angew Chem, Int Ed 2020;59:17472–6. https://doi.org/10.1002/anie.202007621.

[88] Kim JS, Jung WD, Shin SS, Yang S, Park S, Lee JH, et al. Roles of polymerized anionic clusters stimulating for hydrolysis deterioration in Li7P3S11. J Phys Chem C 2021;125:19509–16. https://doi.org/10.1021/acs.jpcc.1c05034.

[89] Hayashi A, Muramatsu H, Ohtomo T, Hama S, Tatsumisago M. Improvement of chemical stability of Li3PS4 glass electrolytes by adding MxOy (M = Fe, Zn, and Bi) nanoparticles. J Mater Chem A 2013;1:6320–6. https://doi.org/10.1039/c3ta10247e.

[90] Zhao F, Alahakoon SH, Adair K, Zhang S, Xia W, Li W, et al. An air-stable and Li-Metal-Compatible glass-ceramic electrolyte enabling high-performance all-solid-state Li metal batteries. Adv Mater 2021;33:2006577. https://doi.org/10.1002/adma.202006577.

[91] Lu P, Liu L, Wang S, Xu J, Peng J, Yan W, et al. Superior all-solid-state batteries enabled by a gas-phase-synthesized sulfide electrolyte with ultrahigh moisture stability and ionic conductivity. Adv Mater 2021;33:2100921. https://doi.org/10.1002/adma.202100921.

[92] Zhao F, Liang J, Yu C, Sun Q, Li X, Adair K, et al. A versatile Sn-substituted argyrodite sulfide electrolyte for all-solid-state Li metal batteries. Adv Energy Mater 2020;10:1903422. https://doi.org/10.1002/aenm.201903422.

[93] Liang J, Chen N, Li X, Li X, Adair KR, Li J, et al. Li10Ge(P1-xSb x)2S12 lithium-ion conductors with enhanced atmospheric stability. Chem Mater 2020;32:2664–72. https://doi.org/10.1021/acs.chemmater.9b04764.

[94] Jung WD, Jeon M, Shin SS, Kim JS, Jung HG, Kim BK, et al. Functionalized sulfide solid electrolyte with air-stable and chemical-resistant oxysulfide nanolayer for all-solid-state batteries. ACS Omega 2020;5:26015–22. https://doi.org/10.1021/acsomega.0c03453.

[95] Xu J, Li Y, Lu P, Yan W, Yang M, Li H, et al. Water-stable sulfide solid electrolyte membranes directly applicable in all-solid-state batteries enabled by superhydrophobic Li + -conducting protection layer. Adv Energy Mater 2022;12:2102348. https://doi.org/10.1002/aenm.202102348.

[96] Tan DHS, Banerjee A, Deng Z, Wu EA, Nguyen H, Doux JM, et al. Enabling thin and flexible solid-state composite electrolytes by the scalable solution process. ACS Appl Energy Mater 2019;2:6542–50. https://doi.org/10.1021/acsaem.9b01111.

[97] Zheng Y, Yao Y, Ou J, Li M, Luo D, Dou H, et al. A review of composite solid-state electrolytes for lithium batteries: fundamentals, key materials and advanced structures. Chem Soc Rev 2020;49:8790–839. https://doi.org/10.1039/d0cs00305k.

[98] Ren HT, Zhang ZQ, Zhang JZ, Peng LF, He ZY, Yu M, et al. Improvement of stability and solid-state battery performances of annealed 70Li2S–30P2S5 electrolytes by additives. Rare Met 2022;41:106–14. https://doi.org/10.1007/s12598-021-01804-2.

[99] Han F, Zhu Y, He X, Mo Y, Wang C. Electrochemical stability of Li10GeP2S12 and Li7La3Zr2O12 solid electrolytes. Adv Energy Mater 2016;6:1501590. https://doi.org/10.1002/aenm.201501590.

[100] Zhu Y, He X, Mo Y. First principles study on electrochemical and chemical stability of solid electrolyte-electrode interfaces in all-solid-state Li-ion batteries. J Mater Chem A 2016;4:3253–66. https://doi.org/10.1039/c5ta08574h.

[101] Zhang Z, Zhang L, Yan X, Wang H, Liu Y, Yu C, et al. All-in-one improvement toward Li6PS5Br-Based solid electrolytes triggered by compositional tune. J Power Sources 2019;410–411:162–70. https://doi.org/10.1016/j.jpowsour.2018.11.016.

[102] Xu H, Yu Y, Wang Z, Shao G. A theoretical approach to address interfacial problems in all-solid-state lithium ion batteries: tuning materials chemistry for electrolyte and buffer coatings based on Li6PA5Cl hali-chalcogenides. J Mater Chem A 2019;7:5239–47. https://doi.org/10.1039/c8ta11151k.

[103] Wu F, Fitzhugh W, Ye L, Ning J, Li X. Advanced sulfide solid electrolyte by core-shell structural design. Nat Commun 2018;9:4037. https://doi.org/10.1038/s41467-018-06123-2.

[104] Nakamura T, Amezawa K, Kulisch J, Zeier WG, Janek J. Guidelines for all-solid-state battery design and electrode buffer layers based on chemical potential profile calculation. ACS Appl Mater Interfaces 2019;11:19968. https://doi.org/10.1021/acsami.9b03053. –76.

[105] Zhou L, Park KH, Sun X, Lalère F, Adermann T, Hartmann P, et al. Solvent-engineered design of argyrodite Li 6 PS 5 X (X = Cl, Br, I) solid electrolytes with high ionic conductivity. ACS Energy Lett 2019;4:265–70. https://doi.org/10.1021/acsenergylett.8b01997.

[106] Meng X. Atomic layer deposition of solid-state electrolytes for next-generation lithium-ion batteries and beyond: opportunities and challenges. Energy Storage Mater 2020;30:296–328. https://doi.org/10.1016/j.ensm.2020.05.001.

[107] Meng X, Elam JW. Atomic-scale rational designs of superionic sulfide-based solid-state electrolytes by atomic layer deposition. ECS Meet. Abstr. 2019;MA2019– 01:155. https://doi.org/10.1149/ma2019-01/2/155.

[108] Zhang X, Wang B, Zhao S, Li H, Yu H. Oxygen anionic redox activated high-energy cathodes: status and prospects. ETransportation 2021;8:100118. https://doi.org/10.1016/j.etran.2021.100118.

[109] Zhang SS. Problems and their origins of Ni-rich layered oxide cathode materials. Energy Storage Mater 2020;24:247–54. https://doi.org/10.1016/j.ensm.2019.08.013.

[110] Lewis JA, Tippens J, Cortes FJQ, McDowell MT. Chemo-mechanical challenges in solid-state batteries. Trends Chem 2019;1:845–57. https://doi.org/10.1016/j.trechm.2019.06.013.

[111] Zhao X, Tian Y, Lun Z, Cai Z, Chen T, Ouyang B, et al. Design principles for zero-strain Li-ion cathodes. Joule 2022;6:1654–71. https://doi.org/10.1016/j.joule.2022.05.018.

[112] Zhang R, Wang C, Zou P, Lin R, Ma L, Yin L, et al. Compositionally complex doping for zero-strain zero-cobalt layered cathodes. Nature 2022;610:67–73. https://doi.org/10.1038/s41586-022-05115-z.

[113] Li W, Asl HY, Xie Q, Manthiram A. Collapse of LiNi 1– x – y Co x Mn y O 2 lattice at deep charge irrespective of nickel content in lithium-ion batteries. J Am Chem Soc 2019;141:5097–101. https://doi.org/10.1021/jacs.8b13798.

[114] Singh A, Pal S. Chemo-mechanical modeling of inter- and intra-granular fracture in heterogeneous cathode with polycrystalline particles for lithium-ion battery. J Mech Phys Solid 2022;163:104839. https://doi.org/10.1016/j.jmps.2022.104839.

[115] Jung SH, Kim U, Kim J, Jun S, Yoon CS, Jung YS, et al. Ni-Rich layered cathode materials with electrochemo-mechanically compliant microstructures for all-solid-state Li batteries. Adv Energy Mater 2020;10:1903360. https://doi.org/10.1002/aenm.201903360.

[116] Kim U-H, Lee S, Park N, Kim SJ, Yoon CS, Sun Y-K. High-energy-density Li-ion battery reaching full charge in 12 min. ACS Energy Lett 2022;7:3880–8. https://doi.org/10.1021/acsenergylett.2c02032.

[117] Han Y, Jung SH, Kwak H, Jun S, Kwak HH, Lee JH, et al. Single- or poly-crystalline Ni-rich layered cathode, sulfide or halide solid electrolyte: which will be the winners for all-solid-state batteries? Adv Energy Mater 2021;11:2100126. https://doi.org/10.1002/aenm.202100126.
[118] Wang C, Yu R, Hwang S, Liang J, Li X, Zhao C, et al. Single crystal cathodes enabling high-performance all-solid-state lithium-ion batteries. Energy Storage Mater 2020;30:98–103. https://doi.org/10.1016/j.ensm.2020.05.007.
[119] Li X, Peng W, Tian R, Song D, Wang Z, Zhang H, et al. Excellent performance single-crystal NCM cathode under high mass loading for all-solid-state lithium batteries. Electrochim Acta 2020;363:137185. https://doi.org/10.1016/j.electacta.2020.137185.
[120] Liu X, Xu G-L, Kolluru VSC, Zhao C, Li Q, Zhou X, et al. Origin and regulation of oxygen redox instability in high-voltage battery cathodes. Nat Energy 2022;7:808–17. https://doi.org/10.1038/s41560-022-01036-3.
[121] Shi T, Tu Q, Tian Y, Xiao Y, Miara LJ, Kononova O, et al. High active material loading in all-solid-state battery electrode via particle size optimization. Adv Energy Mater 2020;10:1902881. https://doi.org/10.1002/aenm.201902881.
[122] Dixit MB, Parejiya A, Muralidharan N, Essehli R, Amin R, Belharouak I. Understanding implications of cathode architecture on energy density of solid-state batteries. Energy Storage Mater 2021;40:239–49. https://doi.org/10.1016/j.ensm.2021.05.001.
[123] Mistry A, Heenan T, Smith K, Shearing P, Mukherjee PP. Asphericity can cause nonuniform lithium intercalation in battery active particles. ACS Energy Lett 2022;7:1871–9. https://doi.org/10.1021/acsenergylett.2c00870.
[124] Xing X, Li Y, Wang S, Liu H, Wu Z, Yu S, et al. Graphite-based lithium-free 3D hybrid anodes for high energy density all-solid-state batteries. ACS Energy Lett 2021;6:1831–8. https://doi.org/10.1021/acsenergylett.1c00627.
[125] Zhang Z, Chen S, Yang J, Wang J, Yao L, Yao X, et al. Interface Re-engineering of Li10GeP2S12 electrolyte and lithium anode for all-solid-state lithium batteries with ultralong cycle life. ACS Appl Mater Interfaces 2018;10:2556–65. https://doi.org/10.1021/acsami.7b16176.
[126] Iwao M, Sakurai R, Nakamura H, Hayakawa E, Ohsaki S, Watano S. Solid electrolyte/graphite composite particle for an all-solid-state lithium-ion battery. Adv Powder Technol 2022;33:103633. https://doi.org/10.1016/j.apt.2022.103633.
[127] Yang S, Yamamoto K, Mei X, Sakuda A, Uchiyama T, Watanabe T, et al. High rate capability from a graphite anode through surface modification with lithium iodide for all-solid-state batteries. ACS Appl Energy Mater 2022;5:667–73. https://doi.org/10.1021/acsaem.1c03166.
[128] Huo H, Janek J. Silicon as emerging anode in solid-state batteries. ACS Energy Lett 2022;7:4005–16. https://doi.org/10.1021/acsenergylett.2c01950.
[129] Lu Y, Zhao C-Z, Zhang R, Yuan H, Hou L-P, Fu Z-H, et al. The carrier transition from Li atoms to Li vacancies in solid-state lithium alloy anodes. Sci Adv 2021;7. https://doi.org/10.1126/sciadv.abi5520. eabi5520.
[130] Whiteley JM, Kim JW, Kang CS, Cho JS, Oh KH, Lee S-H. Tin networked electrode providing enhanced volumetric capacity and pressureless operation for all-solid-state Li-ion batteries. J Electrochem Soc 2015;162:A711–5. https://doi.org/10.1149/2.0751504jes.
[131] Wang C, Adair K, Sun X. All-solid-state lithium metal batteries with sulfide electrolytes: understanding interfacial ion and electron transport. Acc Mater Res 2022;3:21–32. https://doi.org/10.1021/accountsmr.1c00137.
[132] Huang W, Zhao C, Wu P, Yuan H, Feng W, Liu Z, et al. Anode-free solid-state lithium batteries: a review. Adv Energy Mater 2022;12:2201044. https://doi.org/10.1002/aenm.202201044.
[133] Mukhopadhyay A, Sheldon BW. Deformation and stress in electrode materials for Li-ion batteries. Prog Mater Sci 2014;63:58–116. https://doi.org/10.1016/j.pmatsci.2014.02.001.
[134] Richards WD, Miara LJ, Wang Y, Kim JC, Ceder G. Interface stability in solid-state batteries. Chem Mater 2016;28:266–73. https://doi.org/10.1021/acs.chemmater.5b04082.
[135] Cao D, Sun X, Li Q, Natan A, Xiang P, Zhu H. Lithium dendrite in all-solid-state batteries: growth mechanisms, suppression strategies, and characterizations. Matter 2020;3:57–94. https://doi.org/10.1016/j.matt.2020.03.015.
[136] Liu H, Sun Q, Zhang H, Cheng J, Li Y, Zeng Z, et al. The application road of silicon-based anode in lithium-ion batteries: from liquid electrolyte to solid-state electrolyte. Energy Storage Mater 2023;55:244–63. https://doi.org/10.1016/j.ensm.2022.11.054.
[137] Paul PP, Chen B-R, Langevin SA, Dufek EJ, Nelson Weker J, Ko JS. Interfaces in all solid state Li-metal batteries: a review on instabilities, stabilization strategies, and scalability. Energy Storage Mater 2022;45:969–1001. https://doi.org/10.1016/j.ensm.2021.12.021.
[138] Krauskopf T, Richter FH, Zeier WG, Janek J. Physicochemical concepts of the lithium metal anode in solid-state batteries. Chem Rev 2020;120:7745–94. https://doi.org/10.1021/acs.chemrev.0c00431.
[139] Kasemchainan J, Zekoll S, Spencer Jolly D, Ning Z, Hartley GO, Marrow J, et al. Critical stripping current leads to dendrite formation on plating in lithium anode solid electrolyte cells. Nat Mater 2019;18:1105–11. https://doi.org/10.1038/s41563-019-0438-9.
[140] Singh DK, Henss A, Mogwitz B, Gautam A, Horn J, Krauskopf T, et al. Li6PS5Cl microstructure and influence on dendrite growth in solid-state batteries with lithium metal anode. Cell Reports Phys Sci 2022;3:101043. https://doi.org/10.1016/j.xcrp.2022.101043.
[141] Luo S, Wang Z, Li X, Liu X, Wang H, Ma W, et al. Growth of lithium-indium dendrites in all-solid-state lithium-based batteries with sulfide electrolytes. Nat Commun 2021;12:6968. https://doi.org/10.1038/s41467-021-27311-7.
[142] Trevey J, Jang JS, Jung YS, Stoldt CR, Lee SH. Glass-ceramic Li2S-P2S5 electrolytes prepared by a single step ball billing process and their application for all-solid-state lithium-ion batteries. Electrochem Commun 2009;11:1830–3. https://doi.org/10.1016/j.elecom.2009.07.028.
[143] Dunlap NA, Kim S, Jeong JJ, Oh KH, Lee SH. Simple and inexpensive coal-tar-pitch derived Si-C anode composite for all-solid-state Li-ion batteries. Solid State Ionics 2018;324:207–17. https://doi.org/10.1016/j.ssi.2018.07.013.
[144] Li H, Li H, Lai Y, Yang Z, Yang Q, Liu Y, et al. Revisiting the preparation progress of nano-structured Si anodes toward industrial application from the perspective of cost and scalability. Adv Energy Mater 2022;12:2102181. https://doi.org/10.1002/aenm.202102181.
[145] Yamamoto M, Terauchi Y, Sakuda A, Takahashi M. Slurry mixing for fabricating silicon-composite electrodes in all-solid-state batteries with high areal capacity and cycling stability. J Power Sources 2018;402:506–12. https://doi.org/10.1016/j.jpowsour.2018.09.070.
[146] Raj V, Npb Aetukuri, Nanda J. Solid state lithium metal batteries – issues and challenges at the lithium-solid electrolyte interface. Curr Opin Solid State Mater Sci 2022;26:100999. https://doi.org/10.1016/j.cossms.2022.100999.
[147] Albertus P, Anandan V, Ban C, Balsara N, Belharouak I, Buettner-Garrett J, et al. Challenges for and pathways toward Li-Metal-Based all-solid-state batteries. ACS Energy Lett 2021. https://doi.org/10.1021/acsenergylett.1c00445. 1399–404.
[148] Yang C, Zhang L, Liu B, Xu S, Hamann T, McOwen D, et al. Continuous plating/stripping behavior of solid-state lithium metal anode in a 3D ion-conductive framework. Proc Natl Acad Sci USA 2018;115:3770–5. https://doi.org/10.1073/pnas.1719758115.
[149] Zheng B, Zhu J, Wang H, Feng M, Umeshbabu E, Li Y, et al. Stabilizing Li10SnP2S12/Li interface via an in situ formed solid electrolyte interphase layer. ACS Appl Mater Interfaces 2018;10:25473–82. https://doi.org/10.1021/acsami.8b08860.
[150] Shi Y, Zhou D, Li M, Wang C, Wei W, Liu G, et al. Surface engineered Li metal anode for all-solid-state lithium metal batteries with high capacity. Chemelectrochem 2021;8:386–9. https://doi.org/10.1002/celc.202100010.
[151] Liang J, Li X, Zhao Y, Goncharova LV, Li W, Adair KR, et al. An air-stable and dendrite-free Li anode for highly stable all-solid-state sulfide-based Li batteries. Adv Energy Mater 2019;9:1902125. https://doi.org/10.1002/aenm.201902125.
[152] Haruyama J, Sodeyama K, Han L, Takada K, Tateyama Y. Space-charge layer effect at interface between oxide cathode and sulfide electrolyte in all-solid-state lithium-ion battery. Chem Mater 2014;26:4248–55. https://doi.org/10.1021/cm5016959.
[153] Lu G, Geng F, Gu S, Li C, Shen M, Hu B. Distinguishing the effects of the space-charge layer and interfacial side reactions on Li10GeP2S12 -based all-solid-state batteries with stoichiometric-controlled LiCoO2. ACS Appl Mater Interfaces 2022;14:25556–65. https://doi.org/10.1021/acsami.2c05239.
[154] De Klerk NJJ, Wagemaker M. Space-charge layers in all-solid-state batteries; important or negligible? ACS Appl Energy Mater 2018;1:5609–18. https://doi.org/10.1021/acsaem.8b01141.
[155] Takada K, Ohta N, Zhang L, Xu X, Hang BT, Ohnishi T, et al. Interfacial phenomena in solid-state lithium battery with sulfide solid electrolyte. Solid State Ionics 2012;225:594–7. https://doi.org/10.1016/j.ssi.2012.01.009.
[156] Takada K, Ohta N, Tateyama Y. Recent progress in interfacial nanoarchitectonics in solid-state batteries. J Inorg Organomet Polym Mater 2015;25:205–13. https://doi.org/10.1007/s10904-014-0127-8.
[157] Ohta N, Takada K, Zhang L, Ma R, Osada M, Sasaki T. Enhancement of the high-rate capability of solid-state lithium batteries by nanoscale interfacial modification. Adv Mater 2006;18:2226–9. https://doi.org/10.1002/adma.200502604.
[158] Takada K, Ohta N, Zhang L, Fukuda K, Sakaguchi I, Ma R, et al. Interfacial modification for high-power solid-state lithium batteries. Solid State Ionics 2008;179:1333–7. https://doi.org/10.1016/j.ssi.2008.02.017.
[159] Yamamoto K, Iriyama Y, Asaka T, Hirayama T, Fujita H, Fisher CAJ, et al. Dynamic visualization of the electric potential in an all-solid-state rechargeable lithium battery. Angew Chem, Int Ed 2010;49:4414–7. https://doi.org/10.1002/anie.200907319.
[160] Yamamoto K, Iriyama Y, Asaka T, Hirayama T, Fujita H, Nonaka K, et al. Direct observation of lithium-ion movement around an in-situ-formed- negative-electrode/solid-state-electrolyte interface during initial charge-discharge reaction. Electrochem Commun 2012;20:113–6. https://doi.org/10.1016/j.elecom.2012.04.013.
[161] Nomura Y, Yamamoto K, Hirayama T, Ouchi S, Igaki E, Saitoh K, et al. Direct observation of a Li-ionic space-charge layer formed at an electrode/solid-electrolyte interface. Adv Mater 2019;58:5346–50. https://doi.org/10.1002/ANGE.201814669.
[162] Wang L, Xie R, Chen B, Yu X, Ma J, Li C, et al. In-situ visualization of the space-charge-layer effect on interfacial lithium-ion transport in all-solid-state batteries. Nat Commun 2020;11:5889. https://doi.org/10.1038/s41467-020-19726-5.
[163] Gao B, Jalem R, Tateyama Y. First-principles study of microscopic electrochemistry at the LiCoO2 cathode/LiNbO3Coating/β-Li3PS4Solid electrolyte interfaces in an all-solid-state battery. ACS Appl Mater Interfaces 2021;13:11765–73. https://doi.org/10.1021/acsami.0c19091.
[164] Okuno Y, Haruyama J, Tateyama Y. Comparative study on sulfide and oxide electrolyte interfaces with cathodes in all-solid-state battery via first-principles calculations. ACS Appl Energy Mater 2020;3:11061–72. https://doi.org/10.1021/acsaem.0c02033.
[165] Takada K, Ohno T, Ohta N, Ohnishi T, Tanaka Y. Positive and negative aspects of interfaces in solid-state batteries. ACS Energy Lett 2018;3:98–103. https://doi.org/10.1021/acsenergylett.7b01105.

[166] Gao B, Jalem R, Ma Y, Tateyama Y. Li+ transport mechanism at the heterogeneous cathode/solid electrolyte interface in an all-solid-state battery via the first-principles structure prediction scheme. Chem Mater 2020;32:85–96. https://doi.org/10.1021/acs.chemmater.9b02311.
[167] Zhang J, Zheng C, Li L, Xia Y, Huang H, Gan Y, et al. Unraveling the intra and intercycle interfacial evolution of Li6PS5Cl-based all-solid-state lithium batteries. Adv Energy Mater 2020;10:1903311. https://doi.org/10.1002/aenm.201903311.
[168] Gogotsi Y, Penner RM. Energy storage in nanomaterials - capacitive, pseudocapacitive, or battery-like? ACS Nano 2018;12. https://doi.org/10.1021/acsnano.8b01914. 2081–3.
[169] Ohta N, Takada K, Sakaguchi I, Zhang L, Ma R, Fukuda K, et al. LiNbO3-coated LiCoO2 as cathode material for all solid-state lithium secondary batteries. Electrochem Commun 2007;9:1486–90. https://doi.org/10.1016/j.elecom.2007.02.008.
[170] Sakuda A, Hayashi A, Tatsumisago M. Interfacial observation between LiCoO2 electrode and Li2S-P2S5 solid electrolytes of all-solid-state lithium secondary batteries using transmission electron microscopy. Chem Mater 2010;22:949–56. https://doi.org/10.1021/cm901819c.
[171] Wenzel S, Leichtweiss T, Krüger D, Sann J, Janek J. Interphase formation on lithium solid electrolytes - an in situ approach to study interfacial reactions by photoelectron spectroscopy. Solid State Ionics 2015;278:98–105. https://doi.org/10.1016/j.ssi.2015.06.001.
[172] Haruyama J, Sodeyama K, Tateyama Y. Cation mixing properties toward Co diffusion at the LiCoO2 cathode/sulfide electrolyte interface in a solid-state battery. ACS Appl Mater Interfaces 2017;9:286–92. https://doi.org/10.1021/acsami.6b08435.
[173] Auvergniot J, Cassel A, Ledeuil JB, Viallet V, Seznec V, Dedryvère R. Interface stability of argyrodite Li6PS5Cl toward LiCoO2, LiNi1/3Co1/3Mn1/3O2, and LiMn2O4 in bulk all-solid-state batteries. Chem Mater 2017;29:3883–90. https://doi.org/10.1021/acs.chemmater.6b04990.
[174] Walther F, Koerver R, Fuchs T, Ohno S, Sann J, Rohnke M, et al. Visualization of the interfacial decomposition of composite cathodes in argyrodite-based all-solid-state batteries using time-of-flight secondary-ion mass spectrometry. Chem Mater 2019;31:3745–55. https://doi.org/10.1021/acs.chemmater.9b00770.
[175] Wang C, Hwang S, Jiang M, Liang J, Sun Y, Adair K, et al. Deciphering interfacial chemical and electrochemical reactions of sulfide-based all-solid-state batteries. Adv Energy Mater 2021;11:2100210. https://doi.org/10.1002/aenm.202100210.
[176] Strauss F, Teo JH, Schiele A, Bartsch T, Hatsukade T, Hartmann P, et al. Gas evolution in lithium-ion batteries: solid versus liquid electrolyte. ACS Appl Mater Interfaces 2020;12:20462–8. https://doi.org/10.1021/acsami.0c02872.
[177] Zuo T, Rueß R, Pan R, Walther F, Rohnke M, Hori S, et al. A mechanistic investigation of the Li10GeP2S12|LiNi1-x-yCoxMnyO2 interface stability in all-solid-state lithium batteries. Nat Commun 2021;12:6669. https://doi.org/10.1038/s41467-021-26895-4.
[178] Chen B, Ju J, Ma J, Zhang J, Xiao R, Cui G, et al. An insight into intrinsic interfacial properties between Li metals and Li10GeP2S12 solid electrolytes. Phys Chem Chem Phys 2017;19:31436–42. https://doi.org/10.1039/c7cp05253g.
[179] Wenzel S, Weber DA, Leichtweiss T, Busche MR, Sann J, Janek J. Interphase formation and degradation of charge transfer kinetics between a lithium metal anode and highly crystalline Li7P3S11 solid electrolyte. Solid State Ionics 2016;286:24–33. https://doi.org/10.1016/j.ssi.2015.11.034.
[180] Wenzel S, Randau S, Leichtweiß T, Weber DA, Sann J, Zeier WG, et al. Direct observation of the interfacial instability of the fast ionic conductor Li10GeP2S12 at the lithium metal anode. Chem Mater 2016;28:2400–7. https://doi.org/10.1021/acs.chemmater.6b00610.
[181] Wenzel S, Sedlmaier SJ, Dietrich C, Zeier WG, Janek J. Interfacial reactivity and interphase growth of argyrodite solid electrolytes at lithium metal electrodes. Solid State Ionics 2018;318:102–12. https://doi.org/10.1016/j.ssi.2017.07.005.
[182] Sakuma M, Suzuki K, Hirayama M, Kanno R. Reactions at the electrode/electrolyte interface of all-solid-state lithium batteries incorporating Li-M (M = Sn, Si) alloy electrodes and sulfide-based solid electrolytes. Solid State Ionics 2016;285:101–5. https://doi.org/10.1016/j.ssi.2015.07.010.
[183] Li X, Jin L, Song D, Zhang H, Shi X, Wang Z, et al. LiNbO3-coated LiNi0.8Co0.1Mn0.1O2 cathode with high discharge capacity and rate performance for all-solid-state lithium battery. J Energy Chem 2020;40:39–45. https://doi.org/10.1016/j.jechem.2019.02.006.
[184] Liang Y, Liu H, Wang G, Wang C, Li D, Ni Y, et al. Heuristic design of cathode hybrid coating for power-limited sulfide-based all-solid-state lithium batteries. Adv Energy Mater 2022;12:2201555. https://doi.org/10.1002/aenm.202201555.
[185] Wang Y, Wang Z, Wu D, Niu Q, Lu P, Ma T, et al. Stable Ni-rich layered oxide cathode for sulfide-based all-solid-state lithium battery. eScience 2022;2:537–45. https://doi.org/10.1016/j.esci.2022.06.001.
[186] Yao X, Huang N, Han F, Zhang Q, Wan H, Mwizerwa JP, et al. High-performance all-solid-state lithium–sulfur batteries enabled by amorphous sulfur-coated reduced graphene oxide cathodes. Adv Energy Mater 2017;7:1602923. https://doi.org/10.1002/aenm.201602923.
[187] Ye L, Li X. A dynamic stability design strategy for lithium metal solid state batteries. Nature 2021;593:218–22. https://doi.org/10.1038/s41586-021-03486-3.
[188] Yang M, Mo Y. Interfacial defect of lithium metal in solid-state batteries. Angew Chem, Int Ed 2021;133:21664–71. https://doi.org/10.1002/ange.202108144.
[189] Schmalzried H, Janek J. Chemical kinetics of phase boundaries in solids. Berichte Der Bunsengesellschaft Für Phys Chemie 1998;102:127–43. https://doi.org/10.1002/bbpc.19981020202.
[190] Panahian Jand S, Kaghazchi P. Theoretical study of cubic-Li7La3Zr2O12 (001)/LiCoO2 (10-14) interface. MRS Commun 2018;8:591–6. https://doi.org/10.1557/mrc.2018.33.
[191] Doux J, Nguyen H, Tan DHS, Banerjee A, Wang X, Wu EA, et al. Stack pressure considerations for room-temperature all-solid-state lithium metal batteries. Adv Energy Mater 2020;10:1903253. https://doi.org/10.1002/aenm.201903253.
[192] Krauskopf T, Hartmann H, Zeier WG, Janek J. Toward a fundamental understanding of the lithium metal anode in solid-state batteries - an electrochemo-mechanical study on the garnet-type solid electrolyte Li 6.25 Al 0.25 La 3 Zr 2 O 12. ACS Appl Mater Interfaces 2019;11:14463–77. https://doi.org/10.1021/acsami.9b02537.
[193] Lu Y, Zhao C-Z, Hu J-K, Sun S, Yuan H, Fu Z-H, et al. The void formation behaviors in working solid-state Li metal batteries. Sci Adv 2022;8. https://doi.org/10.1126/sciadv.add0510. eadd0510.
[194] Sun F, Wang C, Osenberg M, Dong K, Zhang S, Yang C, et al. Clarifying the electro-chemo-mechanical coupling in Li10SnP2S12 based all-solid-state batteries. Adv Energy Mater 2022;12:2103714. https://doi.org/10.1002/aenm.202103714.
[195] Koerver R, Aygün I, Leichtweiß T, Dietrich C, Zhang W, Binder JO, et al. Capacity fade in solid-state batteries: interphase formation and chemomechanical processes in nickel-rich layered oxide cathodes and lithium thiophosphate solid electrolytes. Chem Mater 2017;29:5574–82. https://doi.org/10.1021/acs.chemmater.7b00931.
[196] Li X, Sun Y, Wang Z, Wang X, Zhang H, Song D, et al. High-rate and long-life Ni-rich oxide cathode under high mass loading for sulfide-based all-solid-state lithium batteries. Electrochim Acta 2021;391:138917. https://doi.org/10.1016/j.electacta.2021.138917.
[197] Dewald GF, Ohno S, Hering JGC, Janek J, Zeier WG. Analysis of charge carrier transport toward optimized cathode composites for all-solid-state Li−S batteries. Batter Supercaps 2021;4:183–94. https://doi.org/10.1002/batt.202000194.
[198] Minnmann P, Quillman L, Burkhardt S, Richter FH, Janek J. Editors' choice—quantifying the impact of charge transport bottlenecks in composite cathodes of all-solid-state batteries. J Electrochem Soc 2021;168:040537. https://doi.org/10.1149/1945-7111/abf8d7.
[199] Parikh D, Christensen T, Li J. Correlating the influence of porosity, tortuosity, and mass loading on the energy density of LiNi0.6Mn0.2Co0.2O2 cathodes under extreme fast charging (XFC) conditions. J Power Sources 2020;474:228601. https://doi.org/10.1016/j.jpowsour.2020.228601.
[200] Pouraghajan F, Thompson AI, Hunter EE, Mazzeo B, Christensen J, Subbaraman R, et al. The effects of cycling on ionic and electronic conductivities of Li –ion battery electrodes. J Power Sources 2021;492:229636. https://doi.org/10.1016/j.jpowsour.2021.229636.
[201] Liu L, Xu J, Wang S, Wu F, Li H, Chen L. Practical evaluation of energy densities for sulfide solid-state batteries. ETransportation 2019;1:100010. https://doi.org/10.1016/j.etran.2019.100010.
[202] Yang X, Doyle-Davis K, Gao X, Sun X. Recent progress and perspectives on designing high-performance thick electrodes for all-solid-state lithium batteries. ETransportation 2022;11:100152. https://doi.org/10.1016/j.etran.2021.100152.
[203] Zhang W, Weber DA, Weigand H, Arlt T, Manke I, Schröder D, et al. Interfacial processes and influence of composite cathode microstructure controlling the performance of all-solid-state lithium batteries. ACS Appl Mater Interfaces 2017;9:17835–45. https://doi.org/10.1021/acsami.7b01137.
[204] Davis AL, Goel V, Liao DW, Main MN, Kazyak E, Lee J, et al. Rate limitations in composite solid-state battery electrodes: revealing heterogeneity with operando microscopy. ACS Energy Lett 2021;6:2993–3003. https://doi.org/10.1021/acsenergylett.1c01063.
[205] Sangrós Giménez C, Helmers L, Schilde C, Diener A, Kwade A. Modeling the electrical conductive paths within all-solid-state battery electrodes. Chem Eng Technol 2020;43:819–29. https://doi.org/10.1002/ceat.201900501.
[206] Mizuno F, Hayashi A, Tadanaga K, Tatsumisago M. Design of composite positive electrode in all-solid-state secondary batteries with Li2S-P2S5 glass-ceramic electrolytes. J Power Sources 2005;146:711–4. https://doi.org/10.1016/j.jpowsour.2005.03.161.
[207] Zhang W, Leichtweiß T, Culver SP, Koerver R, Das D, Weber DA, et al. The detrimental effects of carbon additives in Li10GeP2S12-based solid-state batteries. ACS Appl Mater Interfaces 2017;9:35888–96. https://doi.org/10.1021/acsami.7b11530.
[208] Deng S, Sun Y, Li X, Ren Z, Liang J, Doyle-Davis K, et al. Eliminating the detrimental effects of conductive agents in sulfide-based solid-state batteries. ACS Energy Lett 2020;5:1243–51. https://doi.org/10.1021/acsenergylett.0c00256.
[209] Tan DHS, Wu EA, Nguyen H, Chen Z, Marple MAT, Doux J-M, et al. Elucidating reversible electrochemical redox of Li 6 PS 5 Cl solid electrolyte. ACS Energy Lett 2019;4:2418–27. https://doi.org/10.1021/acsenergylett.9b01693.
[210] Strauss F, Bartsch T, De Biasi L, Kim AY, Janek J, Hartmann P, et al. Impact of cathode material particle size on the capacity of bulk-type all-solid-state batteries. ACS Energy Lett 2018;3:992–6. https://doi.org/10.1021/acsenergylett.8b00275.
[211] Jiang W, Zhu X, Huang R, Zhao S, Fan X, Ling M, et al. Revealing the design principles of Ni-rich cathodes for all-solid-state batteries. Adv Energy Mater 2022;12:2103473. https://doi.org/10.1002/aenm.202103473.
[212] Rosero-Navarro NC, Miura A, Tadanaga K. Composite cathode prepared by argyrodite precursor solution assisted by dispersant agents for bulk-type all-solid-state batteries. J Power Sources 2018;396:33–40. https://doi.org/10.1016/j.jpowsour.2018.06.011.
[213] Calpa M, Rosero-Navarro NC, Miura A, Tadanaga K. Electrochemical performance of bulk-type all-solid-state batteries using small-sized Li7P3S11 solid electrolyte prepared by liquid phase as the ionic conductor in the composite cathode.

Electrochim Acta 2019;296:473–80. https://doi.org/10.1016/j.electacta.2018.11.035.
[214] Rajagopal R, Subramanian Y, Ryu KS. Improving the electrochemical performance of cathode composites using different sized solid electrolytes for all solid-state lithium batteries. RSC Adv 2021;11:32981–7. https://doi.org/10.1039/d1ra05897e.
[215] Park C, Lee S, Kim K, Kim M, Choi S, Shin D. Electrochemical properties of composite cathode using bimodal sized electrolyte for all-solid-state batteries. J Electrochem Soc 2019;166:A5318–22. https://doi.org/10.1149/2.0481903jes.
[216] Rosero-Navarro NC, Kinoshita T, Miura A, Higuchi M, Tadanaga K. Effect of the binder content on the electrochemical performance of composite cathode using Li6PS5Cl precursor solution in an all-solid-state lithium battery. Ionics 2017;23:1619–24. https://doi.org/10.1007/s11581-017-2106-x.
[217] Bielefeld A, Weber DA, Janek J. Modeling effective ionic conductivity and binder influence in composite cathodes for all-solid-state batteries. ACS Appl Mater Interfaces 2020;12:12821–33. https://doi.org/10.1021/acsami.9b22788.
[218] Zhang J, Zhong H, Zheng C, Xia Y, Liang C, Huang H, et al. All-solid-state batteries with slurry coated LiNi0.8Co0.1Mn0.1O2 composite cathode and Li6PS5Cl electrolyte: effect of binder content. J Power Sources 2018;391:73–9. https://doi.org/10.1016/j.jpowsour.2018.04.069.
[219] Hippauf F, Schumm B, Doerfler S, Althues H, Fujiki S, Shiratsushi T, et al. Overcoming binder limitations of sheet-type solid-state cathodes using a solvent-free dry-film approach. Energy Storage Mater 2019;21:390–8. https://doi.org/10.1016/j.ensm.2019.05.033.
[220] Kirsch DJ, Lacey SD, Kuang Y, Pastel G, Xie H, Connell JW, et al. Scalable dry processing of binder-free lithium-ion battery electrodes enabled by holey graphene. ACS Appl Energy Mater 2019;2:2990–7. https://doi.org/10.1021/acsaem.9b00066.
[221] Li Y, Wu Y, Ma T, Wang Z, Gao Q, Xu J, et al. Long-life sulfide all-solid-state battery enabled by substrate-modulated dry-process binder. Adv Energy Mater 2022;12:2201732. https://doi.org/10.1002/aenm.202201732.
[222] Yamamoto M, Terauchi Y, Sakuda A, Takahashi M. Binder-free sheet-type all-solid-state batteries with enhanced rate capabilities and high energy densities. Sci Rep 2018;8:2–11. https://doi.org/10.1038/s41598-018-19398-8.
[223] Lu Y, Zhao CZ, Yuan H, Hu JK, Huang JQ, Zhang Q. Dry electrode technology, the rising star in solid-state battery industrialization. Matter 2022;5:876–98. https://doi.org/10.1016/j.matt.2022.01.011.
[224] Hong SB, Lee YJ, Kim UH, Bak C, Lee YM, Cho W, et al. All-solid-state lithium batteries: Li+-Conducting ionomer binder for dry-processed composite cathodes. ACS Energy Lett 2022;7:1092–100. https://doi.org/10.1021/acsenergylett.1c02756.
[225] Oh DY, Nam YJ, Park KH, Jung SH, Kim KT, Ha AR, et al. Slurry-fabricable Li + -conductive polymeric binders for practical all-solid-state lithium-ion batteries enabled by solvate ionic liquids. Adv Energy Mater 2019;9:1802927. https://doi.org/10.1002/aenm.201802927.
[226] Shin DO, Kim H, Jung S, Byun S, Choi J, Kim MP, et al. Electrolyte-free graphite electrode with enhanced interfacial conduction using Li+-conductive binder for high-performance all-solid-state batteries. Energy Storage Mater 2022;49:481–92. https://doi.org/10.1016/j.ensm.2022.04.029.
[227] Hayakawa E, Nakamura H, Ohsaki S, Watano S. Dry mixing of cathode composite powder for all-solid-state batteries using a high-shear mixer. Adv Powder Technol 2022;33:103705. https://doi.org/10.1016/j.apt.2022.103705.
[228] Noh S, Nichols WT, Cho M, Shin D. Importance of mixing protocol for enhanced performance of composite cathodes in all-solid-state batteries using sulfide solid electrolyte. J Electroceram 2018;40:293–9.
[229] Kim DH, Lee HA, Song YB, Park JW, Lee SM, Jung YS. Sheet-type Li6PS5Cl-infiltrated Si anodes fabricated by solution process for all-solid-state lithium-ion batteries. J Power Sources 2019;426:143–50. https://doi.org/10.1016/j.jpowsour.2019.04.028.
[230] Huang G, Zhong Y, Xia X, Wang X, Gu C, Tu J. Surface-modified and sulfide electrolyte-infiltrated LiNi0.6Co0.2Mn0.2O2 cathode for all-solid-state lithium batteries. J Colloid Interface Sci 2023;632:11–8. https://doi.org/10.1016/j.jcis.2022.11.048.
[231] Alabdali M, Zanotto FM, Viallet V, Seznec V, Franco AA. Microstructurally resolved modeling of all solid-state batteries: latest progresses, opportunities, and challenges. Curr Opin Electrochem 2022;36:101127. https://doi.org/10.1016/j.coelec.2022.101127.
[232] Park J, Kim KT, Oh DY, Jin D, Kim D, Jung YS, et al. Digital twin-driven all-solid-state battery: unraveling the physical and electrochemical behaviors. Adv Energy Mater 2020;10:2001563. https://doi.org/10.1002/aenm.202001563.
[233] Bielefeld A, Weber DA, Janek J. Microstructural modeling of composite cathodes for all-solid-state batteries. J Phys Chem C 2019;123:1626–34. https://doi.org/10.1021/acs.jpcc.8b11043.
[234] Bielefeld A, Weber DA, Rueß R, Glavas V, Janek J. Influence of lithium ion kinetics, particle morphology and voids on the electrochemical performance of composite cathodes for all-solid-state batteries. J Electrochem Soc 2022;169:020539. https://doi.org/10.1149/1945-7111/ac50df.
[235] Neumann A, Randau S, Becker-Steinberger K, Danner T, Hein S, Ning Z, et al. Analysis of interfacial effects in all-solid-state batteries with thiophosphate solid electrolytes. ACS Appl Mater Interfaces 2020;12:9277–91. https://doi.org/10.1021/acsami.9b21404.
[236] Yamakawa S, Ohta S, Kobayashi T. Effect of positive electrode microstructure in all-solid-state lithium-ion battery on high-rate discharge capability. Solid State Ionics 2020;344:115079. https://doi.org/10.1016/j.ssi.2019.115079.
[237] Lombardo T, Caro F, Ngandjong AC, Hoock J, Duquesnoy M, Delepine JC, et al. The ARTISTIC online calculator: exploring the impact of lithium-ion battery electrode manufacturing parameters interactively through your browser. Batter Supercaps 2022;5:e202100324. https://doi.org/10.1002/batt.202100324.
[238] Ngandjong AC, Rucci A, Maiza M, Shukla G, Vazquez-Arenas J, Franco AA. Multiscale simulation platform linking lithium ion battery electrode fabrication process with performance at the cell level. J Phys Chem Lett 2017;8:5966–72. https://doi.org/10.1021/acs.jpclett.7b02647.
[239] Zanotto FM, Dominguez DZ, Ayerbe E, Boyano I, Burmeister C, Duquesnoy M, et al. Data specifications for battery manufacturing digitalization: current status, challenges, and opportunities. Batter Supercaps 2022:202200224. https://doi.org/10.1002/batt.202200224.
[240] Alabdali M, Zanotto FM, Duquesnoy M, Viallet V, Seznec V, Franco AA. Three dimensional physical modeling of the wet manufacturing process of solid state battery electrodes. 2022. 10.26434/chemrxiv-2022-qvs9z.
[241] Conforto G, Ruess R, Schröder D, Trevisanello E, Fantin R, Richter FH, et al. Editors' choice—quantification of the impact of chemo-mechanical degradation on the performance and cycling stability of NCM-based cathodes in solid-state Li-ion batteries. J Electrochem Soc 2021;168:070546. https://doi.org/10.1149/1945-7111/ac13d2.
[242] Shi T, Zhang Y, Tu Q, Wang Y, Scott MC, Ceder G. Characterization of mechanical degradation in an all-solid-state battery cathode. J Mater Chem A 2020;8:17399–404. https://doi.org/10.1039/D0TA06985J.
[243] Koerver R, Zhang W, De Biasi L, Schweidler S, Kondrakov AO, Kolling S, et al. Chemo-mechanical expansion of lithium electrode materials-on the route to mechanically optimized all-solid-state batteries. Energy Environ Sci 2018;11:2142–58. https://doi.org/10.1039/c8ee00907d.
[244] Li R, Li W, Singh A, Ren D, Hou Z, Ouyang M. Effect of external pressure and internal stress on battery performance and lifespan. Energy Storage Mater 2022;52:395–429. https://doi.org/10.1016/j.ensm.2022.07.034.
[245] Ruess R, Schweidler S, Hemmelmann H, Conforto G, Bielefeld A, Weber DA, et al. Influence of NCM particle cracking on kinetics of lithium-ion batteries with liquid or solid electrolyte. J Electrochem Soc 2020;167:100532. https://doi.org/10.1149/1945-7111/ab9a2c.
[246] Liu X, Zheng B, Zhao J, Zhao W, Liang Z, Su Y, et al. Electrochemo-mechanical effects on structural integrity of Ni-rich cathodes with different microstructures in all solid-state batteries. Adv Energy Mater 2021;11:2003583. https://doi.org/10.1002/aenm.202003583.
[247] Teo JH, Strauss F, Walther F, Ma Y, Payandeh S, Scherer T, et al. The interplay between (electro) chemical and (chemo) mechanical effects in the batteries. Mater Futur 2022;1:015102.
[248] Yamamoto M, Terauchi Y, Sakuda A, Kato A, Takahashi M. Effects of volume variations under different compressive pressures on the performance and microstructure of all-solid-state batteries. J Power Sources 2020;473:228595. https://doi.org/10.1016/j.jpowsour.2020.228595.
[249] Okuno R, Yamamoto M, Kato A, Takahashi M. High cycle stability of nanoporous Si composites in all-solid-state lithium-ion batteries. J Electrochem Soc 2022;169:080502. https://doi.org/10.1149/1945-7111/ac81f6.
[250] Kim JY, Jung S, Kang SH, Park J, Lee MJ, Jin D, et al. Graphite–Silicon diffusion-dependent electrode with short effective diffusion length for high-performance all-solid-state batteries. Adv Energy Mater 2022;12:2103108. https://doi.org/10.1002/aenm.202103108.
[251] Okuno R, Yamamoto M, Kato A, Takahashi M. Stable cyclability caused by highly dispersed nanoporous Si composite anodes with sulfide-based solid electrolyte. J Electrochem Soc 2020;167:140522. https://doi.org/10.1149/1945-7111/abc3ff.
[252] Okuno R, Yamamoto M, Kato A, Terauchi Y, Takahashi M. Microstructures of nanoporous-Si composite anodes in sulfide-based all-solid-state lithium-ion batteries. IOP Conf Ser Mater Sci Eng 2019;625:012012. https://doi.org/10.1088/1757-899X/625/1/012012.
[253] Doux JM, Yang Y, Tan DHS, Nguyen H, Wu EA, Wang X, et al. Pressure effects on sulfide electrolytes for all solid-state batteries. J Mater Chem A 2020;8:5049–55. https://doi.org/10.1039/c9ta12889a.
[254] So M, Inoue G, Hirate R, Nunoshita K, Ishikawa S, Tsuge Y. Effect of mold pressure on compaction and ion conductivity of all-solid-state batteries revealed by the discrete element method. J Power Sources 2021;508:230344. https://doi.org/10.1016/j.jpowsour.2021.230344.
[255] Cronau M, Szabo M, König C, Wassermann TB, Roling B. How to measure a reliable ionic conductivity? The stack pressure dilemma of microcrystalline sulfide-based solid electrolytes. ACS Energy Lett 2021;6:3072–7. https://doi.org/10.1021/acsenergylett.1c01299.
[256] Sakuda A, Hayashi A, Tatsumisago M. Sulfide solid electrolyte with favorable mechanical property for all-solid-state lithium battery. Sci Rep 2013;3:2–6. https://doi.org/10.1038/srep02261.
[257] Yamamoto M, Takahashi M, Terauchi Y, Kobayashi Y, Ikeda S, Sakuda A. Fabrication of composite positive electrode sheet with high active material content and effect of fabrication pressure for all-solid-state battery. J Ceram Soc Japan 2017;125:391–5. https://doi.org/10.2109/jcersj2.16321.
[258] Piper DM, Yersak TA, Lee S-H. Effect of compressive stress on electrochemical performance of silicon anodes. J Electrochem Soc 2013;160:A77–81. https://doi.org/10.1149/2.064301jes.
[259] Janek J, Zeier WG. Challenges in speeding up solid-state battery development. Nat Energy 2023;8:230–40. https://doi.org/10.1038/s41560-023-01208-9.
[260] Volkswagen. PV8450: lithium-ion cells for automotive applications test conditions. 2015.
[261] Ruiz V, Pfrang A, Kriston A, Omar N, Van den Bossche P, Boon-Brett L. A review of international abuse testing standards and regulations for lithium ion batteries

in electric and hybrid electric vehicles. Renew Sustain Energy Rev 2018;81:1427–52. https://doi.org/10.1016/j.rser.2017.05.195.
[262] FreedomCAR battery test manual for power-assist hybrid electric vehicles. 2003.11069.
[263] Zhang Y, Sun X, Cao D, Gao G, Yang Z, Zhu H, et al. Self-Stabilized LiNi0.8Mn0.1Co0.1O2 in thiophosphate-based all-solid-state batteries through extra LiOH. Energy Storage Mater 2021;41:505–14. https://doi.org/10.1016/j.ensm.2021.06.024.
[264] Shi J, Ma Z, Han K, Wan Q, Wu D, Qu X, et al. Coupling novel Li7TaO6 surface buffering with bulk Ta-doping to achieve long-life sulfide-based all-solid-state lithium batteries. J Mater Chem A 2022. https://doi.org/10.1039/d2ta06703j.21336–48.
[265] Solid power high-content silicon cell data. https://ir.solidpowerbattery.com/static-files/0850515d-73ca-488e-9fa1-48892f92a695. [Accessed 27 March 2023].
[266] Yoon K, Kim H, Han S, Chan T, Ko K, Jo S, et al. Detrimental effect of high-temperature storage on sulfide-based all-solid-state batteries. Appl Phys Rev 2022;9:031403. https://doi.org/10.1063/5.0088838.
[267] Morino Y. Degradation rate at the Solid–Solid interface of sulfide-based solid Electrolyte–Cathode active material. J Power Sources 2022;541:231672. https://doi.org/10.1016/j.jpowsour.2022.231672.
[268] USABC. Electric vehicle battery test procedures manual- rev, 2; 1996.
[269] Liang Z, Xiang Y, Wang K, Zhu J, Jin Y, Wang H, et al. Understanding the failure process of sulfide-based all-solid-state lithium batteries via operando nuclear magnetic resonance spectroscopy. Nat Commun 2023;14:259. https://doi.org/10.1038/s41467-023-35920-7.
[270] Xiao Y, Xu R, Yan C, Huang J, Zhang Q, Ouyang M. A toolbox of reference electrodes for lithium batteries. Adv Funct Mater 2022;32:2108449. https://doi.org/10.1002/adfm.202108449.
[271] Nam YJ, Park KH, Oh DY, An WH, Jung YS. Diagnosis of failure modes for all-solid-state Li-ion batteries enabled by three-electrode cells. J Mater Chem A 2018;6:14867–75. https://doi.org/10.1039/c8ta03450h.
[272] Feng X, Xu C, He X, Wang L, Gao S, Ouyang M. A graphical model for evaluating the status of series-connected lithium-ion battery pack. Int J Energy Res 2019;43:749–66. https://doi.org/10.1002/er.4305.
[273] Wang X, Wei X, Zhu J, Dai H, Zheng Y, Xu X, et al. A review of modeling, acquisition, and application of lithium-ion battery impedance for onboard battery management. ETransportation 2021;7:100093. https://doi.org/10.1016/j.etran.2020.100093.
[274] Qu D, Ji W, Qu H. Probing process kinetics in batteries with electrochemical impedance spectroscopy. Commun Mater 2022;3:61. https://doi.org/10.1038/s43246-022-00284-w.
[275] Vadhva P, Hu J, Johnson MJ, Stocker R, Braglia M, Brett DJL, et al. Electrochemical impedance spectroscopy for all-solid-state batteries: theory, methods and future outlook. Chemelectrochem 2021;8:1930–47. https://doi.org/10.1002/celc.202100108.
[276] Smith a J, Burns JC, Xiong D, Dahn JR. Interpreting high precision coulometry results on Li-ion cells. J Electrochem Soc 2011;158:A1136. https://doi.org/10.1149/1.3625232.
[277] Stevens Da, Ying RY, Fathi R, Reimers JN, Harlow JE, Dahn JR. Using high precision coulometry measurements to compare the degradation mechanisms of NMC/LMO and NMC-only automotive scale pouch cells. J Electrochem Soc 2014;161:A1364–70. https://doi.org/10.1149/2.0971409jes.
[278] Morino Y, Tsukasaki H, Mori S. Cycle degradation analysis by high precision coulometry for sulfide-based all-solid-state battery cathode under various potentials. Electrochemistry 2022;90. https://doi.org/10.5796/electrochemistry.22-00018. 22–00018.
[279] Are solid-state cells safer?. https://www.solidpowerbattery.com/solid-state-safety/. [Accessed 27 March 2023].
[280] Guo Y, Wu S, He Y-B, Kang F, Chen L, Li H, et al. Solid-state lithium batteries: safety and prospects. eScience 2022;2:138–63. https://doi.org/10.1016/j.esci.2022.02.008.
[281] Bates AM, Preger Y, Torres-Castro L, Harrison KL, Harris SJ, Hewson J. Are solid-state batteries safer than lithium-ion batteries? Joule 2022;6:742–55. https://doi.org/10.1016/j.joule.2022.02.007.
[282] Inoue T, Mukai K. Are all-solid-state lithium-ion batteries really safe ? – verification by differential scanning calorimetry with an all-inclusive microcell. ACS Appl Mater Interfaces 2017;9:1507–15. https://doi.org/10.1021/acsami.6b13224.
[283] Vishnugopi BS, Hasan MT, Zhou H, Mukherjee PP. Interphases and electrode crosstalk dictate the thermal stability of solid-state batteries. ACS Energy Lett 2023;8:398–407. https://doi.org/10.1021/acsenergylett.2c02443.
[284] Tsukasaki H, Otoyama M, Mori Y, Mori S, Morimoto H, Hayashi A, et al. Analysis of structural and thermal stability in the positive electrode for sulfide-based all-solid-state lithium batteries. J Power Sources 2017;367:42–8. https://doi.org/10.1016/j.jpowsour.2017.09.031.
[285] Tsukasaki H, Uchiyama T, Yamamoto K, Mori S, Uchimoto Y, Kowada H, et al. Exothermal mechanisms in the charged LiNi1/3Mn1/3Co1/3O2 electrode layers for sulfide-based all-solid-state lithium batteries. J Power Sources 2019;434:226714. https://doi.org/10.1016/j.jpowsour.2019.226714.
[286] Atarashi A, Tsukasaki H, Otoyama M, Kowada H, Mori S, Hayashi A, et al. Ex situ investigation of exothermal behavior and structural changes of the Li3PS4- LiNi1/3Mn1/3Co1/3O2 electrode composites. Solid State Ionics 2019;342:115046. https://doi.org/10.1016/j.ssi.2019.115046.
[287] Tsukasaki H, Otoyama M, Kimura T, Mori S, Sakuda A, Hayashi A, et al. Exothermal behavior and microstructure of a LiNi1/3Mn1/3Co1/3O2 electrode layer using a Li4SnS4 solid electrolyte. J Power Sources 2020;479:228827. https://doi.org/10.1016/j.jpowsour.2020.228827.
[288] Rui X, Ren D, Liu X, Wang X, Wang K, Lu Y, et al. Distinct thermal runaway mechanisms of sulfide-based all-solid-state batteries. Energy Environ Sci 2023;16:3552–63. https://doi.org/10.1039/D3EE00084B.
[289] Ren D, Feng X, Liu L, Hsu H, Lu L, Wang L, et al. Investigating the relationship between internal short circuit and thermal runaway of lithium-ion batteries under thermal abuse condition. Energy Storage Mater 2021;34:563–73. https://doi.org/10.1016/j.ensm.2020.10.020.
[290] Ren D, Liu X, Feng X, Lu L, Ouyang M, Li J, et al. Model-based thermal runaway prediction of lithium-ion batteries from kinetics analysis of cell components. Appl Energy 2018;228:633–44. https://doi.org/10.1016/j.apenergy.2018.06.126.
[291] Chen R, Nolan AM, Lu J, Wang J, Yu X, Mo Y, et al. The thermal stability of lithium solid electrolytes with metallic lithium. Joule 2020;4:812–21. https://doi.org/10.1016/j.joule.2020.03.012.
[292] Kaboli S, Girard G, Zhu W, Gheorghe Nita A, Vijh A, George C, et al. Thermal evolution of NASICON type solid-state electrolytes with lithium at high temperature via in situ scanning electron microscopy. Chem Commun 2021;57:11076–9. https://doi.org/10.1039/d1cc04059f.
[293] Wang H, Xu H, Zhang Z, Wang Q, Jin C, Wu C, et al. Fire and explosion characteristics of vent gas from lithium-ion batteries after thermal runaway: a comparative study. ETransportation 2022;13:100190. https://doi.org/10.1016/j.etran.2022.100190.
[294] Rui X, Ren D, Liu X, Wang X, Wang K, Lu Y, et al. Distinct thermal runaway mechanisms of sulfide-based all-solid- state batteries. Under Rev 2023. https://doi.org/10.1039/x0xx00000x.
[295] Inada T, Kobayashi T, Sonoyama N, Yamada A, Kondo S, Nagao M, et al. All solid-state sheet battery using lithium inorganic solid electrolyte, thio-LISICON. J Power Sources 2009;194:1085–8. https://doi.org/10.1016/j.jpowsour.2009.06.100.
[296] Kim KT, Oh DY, Jun S, Song YB, Kwon TY, Han Y, et al. Tailoring slurries using cosolvents and Li salt targeting practical all-solid-state batteries employing sulfide solid electrolytes. Adv Energy Mater 2021;11:2003766. https://doi.org/10.1002/aenm.202003766.
[297] Oh DY, Kim KT, Jung SH, Kim DH, Jun S, Jeoung S, et al. Tactical hybrids of Li+-conductive dry polymer electrolytes with sulfide solid electrolytes: toward practical all-solid-state batteries with wider temperature operability. Mater Today 2022;53:7–15. https://doi.org/10.1016/j.mattod.2021.01.006.
[298] Cho W, Park J, Kim K, Yu J, Jeong G. Sulfide-compatible conductive and adhesive glue-like interphase engineering for sheet-type all-solid-state battery. Small 2021;17:1902138. https://doi.org/10.1002/smll.201902138.
[299] Oh DY, Kim DH, Jung SH, Han JG, Choi NS, Jung YS. Single-step wet-chemical fabrication of sheet-type electrodes from solid-electrolyte precursors for all-solid-state lithium-ion batteries. J Mater Chem A 2017;5:20771–9. https://doi.org/10.1039/c7ta06873e.
[300] Lee K, Kim S, Park J, Park SH, Coskun A, Jung DS, et al. Selection of binder and solvent for solution-processed all-solid-state battery. J Electrochem Soc 2017;164:A2075–81. https://doi.org/10.1149/2.1341709jes.
[301] Kim KT, Kwon TY, Jung YS. Scalable fabrication of sheet-type electrodes for practical all-solid-state batteries employing sulfide solid electrolytes. Curr Opin Electrochem 2022;34:101026. https://doi.org/10.1016/j.coelec.2022.101026.
[302] Chen H, Ling M, Hencz L, Ling HY, Li G, Lin Z, et al. Exploring chemical, mechanical, and electrical functionalities of binders for advanced energy-storage devices. Chem Rev 2018;118:8936–82. https://doi.org/10.1021/acs.chemrev.8b00241.
[303] Lee J, Lee T, Char K, Kim KJ, Choi JW. Issues and advances in scaling up sulfide-based all-solid-state batteries. Acc Chem Res 2021;54:3390–402. https://doi.org/10.1021/acs.accounts.1c00333.
[304] Ito S, Fujiki S, Yamada T, Aihara Y, Park Y, Kim TY, et al. A rocking chair type all-solid-state lithium ion battery adopting Li 2O-ZrO2 coated LiNi0.8Co0.15Al 0.05O2 and a sulfide based electrolyte. J Power Sources 2014;248:943–50. https://doi.org/10.1016/j.jpowsour.2013.10.005.
[305] Lee J, Lee K, Lee T, Kim H, Kim K, Cho W, et al. In Situ deprotection of polymeric binders for solution-processible sulfide-based all-solid-state batteries. Adv Mater 2020;32:2001702. https://doi.org/10.1002/adma.202001702.
[306] Kroll M, Duchardt M, Karstens SL, Schlabach S, Lange F, Hochstrasser J, et al. Sheet-type all-solid-state batteries with sulfidic electrolytes: analysis of kinetic limitations based on a cathode morphology study. J Power Sources 2021;505:230064. https://doi.org/10.1016/j.jpowsour.2021.230064.
[307] Chen K, Shinjo S, Sakuda A, Yamamoto K, Uchiyama T, Kuratani K, et al. Morphological effect on reaction distribution influenced by binder materials in composite electrodes for sheet-type all-solid-state lithium-ion batteries with the sulfide-based solid electrolyte. J Phys Chem C 2019;123:3292–8. https://doi.org/10.1021/acs.jpcc.8b09569.
[308] Kim KT, Kwon TY, Song YB, Kim SM, Byun SC, Min HS, et al. Wet-slurry fabrication using PVdF-HFP binder with sulfide electrolytes via synergetic cosolvent approach for all-solid-state batteries. Chem Eng J 2022;450:138047. https://doi.org/10.1016/j.cej.2022.138047.
[309] Jaiser S, Müller M, Baunach M, Bauer W, Scharfer P, Schabel W. Investigation of film solidification and binder migration during drying of Li-Ion battery anodes. J Power Sources 2016;318:210–9. https://doi.org/10.1016/j.jpowsour.2016.04.018.
[310] Ayerbe E, Berecibar M, Clark S, Franco AA, Ruhland J. Digitalization of battery manufacturing: current status, challenges, and opportunities. Adv Energy Mater 2022;12:2102696. https://doi.org/10.1002/aenm.202102696.

[311] Sakuda A, Kuratani K, Yamamoto M, Takahashi M, Takeuchi T, Kobayashi H. All-solid-state battery electrode sheets prepared by a slurry coating process. J Electrochem Soc 2017;164:A2474–8. https://doi.org/10.1149/2.0951712jes.
[312] Kim DH, Oh DY, Park KH, Choi YE, Nam YJ, Lee HA, et al. Infiltration of solution-processable solid electrolytes into conventional Li-Ion-Battery electrodes for all-solid-state Li-ion batteries. Nano Lett 2017;17:3013–20. https://doi.org/10.1021/acs.nanolett.7b00330.
[313] Song YB, Kim DH, Kwak H, Han D, Kang S, Lee JH, et al. Tailoring solution-processable Li argyrodites Li6+ xP1- xMxS5I (M = Ge, Sn) and their microstructural evolution revealed by cryo-TEM for all-solid-state batteries. Nano Lett 2020;20:4337–45. https://doi.org/10.1021/acs.nanolett.0c01028.
[314] Li Y, Wu Y, Wang Z, Xu J, Ma T, Chen L, et al. Progress in solvent-free dry-film technology for batteries and supercapacitors. Mater Today 2022;55:92–109. https://doi.org/10.1016/j.mattod.2022.04.008.
[315] Li J, Li Y, Zhang S, Liu T, Li D, Ci L. Long cycle life all-solid-state batteries enabled by solvent-free approach for sulfide solid electrolyte and cathode films. Chem Eng J 2022;455:140605. https://doi.org/10.1016/j.cej.2022.140605.
[316] Liu L, Xu J, Wang S, Wu F, Li H, Chen L. Practical evaluation of energy densities for sulfide solid-state batteries. ETransportation 2019;1:100010. https://doi.org/10.1016/j.etran.2019.100010.
[317] Cao D, Li Q, Sun X, Wang Y, Zhao X, Cakmak E, et al. Amphipathic binder integrating ultrathin and highly ion-conductive sulfide membrane for cell-level high-energy-density all-solid-state batteries. Adv Mater 2021;33:2105505. https://doi.org/10.1002/adma.202105505.
[318] Chen YT, Duquesnoy M, Tan DHS, Doux JM, Yang H, Deysher G, et al. Fabrication of high-quality thin solid-state electrolyte films assisted by machine learning. ACS Energy Lett 2021;6:1639–48. https://doi.org/10.1021/acsenergylett.1c00332.
[319] Zhang Z, Wu L, Zhou D, Weng W, Yao X. Flexible sulfide electrolyte thin membrane with ultrahigh ionic conductivity for all-solid-state lithium batteries. Nano Lett 2021;21:5233–9. https://doi.org/10.1021/acs.nanolett.1c01344.
[320] Li Y, Cao D, Arnold W, Ren Y, Liu C, Jasinski JB, et al. Regulated lithium ionic flux through well-aligned channels for lithium dendrite inhibition in solid-state batteries. Energy Storage Mater 2020;31:344–51. https://doi.org/10.1016/j.ensm.2020.06.029.
[321] Xu R, Yue J, Liu S, Tu J, Han F, Liu P, et al. Cathode-supported all-solid-state lithium-sulfur batteries with high cell-level energy density. ACS Energy Lett 2019;4:1073–9. https://doi.org/10.1021/acsenergylett.9b00430.
[322] Liu H, He P, Wang G, Liang Y, Wang C, Fan LZ. Thin, flexible sulfide-based electrolyte film and its interface engineering for high performance solid-state lithium metal batteries. Chem Eng J 2022;430:132991. https://doi.org/10.1016/j.cej.2021.132991.
[323] Kim DH, Lee YH, Song YB, Kwak H, Lee SY, Jung YS. Thin and flexible solid electrolyte membranes with ultrahigh thermal stability derived from solution-processable Li argyrodites for all-solid-state Li-ion batteries. ACS Energy Lett 2020;5:718–27. https://doi.org/10.1021/acsenergylett.0c00251.
[324] Zhu G, Zhao C, Peng H, Yuan H, Hu J, Nan H, et al. A self-limited free-standing sulfide electrolyte thin film for all-solid-state lithium metal batteries. Adv Funct Mater 2021;31:2101985. https://doi.org/10.1002/adfm.202101985.
[325] Yersak T, Salvador JR, Schmidt RD, Cai M. Hot pressed, fiber-reinforced (Li2S)70 (P2S5)30 solid-state electrolyte separators for Li metal batteries. ACS Appl Energy Mater 2019;2:3523–31. https://doi.org/10.1021/acsaem.9b00290.
[326] Wang C, Yu R, Duan H, Lu Q, Li Q, Adair KR, et al. Solvent-free approach for interweaving freestanding and ultrathin inorganic solid electrolyte membranes. ACS Energy Lett 2022;7:410–6. https://doi.org/10.1021/acsenergylett.1c02261.
[327] Ates T, Keller M, Kulisch J, Adermann T, Passerini S. Development of an all-solid-state lithium battery by slurry-coating procedures using a sulfidic electrolyte. Energy Storage Mater 2019;17:204–10. https://doi.org/10.1016/j.ensm.2018.11.011.
[328] Yokota M, Matsunaga T. Effect of roll press on consolidation and electric/ionic-path formation of electrodes for all-solid-state battery. J Power Sources Adv 2021;12:100078. https://doi.org/10.1016/j.powera.2021.100078.
[329] Yersak TA, Hao F, Kang C, Salvador JR, Zhang Q, Malabet HJG, et al. Consolidation of composite cathodes with NCM and sulfide solid-state electrolytes by hot pressing for all-solid-state Li metal batteries. J Solid State Electrochem 2022;26:709–18. https://doi.org/10.1007/s10008-021-05104-8.
[330] Dixit M, Beamer C, Amin R, Shipley J, Eklund R, Muralidharan N, et al. The role of isostatic pressing in large-scale production of solid-state batteries. ACS Energy Lett 2022. https://doi.org/10.1021/acsenergylett.2c01936. 3936–46.
[331] Cao D, Sun X, Wang Y, Zhu H. Bipolar stackings high voltage and high cell level energy density sulfide based all-solid-state batteries. Energy Storage Mater 2022;48:458–65. https://doi.org/10.1016/j.ensm.2022.03.012.
[332] Jung K-N, Shin H-S, Park M-S, Lee J-W. Solid-state lithium batteries: bipolar design, fabrication, and electrochemistry. Chemelectrochem 2019. https://doi.org/10.1002/celc.201900736. 3842–59.
[333] A new bread of battery. 2021. https://ir.solidpowerbattery.com/static-files/11d0e8d6-2fd0-43a2-9169-f02d0bebe801. [Accessed 27 March 2023].
[334] (in Japanese) NEDO's report in 2021. 2021. https://www.nedo.go.jp/content/100936690.pdf. [Accessed 27 March 2023].
[335] Zhu Y. Report about INTER BATTERY 2022. 2022 (in Chinese), https://zhuanlan.zhihu.com/p/495694270. [Accessed 27 March 2023].
[336] SVOLT unveils its second-generation L600 short blade battery. 2021. https://pushevs.com/2021/11/22/svolt-unveils-its-second-generation-l600-short-blade-battery/. [Accessed 27 March 2023].